Biomimetic Implants For Enhancing Implant-epithelial Sealing

A Thesis

By

Ahmed Saad

Submitted to Department of Mining at Material Engineering at McGill University
in fulfillment of the requirements for the degree of
Master of Science

Supervised by

Supervisor: Prof. Marta Cerruti

Co-supervisor: Prof. Faleh Tamimi

December 2020

Acknowledgments

First, I praise God for granting me strength and health and for guiding me through every step I take throughout life and during my master's degree.

Second, I would like to express my greatest gratitude to my supervisor Prof. Marta Cerruti for her endless guidance and support throughout my degree. Prof. Marta has been and will continue to be a great mentor to me and a successful role model that I will work to hopefully be like one day. I would like to specifically express my appreciation to Prof. Marta for her continuous patience towards my repeating mistakes and for continuous support to get the best of me. I extend my gratitude to my co-supervisor Prof. Faleh Tamimi who is a world-class researcher and a supporting and caring mentor. I learnt a lot from Dr. Faleh as his discussions and recommendations have always been fruitful.

Third, I would like to thank the collaborators whose work was pivotal for this thesis. Dr. Wang Min from Prof. Tamimi's lab and Dr. Osama EL-Kashty from Prof. Tran's lab for their assistance in cell culture experiments. Also, I am really thankful for my group members who helped me a lot during this work especially Dr. Emily Buck for her assistance and for sharing her knowledge on diazonium chemistry with me and Dr. Alaa Mansour for assisting me with protein extraction from teeth. Also, I want to thank all of other members in both Dr. Cerruti's lab and Dr. Tamimi's lab.

I am extremely thankful for Abdulla Al Ghurair Foundation for Education (AGFE) for their financial assistance through their full scholarship that they award me.

On a personal level, I would like to express my endless appreciation to my parents and my fiancée for their unconditional support and care. I want to thank my parents for the compromises they made so that I can get good education. No words can describe how much I am thankful for them. Last but not least, I would like to express all of the appreciation to my fiancée Kristen for always making my life better. Thank you for adding a wonderful meaning to my life journey.

Abstract

Devices that penetrate through the skin are known as percutaneous devices. Examples include dental implants, transcutaneous orthopaedic implants and catheters. Percutaneous devices are made from inert materials to prevent inducing allergic reactions of the human body. However, their inertness prevents the formation of a tight sealing with the skin that is in contact with the device. The lack of proper sealing leads to infection at the implantation site that eventually can cause device failure. Yet, infections do not occur around natural organs that penetrate the skin such as teeth and nails. The absence of infection is attributed to the strong attachment between these organs and the epithelial cells in the outermost layer of the skin. Research focused specifically on teeth has shown that the strong attachment between teeth and epithelial cells occurs via a set of extracellular matrix proteins known as basal lamina (BL) proteins that adsorb on teeth. Another study showed that tooth proteins are able to adsorb more BL proteins compared to tooth minerals. In this work, the first goal is to identify the tooth protein that shows strongest affinity to BL proteins. The second goal is to conjugate this protein on percutaneous device surfaces to increase BL proteins adsorption and epithelial cell integration.

To achieve the first goal, we developed a model for investigating interaction between tooth proteins and BL proteins. We used Matrigel to synthesize gel disks of BL proteins. A solution of tooth proteins was added on these disks and then washed away after 30 minutes to remove weakly bound proteins. Collagen protein was identified as the tooth protein with the highest affinity towards BL proteins.

In the second goal, we tested different classes of percutaneous devices including titanium alloy (Ti-6Al-4V) (used in dental and transcutaneous orthopaedic implants), and polymers such as Polyetheretherketone “PEEK” (used in dental implants and bone replacement). We immobilized collagen proteins on the mentioned biomaterial surfaces using covalent linkage. Then, we characterized the modified surfaces with X-ray photoelectron spectroscopy (XPS) to assess the chemical and elemental composition, and atomic force microscopy (AFM) to assess surface topography. Then, we assessed BL protein adsorption and human periodontal fibroblast cell growth on these surfaces and compared them with non-modified samples. Results showed successful conjugation of collagen proteins on titanium and PEEK surfaces. Also, we found that key BL proteins (particularly laminin, nidogen, and fibronectin) adsorb more on collagen-modified

surfaces than un-modified ones. Finally, cell proliferation was higher on collagen modified surfaces than control surfaces.

The results of this project provide a step towards further understanding of how nature prevents infections around percutaneous tissues. It also has the potential to deliver a new generation of biomaterials and surfaces that can be used for percutaneous devices such as dental implants and catheters to increase their sealing and reduce infections.

Résumé

Les appareils qui pénètrent la peau sont connus comme des appareils percutanés. Des implants dentaires, implants orthopédiques transcutanés, et les cathéters en sont des exemples. Les appareils percutanés sont fabriqués à partir de matériaux inertes afin de prévenir des réactions allergiques dans le corps humain. Cependant, le fait d'être inerte prévient la formation d'un joint étanche avec la peau qui est en contact avec l'appareil. Le manque d'étanchéité mène à des infections au site d'implantation qui peut éventuellement entraîner la défaillance de l'appareil. Pourtant, les infections ne se produisent pas autour d'organes qui pénètrent naturellement la peau, tels que les dents et les ongles. L'absence d'infections est attribuée à l'attachement fort entre les organes et les cellules épithéliales dans la couche externe de la peau. Plusieurs études axées spécifiquement sur les dents a montré que la forte fixation entre les dents et les cellules épithéliales se produit par un ensemble de protéines de la matrice extracellulaire appelées protéines de la lame basale (LB) qui s'adsorbent sur les dents. Une autre étude a montré que les protéines dentaires sont capables d'adsorber plus de protéines LB que les minéraux dentaires. Dans cette étude, le premier objectif est d'identifier la protéine dentaire qui montre la plus forte affinité avec les protéines LB. Le deuxième objectif est de conjuguer cette protéine sur les surfaces des appareils percutanés pour augmenter l'adsorption des protéines LB et l'intégration des cellules épithéliales. Pour atteindre le premier objectif, nous avons développé un modèle pour étudier l'interaction entre les protéines dentaires et les protéines LB. Nous avons utilisé Matrigel pour synthétiser des disques de gel de protéines LB. Une solution de protéines dentaires a été ajoutée sur ces disques, puis lavée après 30 minutes pour éliminer les protéines faiblement liées. La protéine de collagène a été identifiée comme la protéine dentaire ayant la plus forte affinité envers les protéines LB. Dans le deuxième objectif, nous avons testé différentes classes d'appareils percutanés, dont l'alliage de titane (Ti-6Al-4V) (utilisé dans les implants dentaires et implants orthopédiques transcutanés) et des polymères tels que le polyétheréthercétone « PEEK » (utilisé dans les implants dentaires et le remplacement osseux). Les protéines de collagène ont été immobilisées de manière covalente sur les surfaces de biomatériau mentionnées. Ensuite, les surfaces modifiées ont été caractérisées par la spectroscopie des photoélectrons X (XPS) pour évaluer la composition chimique et élémentaire, et microscopie à force atomique (AFM) pour évaluer la topographie de surface. Ensuite, nous avons évalué l'adsorption des protéines LB et la croissance des fibroblastes parodontaux humains sur ces surfaces et les avons comparées avec des échantillons non modifiés. Les résultats ont

démontré une conjugaison des protéines de collagène sur des surfaces en titane et PEEK. En outre, il a été constaté que les protéines LB essentielles (en particulier la laminine, le nidogène, et la fibronectine) s'adsorbent davantage sur les surfaces modifiées par le collagène que sur les surfaces non modifiées. Enfin, la viabilité cellulaire était plus élevée sur les surfaces modifiées au collagène que sur les surfaces de contrôle.

Les résultats de ce projet permettent de mieux comprendre comment la nature prévient les infections autour des tissus percutanés. Il fournit également une nouvelle génération de biomatériaux et de surfaces qui peuvent être utilisés pour les appareils percutanés tels que les implants dentaires et les cathéters pour augmenter leur étanchéité et réduire les infections.

Contents

1. Introduction

1.1. Thesis outline

This thesis is written in the traditional monograph style and is divided into 8 chapters. Chapter one includes a brief introduction and the thesis rationale. Chapter two presents a literature review for the thesis work. It starts with the problem of infection in percutaneous devices and major cause of this problem, which is the lack of sealing between the devices and the skin. Then it discusses dental implants and their materials as an example of percutaneous devices since the work of thesis is focused on materials used mainly in dental implants. After that, it presents previous attempts to enhance implant sealing and discusses their limitations. The chapter then moves to explore the biology of the skin, gingival tissue (the specialized skin around the teeth), and the teeth to understand how they interact and produce a strong seal. The chapter concludes with the importance of tooth proteins in producing a strong seal between the teeth and the gingival tissue and the possibility of utilizing these proteins to modify the surface of an implant to produce similar strong seal. Chapter three describes the specific objectives of the work. Chapter four provides the methodology of the experiments and chapter five presents the results. Chapter six provides a discussion of the results while chapter seven is a conclusion of the thesis and chapter eight is the appendix. Finally, chapter nine contains the literature references cited in this thesis.

1.2. Background

Percutaneous devices encompass any device that, temporarily or permanently, penetrate through the skin [1, 2] as shown in Figure 1.1. Examples include dental implants, transcutaneous orthopaedic implants and catheters. Although percutaneous devices are indispensable for patients who need prosthetic limbs, dental implants, catheters or orthopedic implants, recurrent failures or related complications remain significant issues [3-6]. Most of the failure cases can be traced back directly of indirectly to infections.

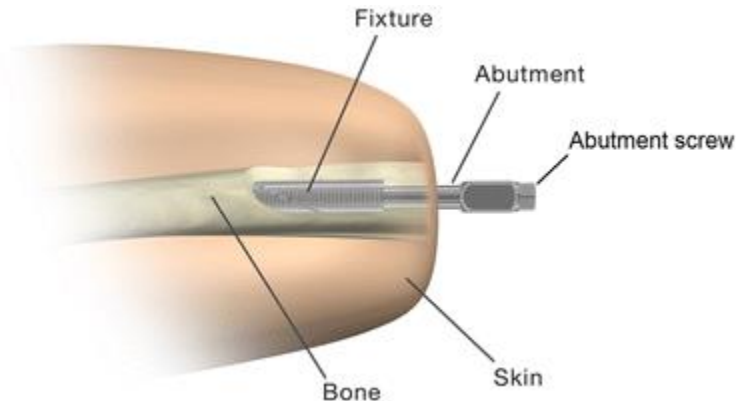

Figure 1.1 shows schematic representation of percutaneous implants. Permission to reprint from [4].

Infections at the implantation site can lead to further complications such as inflammation, swelling and bone resorption (loss of supporting bones), which can lead to having to repeat the implant surgery or implant removal, hence increasing morbidity and healthcare costs [7-9]. For instance, 17% of arm protheses get infected and fail within 5 years of implantation [10]. Moreover, over a million cases of catheter-related infections occurs annually in USA increasing the hospitalization costs by $450 millions. In addition, almost 56% of dental implants develop bacterial mucosal infections which, if not properly treated, can lead to bone resorption and eventually to implant failure and removal [11].

Currently, mild implant infections are treated using antibiotics, which can be effective for such cases [12]. However, antibiotics are not effective against chronic infections because in these cases bacteria develop biofilm that antibiotics cannot eliminate. In addition, antibiotic-resistant bacteria are most likely to develop due to continued use of antibiotics. Eventually, persistent infection can lead to the formation of fibrous tissue and implant failure.

Since antibiotics are not the ideal solution, researchers tried to approach the problem by tackling the original problem which is the lack of strong sealing between percutaneous devices and surrounding skin [13]. Most of the proposed solutions center around concepts such as modifying the surfaces of already known biocompatible materials, creating new composite materials to enhance sealing with soft tissue and developing antibacterial surfaces [14-18].

Despite previous research on improving percutaneous devices, tangible improvements are still limited, mainly due to the lack of complete understanding of the interactions between percutaneous

implants and soft tissues [19]. Many studies showed that protein adsorption is the first step of the body response to foreign materials [19, 20]. This step is critical because the nature of the adsorbed proteins determines the subsequent actions from the body including cell attachment, proliferation and tissue integration [20]. In the case of percutaneous devices, basement membrane proteins (the extracellular matrix (ECM) proteins of the soft tissue of the skin) interact with the device [21]. Therefore, it is necessary to understand the structure and interaction of the basement membrane proteins with soft tissue cells and with percutaneous devices so that these devices can be engineered to induce the desired interactions with the proteins and the cells.

Alongside studying basement membrane structure and function, investigating percutaneous natural analogs such as tooth and nails is important, as well. This is mainly because these organs penetrate and disturb the continuity of the skin, yet they have natural ability to form tight sealing with the surrounding skin (most probably due to their surface properties) [22]. In this work, we will focus on human tooth as an example of natural percutaneous organ with in-depth focus on the interface between the teeth and the gingival tissue.

Teeth are made of two main components, calcium phosphate minerals (mainly hydroxyapatite) and organic components (mainly proteins). Previous research separated the organic and mineral components of the tooth and studied their interactions with basement membrane proteins and the skin cells present in the soft tissue around the tooth, such as periodontal fibroblast and gingival epithelial cells [23]. Results showed that tooth proteins can adsorb more key basement membrane proteins and to promote the growth of fibroblast and epithelial cells compared to tooth minerals. Such results pave the way into further exploration of the role of tooth proteins in mediating the tight sealing between the teeth and the soft tissue in contact with them.

1.3. Thesis rationale

This work explores the interaction between tooth proteins and basement membrane proteins in order to identify key tooth proteins that bind tightly to basement membrane proteins. We will mimic this interaction in vitro by producing a gel substrate of basement membrane proteins and exposing it to liquid solution of tooth proteins then wash away weakly bound tooth proteins and identify only those with high affinity towards basement membrane proteins. The outcomes of this experiment represent a major step in our understanding of how nature produced an incredibly strong sealing between the soft tissue of the skin and natural percutaneous organs. Building on

this, we aim to utilise tooth proteins with high affinity towards basement membrane proteins and attach them to the surface of the implants to improve their soft tissue attachment for the long term.

In summary, this work is an attempt to eliminate infection-induced implant failure by producing biomimetic implants that can have tight attachment and sealing with adjacent soft tissue. Our hypothesis is that attaching to the implant surfaces key tooth proteins that favor adsorption of basement membrane proteins will lead to strong attachment and high proliferation of periodontal epithelial and fibroblast cells of the gingiva.

2. Literature review

2.1. Percutaneous device failure

Percutaneous device failure is still a major hurdle in the advancement of healthcare due to associated health complication and healthcare costs. By understanding what causes the failure, researchers can develop solutions and improve the devices to prevent failure and its complications. Failure can occur due to (1) epidermal marsupialization, (2) permigration, (3) avulsion and (4) infection [1, 24].

In epidermal marsupialization, epidermal cells such as fibroblasts migrate around the implant and surround it creating a pocket-like cavity [1]. Cellular debris and by-products fill the space between the implant and the epidermis and trigger persistent inflammation that eventually leads to device failure as shown in Figure 2.1 a and b. This failure mode is common with smooth, non-porous percutaneous devices. On the other hand, epidermal permigration is common with porous implants in which epidermal cells migrate through the pores (Figure 2.1 c and d)[1]. Although cell migration into the pores represents promising initial step for device integration, the cells lack the ability to develop later stages of connective tissue as dermal and epidermal cells compete with macrophages and other immune cells over the available space, preventing dermal cells from depositing connective tissue, which leads to scar tissue formation. Avulsion is a failure mode where host tissue gets damaged or inflamed due to mechanically induced injury. This can occur because of stresses of the implant on the surrounding tissue at the interface [1]. Infection-related implant failure is the most common and devastating failure mode [24, 25]. In this failure mode, host tissue around the implant gets contaminated by bacteria leading to formation of granulation tissue with large number of acute inflammatory cells. It often occurs due to improper cleaning of the

implantation site or surgical tools or misuse of the device by the patient [7]. Complications of infections vary from mild inflammation to even mortality.

The underlaying cause of most of these failure modes, especially infection, is the lack of proper sealing between the device and the skin [13]. This is mainly due to the inertness of device surfaces and the inability to induce favorable host tissue reactions. Therefore, many previous studies attempted to modify the surface properties of percutaneous devices to induce attachment and integration of host tissue cells and/or to inhibit bacterial adherence and growth. These strategies are detailed in the following section.

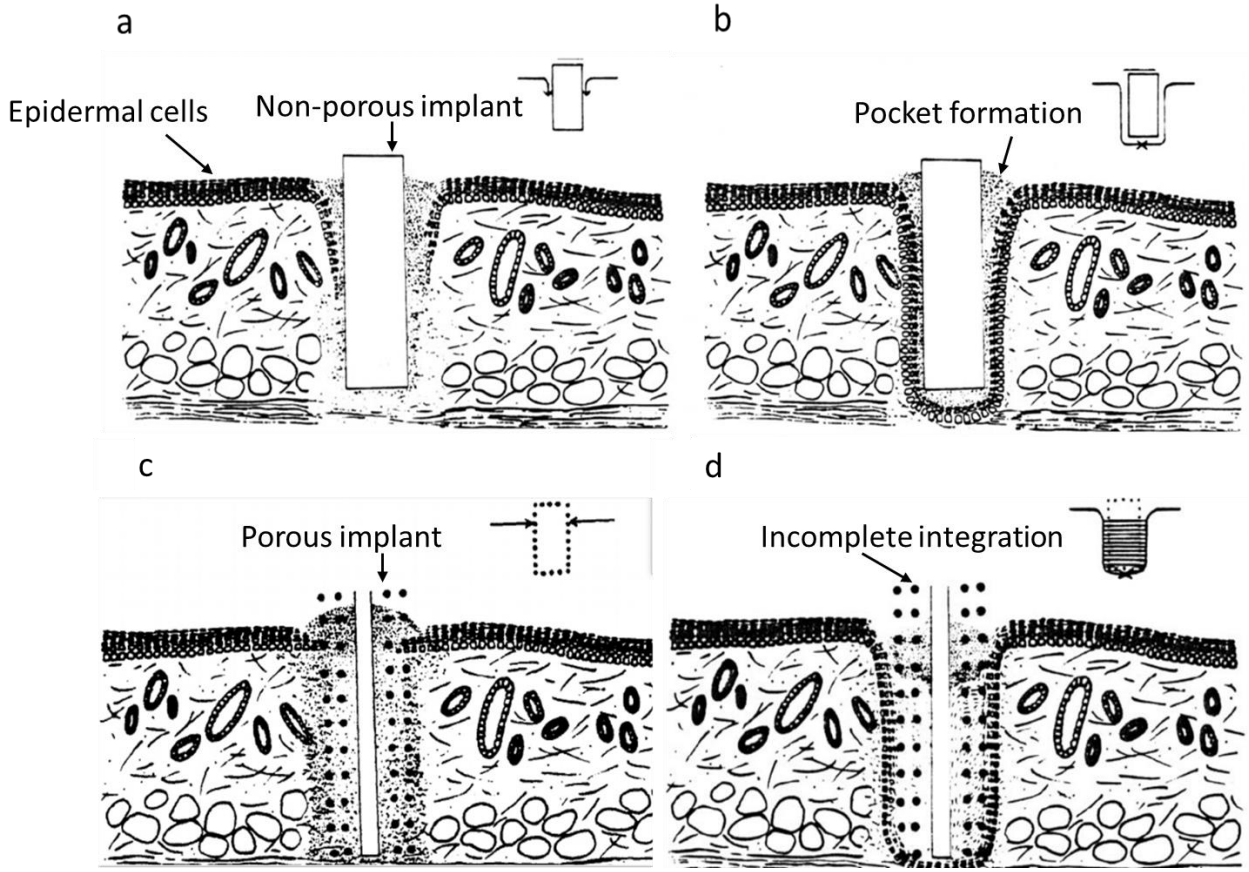

Figure 2.1. A schematic illustration of failure due to epidermal marsupialization and permigration. Parts (a) and (c) show initial reaction of epidermal tissue in marsupialization and permigration, respectively. In (a), cells start to migrate in an apical direction along the percutaneous device while (c) shows infiltration of cells in the pores of the device. Diagrams in the right upper comer illustrate the epidermal cell movement (arrows) in relation to the implant surface. Parts (b) and (d) show the final pocket around the device in marsupialization and permigration, respectively. Permission to reprint from [1]. Copyright (1984) John Wiley and Sons.

2.2. Dental implants as a model of percutaneous devices

Percutaneous devices encompass several types such as dental implants, transcutaneous orthopaedic implants and catheters. Although these types share a common feature of penetrating the skin, they vary in their functions and the materials used to fabricate them. We will focus in this review on a specific type of percutaneous devices which is dental implants.

Throughout history, humans have tried to replace their missing teeth with various materials from their surrounding such as metals, polymers, alloys or even glass [26]. Those materials that replace missing teeth are called dental implants. Nowadays, dental implants are composed of three parts which are not necessarily from the same material. These parts are: (1) the screw, which replaces

the root and fixes the implant into the bones; (2) the crown, which is the top visible part, and (3) the abutment, which connects the two parts together [27]. Figure 2.2 depicts a schematic of different parts of implants.

With the advancement of healthcare, different parameters are used to evaluate the efficiency of a certain material to be used as a dental implant. These parameters are osteointegration, mechanical properties, aesthetic appearance, and soft tissue integration [7, 25, 28]. Osteointegration is the tight connection between implant and bones at the microscopic level. Mechanical properties of the implant need to be within the range of the surrounding cortical and trabecular bones. These mechanical properties include modulus of elasticity, tensile strength, hardness and toughness [29]. For instance, implants should be stiff enough to withstand stresses, but not stiffer than surrounding bones to prevent stress shielding from the bones which leads to bone resorption. Biocompatibility ensures the safety of the implant and that the implant will not initiate adverse reactions to due unfavoured interactions with host tissues [29]. Soft tissue integration refers to the ability of the implant material to induce adhesion of the soft tissue on the implant surface and seal it from outer environment [13]. Aesthetic appearance is a crucial parameter for the material of the visible part of the implant. It is preferable that the visible part of the implant has a similar color and shade to the surrounding teeth [30].

Mechanical properties are affected by bulk properties of the material. On the other hand, osteointegration, soft tissue integration and aesthetic appearance are affected by material surface more than the bulk [31]. Therefore, surface chemistry, composition and morphology are crucial surface properties that need to be optimized to achieve desirable functions. Another important observation is that different parameters are desired for different parts of the implant. For, instance, osteointegration is required for the root while soft tissue integration is required in the middle and top part [32].

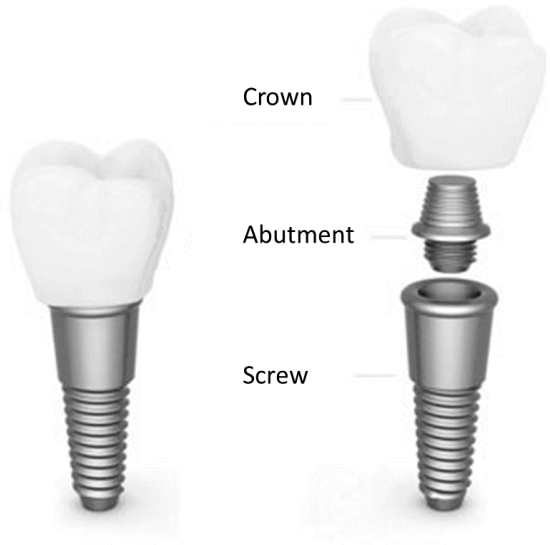

Figure 2.2. A schematic illustration of the three main dental implant parts (i.e. crown, abutment and screw). Adapted from: https://www.irvinedds.com/dental-implants.html.

The standard materials for dental implants are titanium and titanium alloys. However, ceramics such as zirconia are used as well especially for abutment and crown [33]. Moreover, recently several polymers have been explored as alternatives for metals and ceramics because of the ease of modifying their composition to obtain certain physical properties. Some polymers are esthetically pleasing due to having similar color to the teeth [34]. Polyetheretherketone (PEEK) is one of the polymers that has been increasingly used for orthopaedic implants [34]. In the discussion below, we will compare the use of titanium and PEEK as dental implants materials focusing on properties of each material, advantages, disadvantages and improvement strategies. We chose these two materials because they are the subject of the work in this thesis.

2.2.1. Titanium

Titanium is the most common material used for dental implants. It is mostly used to replace the roots of the teeth while ceramic and polymeric materials are used to replace the crown [26]. Commercially pure titanium (cpTi) has four grades that differ according to the content of oxygen and iron; grade 1 has the lowest oxygen and iron content while grade 4 has the highest content of both elements. Iron is added to titanium for corrosion resistance. This variation is reflected in the mechanical properties where the tensile strength gradually increases from grade 1 to grade 4. Titanium alloys are commonly used for dental implants as well. One example of these alloys is Ti-6Al-4V which contains 6% aluminum and 4% vanadium [35, 36].

Advantages of using titanium for dental implants are numerous. For instance, titanium and its alloys possess an interesting combination of high strength and low density. Moreover, sterilization of metals is easy using many of the readily available techniques.

One of the disadvantages of titanium is its gray color, which makes it not aesthetically pleasing when it is in the abutment or the crown of the implant. Moreover, the mismatch in mechanical properties between titanium and bone could create strains and/or stress shielding from the bones that would prevent normal bone remodelling. Table 2.1 shows a comparison of Young's modulus of elasticity of human bone and titanium. The resemblance of modulus of elasticity between PEEK and bones makes it a promising substitute to titanium. The following section discusses other properties of PEEK and its potential use as dental implant material.

Table 2.1. The Young's modulus of human bones and some of the materials used as dental implants.

Material	Young's Modulus (GPa)*
Human Cortical Bone	11.5 – 17.0 [37]
Human Trabecular Bone	0.3 – 3.2 [37]
Titanium	102 -114 [26, 38, 39]
Ti-6Al-4V	113 [26]

Several studies have investigated enhancing titanium implant osteointegration and soft tissue integration. The focus of these studies is to control and optimize surface properties of titanium including topography, roughness, wettability, composition and thickness of the oxide film [33]. Many studies concluded that rougher surfaces promote osteoblast cell adhesion more than smooth surfaces [40]. Moreover, promoting bone formation was achieved by changing surface composition through coating the implant with inorganic components (i.e. hydroxyapatite) or organic phase (e.g. proteins, amino acid sequences and growth factors) [41]. It was shown that hydroxyapatite coating induced more bone contact to the implants, enhanced the fixation of the implants and effectively filled the small gaps between implants and surrounding bones [42-44]. However, the long-term stability of the coating showed dependence on the initial bonding between the implant and the coated layer. Therefore, more studies should be directed into fabricating long-term stable coating to avoid implant failure at later stages. In conclusion, titanium and its alloy are

the current gold standard for implants however, in parallel with trying to improve their properties, other materials are explored as alternatives; one of these materials is Polyetheretherketone.

2.2.2. Polyetheretherketone (PEEK)

PEEK a semi-crystalline thermoplastic polymer which belongs to a family of polymers called poly(aryletherketones) (PAEKs). PAEKs share a common structural feature of having an aromatic backbone chain connected by ether and ketone functional groups. Some of the common properties of this group are the thermal stability, the resistance to chemicals and the biocompatibility. Figure 2.3 depicts the structure of PEEK as a member of PAEK family.

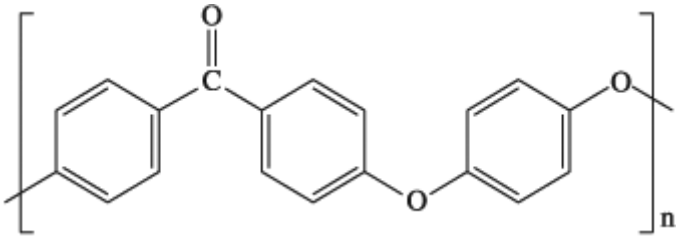

Figure 2.3. The chemical structure of PEEK polymer.

Nowadays, the use of PEEK in orthopedic and spinal implants is widely accepted [45]. It has been used as a replacement for titanium for several reasons; mainly due to its matching stiffness to bones and its radiolucency. PEEK is also used already in the market as implant abutment and as implant fixture [46]. It has also been investigated as a full dental implant material to replace titanium because PEEK has superior qualities such as similar mechanical properties to bones including fatigue strength, wear resistance, tensile strength, and ductility [47]. Young's modulus of PEEK polymer is in the range of 3-4 GPa which is close to that of cortical and tabucular bones [38]. Other advantages are theraml stability, corrosion resistance and biocompatibility [48]. Thermal stability of PEEK is desirable for overcoming the degradation by the heat during sterilization process: with a melting temperature of about 343 °C, PEEK can be easily sterilized by gamma radiation [49]. Chemical resistance of PEEK is another advantage as PEEK does not release toxic by-products like metallic implants. Lastly, PEEK provides aesthetic advantages over metallic implants due to similar appearance to teeth [49].

Despite all of the mentioned advantages, PEEK has some disadvantages such as lack of adhesion to living tissues and adverse immunologic reactions. This is attributed to PEEK bio-inertness not

supporting bone on-growth or soft tissue adhesion [49]. For instance, in an in-vivo study, CFR-PEEK, which is PEEK reinforced with carbon, was coated with titanium and compared with uncoated samples [50]. Both titanium coated and uncoated CFR-PEEK were implanted in dogs and evaluated after 4 and 8 months. The titanium coated samples showed significantly higher bone-implant contact (BIC) than uncoated samples. To overcome bio-inertness of PEEK, it is incorporated in composites containing bone-binding materials, such as hydroxyapatite (HA) [49]. Using a brittle material such as HA compromises the overall mechanical properties of PEEK [48].

Another method to overcome PEEK bio-inertness is surface modification. This method only alters the surface properties and not the bulk and therefore does not affect the mechanical properties of the material. Surface modification can be achieved through (1) changing surface morphology or (2) coating implant surface. Many studies show that surface morphology with rougher surface (Ra ranging from 0.9 to 3.8 μm) increases bone integration [51]. The combination of roughness and functional groups such as phosphonate groups enhanced bone integration and decreased fibrous tissue formation [52, 53]. Another method is implant coating with biomolecules that promote interaction with bones to achieve osteointegration such as proteins and peptides. For instance, bone morphogenic proteins (BMP) are growth factors well-known for improving bone formation [54-56]. Adsorption of BMP-2 alone did not improve MC3T3-E1 cells adhesion while creating a nano porous titanium oxide layer on PEEK surface then depositing BMP-2 cell adhesion in-vitro and bone-implant contact in-vivo in a rabbit model [57]. Covalent attachment of BMP-2 on PEEK with collagen intermediate greatly increased osteogenic differentiation and bone growth around PEEK [58]. These studies showed that introducing biomolecules such as BMPs on the surface of PEEK improves the osteointegration of the implants. Despite of these efforts, limited clinical trials have been done using PEEK as dental implant, therefore, it is still early for PEEK to compete with titanium as a dental implant material. All these modifications mostly aim to improve the osteointegration of the implants without focus on soft tissue integration. Therefore, next section provides a summary of studies that tried to investigate the structural-function relationship to achieve a desirable soft tissue integration.

2.3. Previous approaches to improve soft tissue integration of implants

Several studies have been conducted to improve the integration of percutaneous implant with the surrounding soft tissues. Such integration aims to establish a barrier against bacterial invasion at the interface between the implants and the soft tissues. Table 2.2 provides a summary of previous

studies that were conducted to achieve this integration. The table compares (1) the types of materials used in the studies, (2) the modifications that were done on these materials to improve their integration, (3) the models used to test their hypotheses, and (4) the main findings of the studies.

Titanium and its alloys are the main materials used in studies mentioned in the table. This is because titanium is the most widely used material in percutaneous implants (orthopedic and dental). Some studies were done on polymeric materials including PEEK, polyhydroxymethylmethacrylate (PHEMA), polymethylmethacrylate (PMMA), polydimethylsiloxane (PDMS), and polystyrene (PS). While PEEK (as mentioned in section 2.2) is used in orthopedic and dental implants, the other polymers are mostly used in catheters.

We classified the approaches used in these studies into engineering approaches, biological approaches and hybrids of the two. Engineering approaches include changes in device structure, topography and surface modifications. In general, there are inconsistencies in the reported results regarding the effect of engineering approaches, especially surface topography, on the attachment of the device to the connective tissues. Biological approaches include protein coating or incorporation of antimicrobial agents. Proteins such as collagen I, laminins and fibronectin were coated on or covalently bound to percutaneous devices [59-61]. Many studies report findings suggesting that biological approaches improve cell attachment to percutaneous device in in-vitro models [61-64]. Hybrid approaches are combinations of engineering and biological approaches. There is no particular indication that hybrid approaches achieve superior outcomes compared to either engineering or biological approaches.

In-vitro and in-vivo models were used to test the effect of materials modification on improving soft tissue integration. As shown in Table 2.2, there is no standardized protocols for cell types used in in-vitro testing, animal models, implantation sites and device design, which complicates comparing the findings and drawing definitive conclusions.

The slow progress in obtaining true integration between the devices and the host tissue is due to lack of understanding of the phenomena occurring in the host tissue at the interface with the device at the implantation site. The initial reaction of the body after implantation is protein adsorption on the device. The nature, quantity and conformation of the adsorbed proteins influence subsequent cell adhesion, proliferation and in some cases differentiation. Therefore, it is crucial to understand

the nature and interactions of the proteins in the soft tissue in contact with percutaneous devices if we want to design a device surface that can fully integrate with the host tissue. The following chapters discuss structure and function of the skin and its ECM proteins and their interaction with teeth as a model of natural percutaneous organs that disrupt skin continuity while maintaining a tight seal with it.

Table 2.2. Major previous work on improving the integration between percutaneous devices and soft tissue. Hydroxyapatite (HA), carbon fiber reinforced PEEK (CFRPEEK).

Material	**Approach/ specific modification**	**Results/conclusion**	**Model**	**Reference**
Ti	Engineering /Changing surface topography	Rougher surfaces with Ra around 5 µm or more and acid-itched surfaces have better connective tissue attachment than smooth surfaces.	In-vivo model on rats with a checkpoint after 11 weeks.	[17]
Ti	Engineering/Changing surface topography	Surfaces with pore size of 15 and 30 µm promoted cell growth and cell morphology similar to natural tissue.	In-vitro cell culture using gingival fibroblasts.	[65]
Ti	Engineering/Changing surface topography	Nanotextured Ti promoted cell adhesion and proliferation.	In-vitro cell culture using keratinocytes.	[2]
TiO_2	Engineering/Changing surface topography	TiO_2 nanotubes promoted fibroblasts proliferation, adhesion and morphology but not keratinocytes.	In-vitro cell culture using keratinocytes and dermal fibroblast cells.	[66]
Ti	Engineering/Changing surface topography	Smooth implants showed 7-fold higher bacterial	In-vivo model of New Zealand	[5]

		infection than porous ones.	white rabbits with checkpoint after 4 weeks.	
Ti	Engineering/Changing surface topography	Porous Ti (roughness was 113 μm) prevented infection in 100% of the animals after 9 months, while 25% of smooth Ti implants were infected.	In-vivo model using sheep with a 9-months checkpoint.	[67]
Ti	Engineering/Changing surface topography	There was no statistically significant prevention of infection between smooth and porous percutaneous devices	In-vivo model of rabbits for 24 months period.	[68]
Ti	Engineering/Changing surface topography	Nanoporous surfaces showed higher fibrous ingrowth compared to larger porous implants	In-vivo model of rats with checkpoints of 3-6 weeks.	[69]
Ti	Engineering/Changing surface composition	Fluorinated hydroxyapatite coated implants showed antibacterial activity compared to pristine Ti.	In-vitro antibacterial assays	[70]
Ti	Engineering/Changing surface composition and topography	Ti with TiO_2 nanotubes of 100 nm diameter showed less inflammation and better tissue integration compared to smooth Ti.	In-vivo model using rabbits with a checkpoint of 8 weeks.	[71]
Ti	Engineering/Changing surface composition	Implants coated with HA showed no signs of	In-vivo model using sheep with	[72]

		inflammation. Moreover, HA-coated implants showed more dermal adherence compared to control.	a checkpoint after 4 weeks.	
Ti	Engineering/Changing surface composition	Implants were coated with dimethyl (2-methacryloyloxy-ethyl) phosphonate and 4-vinylpyridine and they showed lower deep tissue infection compared to uncoated implants.	Results are obtained using mice with a checkpoint after 168 days.	[16]
Ti	Engineering/Changing surface composition	Ti coated with TiO_2 with 0.67 wt% Cu showed significant enhancement of fibroblast cell adhesion and proliferation.	In-vitro cell culture using fibroblast cells.	[73]
Ti	Engineering/ Changing surface composition	Titanium coated with PDMS improved cell proliferation and adhesion.	In-vitro cell culture using human dermal fibroblasts.	[74]
PS	Engineering/Changing surface topography	Dentin-like textured surface enhanced ECM deposition of gingival fibroblast. However, proliferation was the same for test and smooth surfaces.	In-vitro cell culture using fibroblast cells.	[75]

Epoxy	Engineering/Changing surface topography	Hexagonal pores (84 µm) showed higher epithelial cell adhesion compared to smooth surface.	In-vitro cell culture using periodontal ligament epithelial cells.	[76]
Porous PHEMA	Engineering/ Changing surface topography & composition	PHEMA samples were modified with spherical pores with diameters of 20, 40, 60 µm. Keratinocyte migration distances were longer in samples with 40, 60 µm compared to 20 µm. Modifying the surface with carbonyldiimidazole didn't affect cells migration.	In-vivo model using mice with checkpoints after 3-14 days.	[77]
PMMA	Engineering/ Changing surface composition	PMMA functionalized with animo groups promoted human gingival epithelial cell proliferation and adhesion.	In vitro cell culture using primary human gingival epithelial cells	[78]
PEEK/Ti /zirconia	No change	No statistically significant differences were found of the viability, morphology, proliferation of human gingival epithelial among the 3 materials.	In vitro cell culture using primary human gingival epithelial cells	[79]

PEEK/Ti	Engineering/ Changing surface topography	Rough PEEK, pristine PEEK, and Ti showed similar soft tissue location in relation to implants.	In-vivo model using Labrador dogs with checkpoint after 4 months.	[80]
PEEK	Engineering/ Changing surface topography	Acid-etched microporous PEEK with macropores of 1.5 mm diameter promoted the close integration of soft tissue and without fibrous capsule formation.	In-vivo model using New Zealand white rabbit with checkpoint after 4 weeks.	[81]
CFR-PEEK	Engineering/ Changing surface topography & composition	Coating CFR-PEEK with TiO2 nanostructure improved adhesion, migration, proliferation, and collagen secretion ability of human gingival fibroblasts.	In-vitro cell culture using of human gingival fibroblast cells.	[82]
Ti	Biological/ Protein conjugation	Conjugating fibronectin to titanium increased fibroblast adhesion and vinculin focal contact.	In-vitro cell culture using fibroblast cells.	[59]
Ti	Biological/ Protein conjugation	Conjugating fibronectin to titanium increased cell alignment, hence, enhancing dermal attachment.	Fibroblast cells and in-vivo model using sheep were used.	[62]
Ti	Biological/ Protein conjugation	Conjugating laminin 332 to titanium increased keratinocytes adhesion	In-vitro cell culture using	[63]

		plaques 20 folds compared to untreated samples.	keratinocyte cells.	
Ti	Biological/ Protein conjugation	Adsorption of E-cadherin on Ti showed higher attachment and cell area compared to pristine Ti.	In-vitro cell culture using murine keratinocyte cells.	[83]
Ti	Biological/ Protein coating	Coating Ti with collagen I increased cell proliferation and gene expression of cell adhesion markers compared to uncoated Ti.	In-vitro cell culture using human gingival fibroblasts.	[61]
Ti	Biological/ Protein coating	Ti was treated with polydopamine then with collagen I. Treatment increased cell proliferation and adhesion compared to uncoated Ti.	In-vitro cell culture using human foreskin fibroblasts and human immortal keratinocytes.	[64]
Ti	Biological/ protein coating	Ti - coated with laminin and ameloblastin – improved cell proliferation and hemidesmosome formation compared to uncoated Ti.	In-vitro cell culture using human keratinocytes.	[84]
Ti	Biological/ Protein coating	Ti was coated with chitosan-collagen matrix incorporating a plasmid	In-vitro cell culture using human gingival	[85]

		coding for C-terminal globular domain of LMMA3 protein. Coated samples improved cell adhesion in-vitro and in-vivo.	epithelial cells and in-vivo using rat model.	
Ti	Biological/ Polymer coating	Polydopamine coated Ti showed higher cell proliferation, adhesion and collagen secretion compared to uncoated Ti.	In-vitro cell culture using human gingival fibroblasts.	[86]
Ti	Hybrid/ Changing surface composition & protein coating	Fibronectin/HA coated Ti increased the strength of cell attachment 7 folds compared to uncoated Ti after 24 hours of incubation	In-vitro model of fibroblast cells was used.	[87]
Ti	Hybrid/ Changing surface topography, composition & protein coating	Porous Ti coated with fibronectin functionalized HA and silver (PT-HAAgFn) did not improve soft-tissue integration compared with uncoated porous Ti (PT). However, PT improved soft tissue integration compared to uncoated non-porous Ti (C).	In-vivo model using sheep model with a checkpoint of 4 weeks after implantation.	[88]

Porous poly HEMA	Hybrid/ Changing surface composition & protein coating	PHEMA were modified with carbonyl diimidazole (CDI) and CDI with laminin 332. None of modified and control samples showed signs of infection. Blood vessels growth and collagen bundle formation were observed in all of the implants, as well.	In-vivo model using mice with checkpoints of 7-28 days.	[89]
Polyethylene-vinyl alcohol	Hybrid/ Changing surface composition/ protein coating	Polymer was coated with HA or HA-laminin. The coating improved the adhesion strength (tensile strength) with the surrounding tissue.	In-vivo model using rats with checkpoint after 14 days of implantation.	[90]
Ti	Hybrid/ Changing surface topography/ protein coating	Smooth Ti functionalized with collagen I showed higher cell adhesion and proliferation compared to rougher unfunctionalized Ti.	In-vitro cell culture using human dermal fibroblasts.	[91]
Ti	Hybrid/ surface topography and protein coating	Ti samples with grooves of 0.1-0.2 µm were coated with keratin fibers. The modified samples increased cell proliferation compared to unmodified Ti.	In-vitro cell culture using human gingival fibroblasts.	[92]

2.4. Skin and its basement membrane

2.4.1. Skin structure

Skin is the largest organ of the human body as it accounts for 8% of the total body mass. It acts as the body's first line of defense against external environment and harmful agents [93]. Anatomically, skin consists of three distinctive layers named epidermis, dermis and the subcutaneous layer (hypodermis) [93, 94]. The skin contains other appendages such as hair and sweat glands as depicted in Figure 2.4. Each layer comprises specific types of cells that provide different physiological roles specific to the layer.

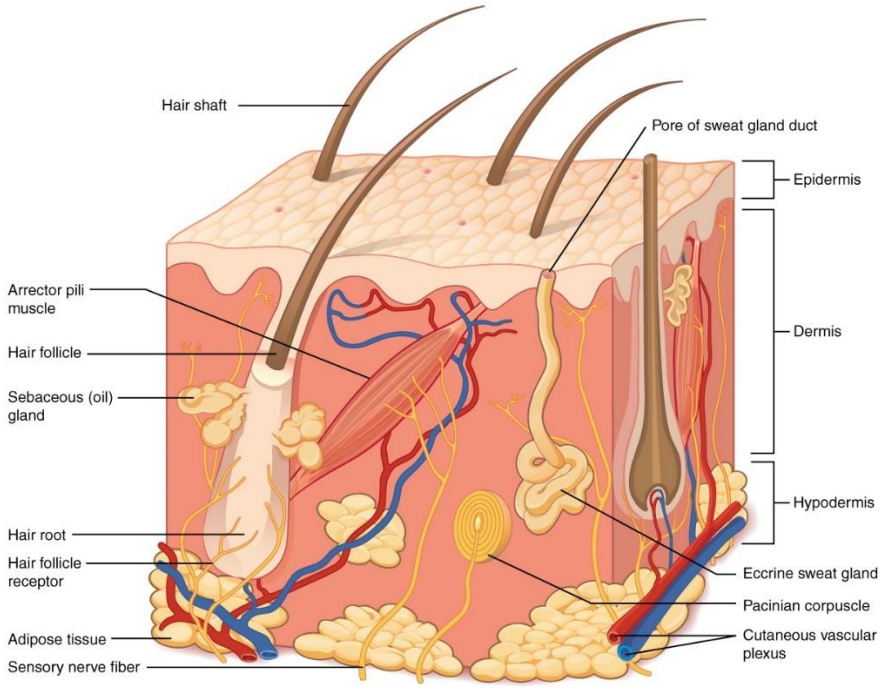

Figure 2.4. Main structure of the skin. Adapted from: https://opentextbc.ca/anatomyandphysiology/

The outermost layer of the skin is the epidermis, which is mainly composed of epithelial cells (keratinocytes) [93]. It is a thin layer with a thickness of 0.1 mm [95]. Keratinocytes provide an impermeable barrier against the outer environment due to the proximity of the cells to each other. Keratinocytes are connected through thickened parts of plasma membrane called desmosomes that contribute to their tight connection and their impermeability [94]. The epidermis is divided into 4 sub-layers depending on the differentiation of keratinocytes in each layer [95]. These layers are (from dermis outwards) basale, spinosum, granulosum and corneum, as shown in Figure 2.5. A fifth

layer is observed in regions with thicker epidermis; this layer is called lucidum. The basal layer is mainly composed of actively dividing cuboidal or columnar keratinocytes. It contains number of stem cells and melanocytes, as well. The spinosum layer is formed as a result of the newly divided keratinocytes which migrated upwards. Cells in this layer are oval to polygonal-shaped. Melanocytes can reside in this layer, as well. The stratum granulosum lays on top of spinosum and contains more flattened, more keratinized non-nucleated cells as the layer moves outwards. The outer-most layer is the corneum, which consists of non-viable very packed cells filled with keratin.

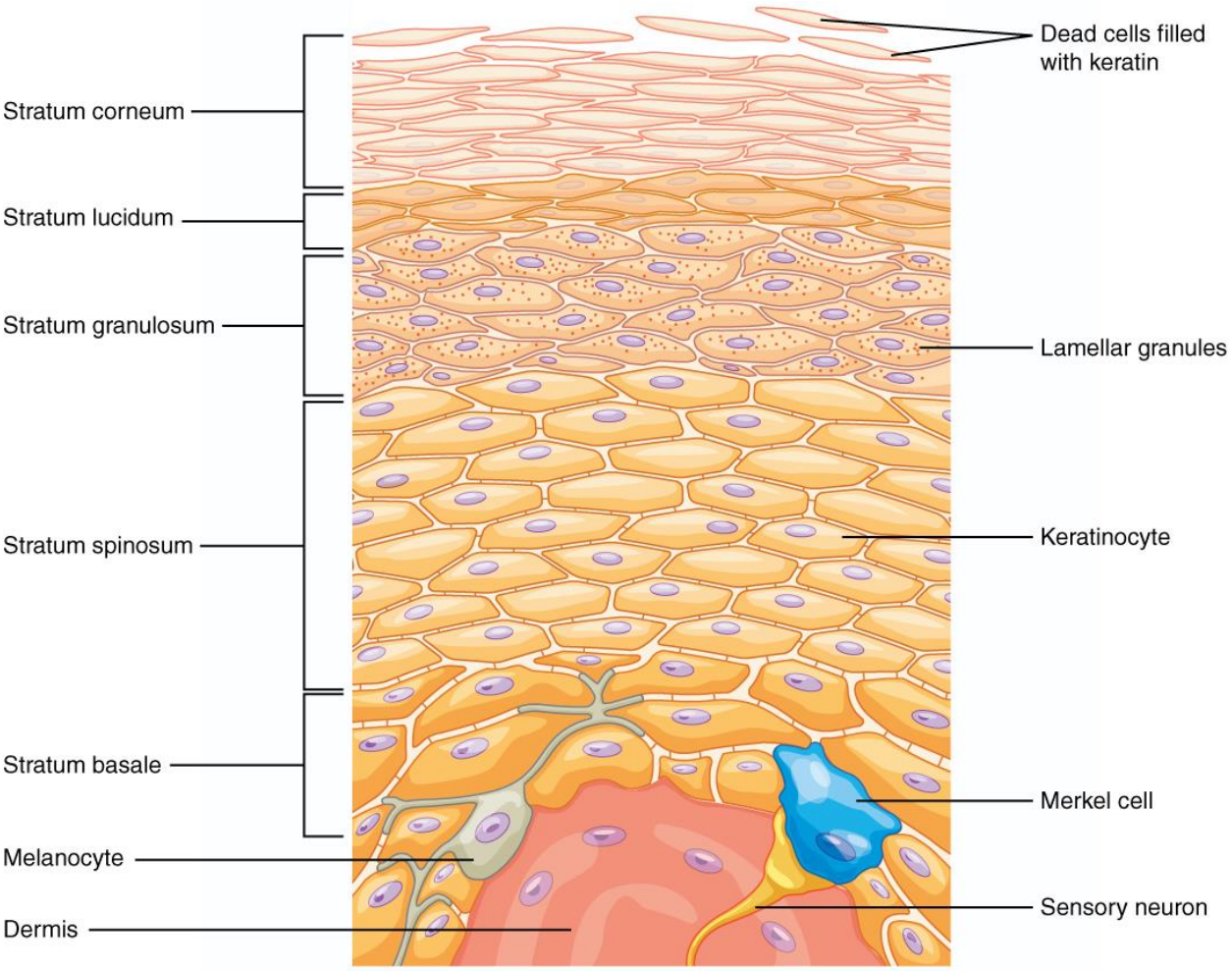

Figure 2.5. Schematic if the sub-layers of the epidermis. Adapted from: https://opentextbc.ca/anatomyandphysiology/

The dermis is the fibrous middle layer of the skin. It is much thicker than the epidermis with a thickness ranging from 0.6 to 3 mm, depending on the region of the skin; it is mostly composed of ECM that is synthesized by fibroblast cells. [95]. It mainly functions as an absorber of the stress

and strain applied on the skin due to its fibrous nature [93, 96]. The dermis includes other types of cells such as histiocytes, mast cells and dermal dendritic cells that are involved in immune responses[94].

The hypodermis is a layer below the dermis, and it serves a connection between the dermis the underlying bone or muscle tissue [95]. It consists of highly vascularized connective tissue and adipose tissue, which functions as fat storage and provides insulation for inner organs.

2.4.2. Structure of basement membrane

The epidermis and the dermis are separated by a layer of specialized ECM called basement membrane [97, 98]. The functions of the basement membrane are numerous including its role in maintaining the integrity of the skin by binding epidermis and dermis together and its crucial role as a substrate for keratinocytes (and other epithelial cell types) adhesion and migration, especially during wound healing [97]. Basement membrane is divided into three layers: lamina lucida, lamina densa and lamina reticularis or sub-basal lamina (Figure 2.6). Lamina lucida and lamina densa are collectively known as basal lamina (BL) [98, 99]. Molecular biology provides further details on the structure and interactions of basement membrane components.

The epithelial cell layer is connected to lamina lucida proteins through thickened plasma membrane structures called hemidesmosomes [100]. The lamina lucida resides below epithelial cells. It is a layer of 20-40 nm thickness rich in laminin glycoproteins such as laminin 332 and laminin 331[101]. These proteins interact with integrin transmembrane proteins of epithelial cells. Lamina densa is the adjacent layer to lamina lucida. It is mainly composed of collagen IV proteins, laminins glycoproteins, nidogen and perlecan proteoglycan [101]. It serves as a linkage between lamina lucida protein filaments and anchorage fibrils originating from the dermis. Lamina reticularis or sub-basal lamina is the last layer of the basement membrane [101]. It has a thickness of 20-60 nm, is mainly composed of collagen VII and function as link between lamina densa and the dermis.

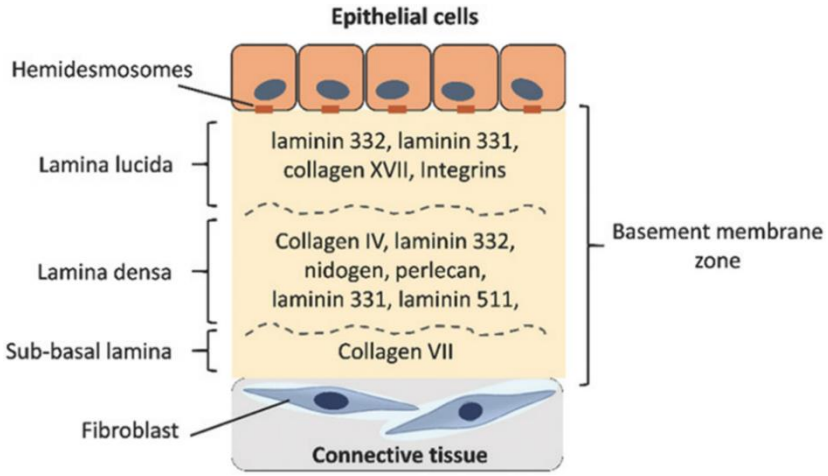

Figure 2.6. Schematic representation of basement membrane molecular structure. Permission to reprint from [13].

2.4.3. Proteins of the basement membrane

The main basement membrane proteins are laminins with different isoforms, collagen IV, nidogen and perlecan [97, 101]. Such proteins interact with each other to maintain the function of the basement membrane. The structure of each protein and their interactions with each other are detailed below.

Laminins

Laminins are a family of glycoproteins composed of three distinctive (heterotrimeric) chains (α, β, γ) assembled in a fork shape [97, 98, 102]. The 3 chains form the unbranched part of the protein coiled up in a helical shape called coiled coil [103]. In this part, the chains are linked together by disulfide bonds [102]. At the branching point, the chains disassemble into distinct branches. The α chain is almost double the size (weight) of β and γ chains because it contains an extra globular-like domain (G-domain) that contains sites of interaction between laminin and cellular receptors such as integrin [98]. The laminin family encompasses at least 15 isoforms found in different body tissues such as skin, kidneys, muscles, lung and vasculature [103]. These isoforms are synthesized from different combinations of 5α, 3β and 2γ chains identified in the vertebrates. The laminin nomenclature uses three numbers representing the numbers of the three chains forming the isoform

[103]. For instance, laminin 332 is composed of α3, β3 and γ2 chains. The schematic of laminin 111 is shown in Figure 2.7.

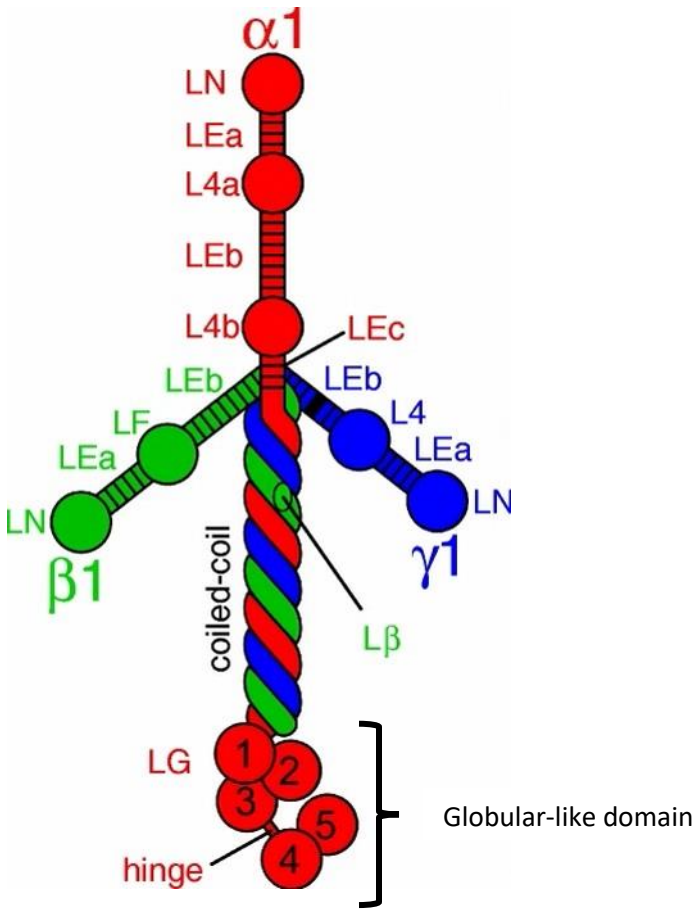

Figure 2.7. Schematic representation of the structure of laminin 111 (one of laminin isoforms) with the different domains on its three polypeptide chains. Permission to reprint from [67].

Laminin 332 is an important isoform as it exists in almost all basement membranes of epithelial tissues. Various domains of laminin 332 are involved in interactions with other molecules. For instance, its β chain has binding sites for laminin 311 and collagen VII [103]. Moreover, the γ chain has binding sites for perlecan, collagen IV and nidogen. In addition, α chain has the crucial role in mediating the binding to α6β4 integrin receptors in epithelial cells [103]. Besides interactions with other basement membrane proteins, laminins interact with each other to form an extended honey-comb like networks as shown in Figure 2.8 [104].

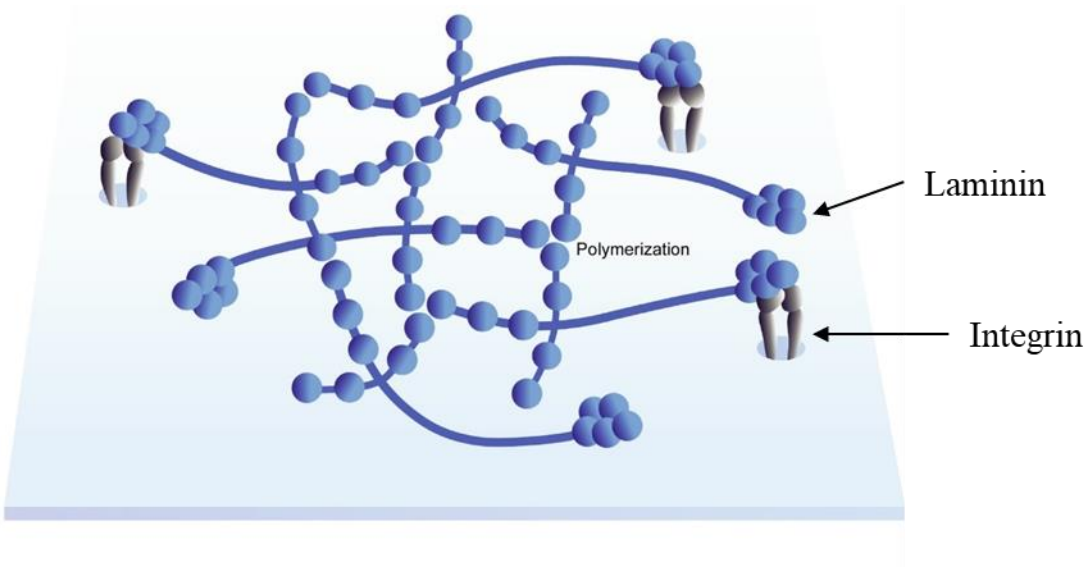

Figure 2.8. Laminin network formation in the basement membrane through interaction between adhesive domains. Reprinted with permission from [97]. Copyright (2018) Academic Press.

Collagen IV

Collagen is the most abundant fibrous protein in the extracellular matrix. There are 16 isoforms of collagen in the body however, this section will focus on collagen type IV because of its abundance and crucial role in the basement membrane [105].

Collagen IV is composed of 3 polypeptide chains that are self-assembled into a triple-helical structure [98]. As shown in Figure 2.9 A, each chain contains 3 domains: a 7S amino-terminal domain, a triple helical collagenous domain and a non-collagenous carboxylic-terminal domain (NC1) [105]. Similar to laminins, collagen IV in the basement membrane can assemble into a network formed by tetramers of collagen IV, which interacts with each other via the 7S amino-terminal domain, and dimers which interact via the non-collagenous carboxylic terminal domain and lateral interactions as shown in Figure 2.9 B [104, 106]. In addition, collagen IV interacts with the laminin network, with other molecules and with epithelial cell surface receptors [107].

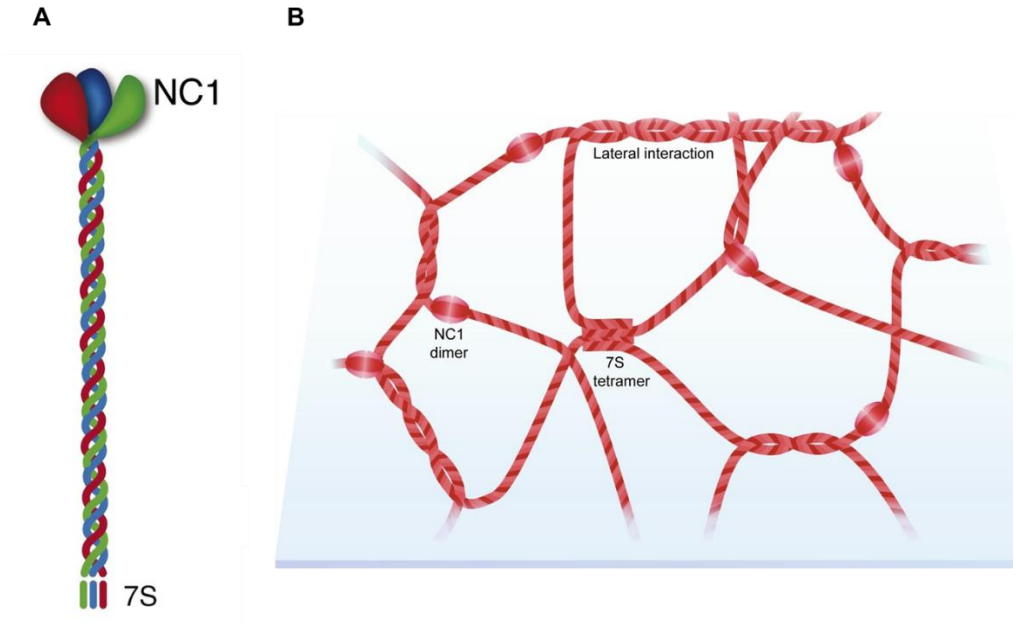

Figure 2.9. (A) A schematic representation of collagen IV structure and (B) a network of collagen IV in basement membrane. Permission to reprint from [97, 108].

Nidogen

Nidogen is another glycoprotein found in the basement membrane. It mainly serves as a linkage between collagen IV and laminins providing stability to the basement membrane structure [97, 109]. Nidogen has two isoforms with a similar structure consisting of 3 globular domains named G1, G2 and G3 with 2 rod-like structures connecting them as shown in Figure 2.10 [98]. Nidogen's G3 domain binds to the γ1 domain of laminins in one of the interactions with the highest affinity in nature [110], while the G2 domain binds to collagen IV. One interesting finding is that nidogen is produced during fetal development by mesenchymal cells and fibroblast cells, and not by epithelial cells [111]. This sheds some light on the role of various cell types in the formation of the basement membrane.

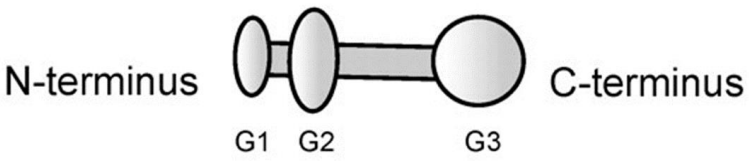

Figure 2.10. A schematic illustration of nidogen molecule. Permission to reprint from [112].

Perlecan

Perlecan – a heparan-sulfate proteoglycan - is another molecule that serves as a linker between laminin and collagen type IV networks [97]. Perlecan binds to basement membrane proteins and glycoproteins, epithelial cell surface receptors and growth factors that are crucial for epithelial cell survival. Perlecan contains 5 distinct domains (domain I-V) connected to each other by a core protein (Figure 2.11)[98]. The first amino-terminal domain (domain I) is linked to 3 glycosaminoglycan chains shown in red in (Figure 2.11). The core protein has binding sites for nidogen's G2 domain and for collagen IV. The glycosaminoglycan chains bind to the non-collagenous domain of collagen IV and the laminin α chain. Other interactions of perlecan domains with other macromolecules are shown in Figure 2.11.

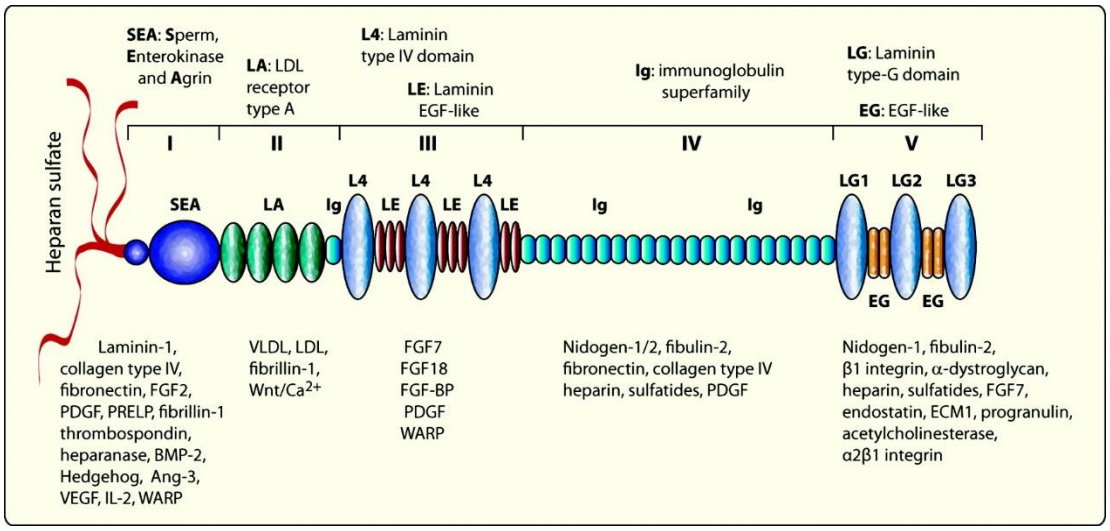

Figure 2.11. A schematic illustration of perlecan molecule with different domains with the respective molecules that interact with each domain. Permission to reprint from [113].

Other proteins have been identified in lower amounts in basement membranes [97]. In fact, a total of 40 basement membrane proteins have been identified in all body tissues or even tumors. Each basement membrane has a specific number and ratios of proteins that fits its functions. Figure 2.12 shows a simplified schematic representation of the complex interactions of the core basement membrane proteins.

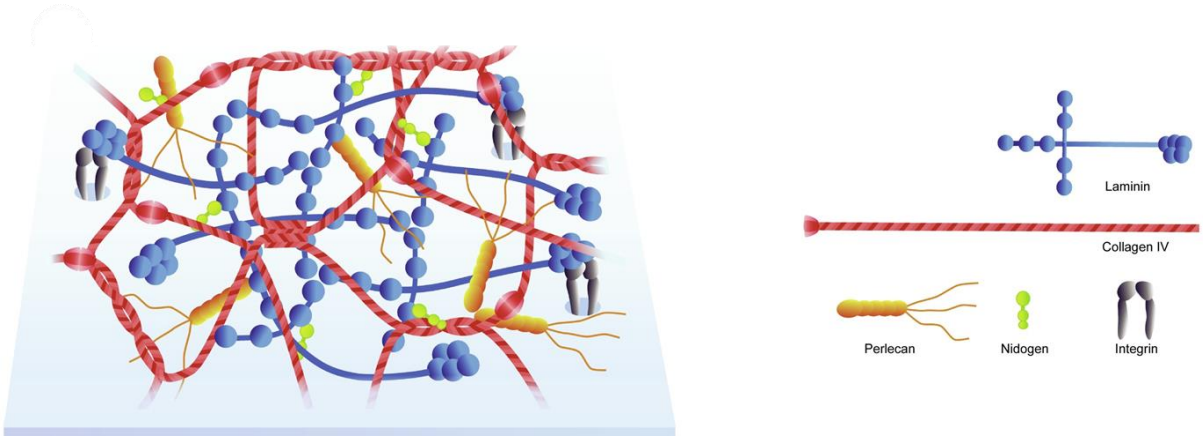

Figure 2.12. A schematic representation of the complex interactions of the core basement membrane proteins. Permission to reprint from [97].

2.5. Periodontal tissue structure and function

2.5.1. General structure of periodontal tissue

The skin structure – as discussed in the previous section - is interrupted by certain organs such as nails and teeth [13]. The interface between the skin and these organs could be an entry way for infective agents; however, these interfaces are surprisingly impermeable to bacteria and harmful agents. This is due to the strong sealing between the skin and these natural percutaneous organs. Understanding how nature creates this interface can be inspiring to produce biomimetic percutaneous devices with a strong sealing with the skin. Our discussion will focus on teeth as percutaneous organs and their surrounding gingival tissue since the focus of the thesis is on dental implants.

Teeth are surrounded by a supporting tissue called the periodontium that is a specialized part of the skin in proximity of the tooth. Periodontium has the same general structure of the skin described in section 2.4, which includes an epithelial cell layer attached to a basement membrane that connect to an underlaying connective tissue. Such general anatomy can differ in few sections of the periodontium to serve a certain function. Therefore, the periodontium can be divided at the macroscopic level into four main parts which are the cementum, the periodontal ligament, the alveolar bone and the gingival tissue (gingival, sulcular, and junctional epithelia) as shown in

Figure 2.13 [114]. Since sometimes, cementum is identified as part of the tooth, details of its composition and function will be mentioned in the section 2.6 which discusses the tooth anatomy.

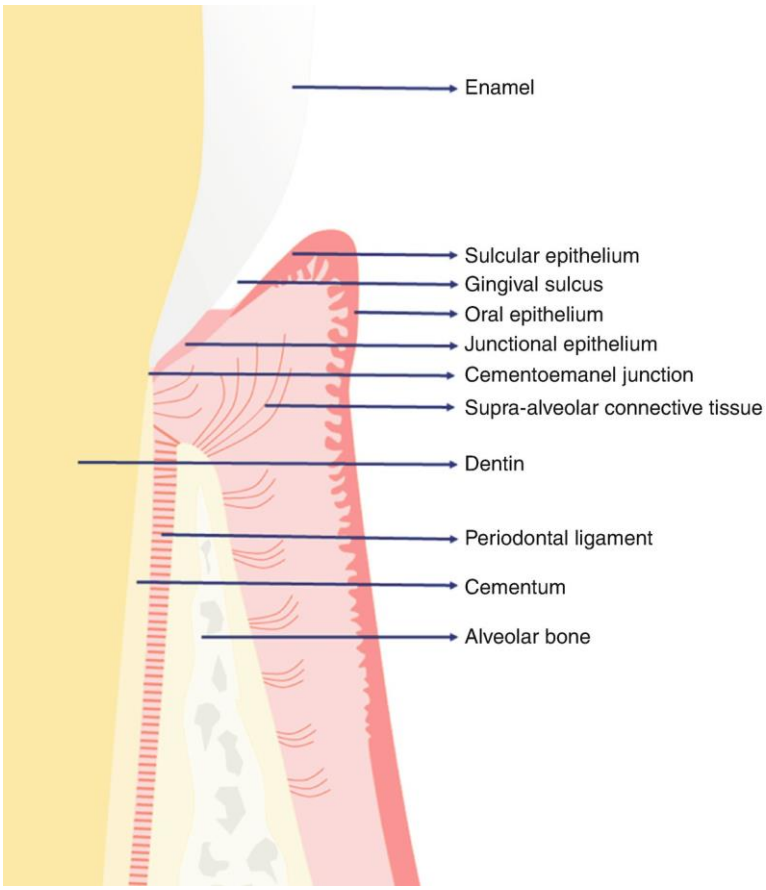

Figure 2.13. A schematics representation of periodontium tissue which consists of gingival, sulcular, and junctional epithelia (gingival tissue), periodontal ligament, alveolar bone and cementum. Dentin and Enamel are different layers that form the tooth. Cementoenamel junction is interface between enamel and cementum. Reprinted with permission to reprint from [115]. Copyright by Springer Nature 2020.

2.5.2. Periodontal ligament

The periodontal ligament is the soft tissue separating the cementum from the alveolar bone [116]. The periodontal ligament functions as a cushion for the teeth when there are external forces such as mastication. It has another role in tissue repair and homeostasis by acting as a cell reservoir. Several cell types are found in the periodontal ligament including osteoblast, osteoclast, epithelial, fibroblast, and mesenchymal stem cells. The ECM consists mainly of collagen fibers of type I, III and XII. The extremities of collagen fiber bundles are embedded in cementum or bone. The periodontal ligament serves as a modulator of mineralization and prevention of fusion between

tooth and bones. Indeed, matrix ‘Gla’ protein, a potent mineralization inhibitor, is also a protein found in periodontal ligament.

2.5.3. Alveolar bone

The alveolar bone is the part of the jaw bones forming the sockets where the teeth reside. It is separated from the teeth by the periodontal ligament. Although, the alveolar bone resides in the deep tissue, late stages of bacterial infection can lead to its resorption and loss.

2.5.4. Gingival tissue

The gingival tissue comprises 3 epithelial types: (1) the gingival epithelium, which covers the outer surface of the gingiva facing the oral cavity, (2) the sulcular epithelium, which resides between the gingival and the junctional epithelium and (3) the junctional epithelium (JE), which faces the tooth as shown in Figure 2.13 [117, 118]. The JE is the one with crucial importance in the current discussion because it is in direct contact with the tooth surface. The main role of the JE is to seal the periodontal tissue into the teeth and protect the body from the outer environment. Figure 2.14 shows the JE and components surrounding it. The JE is a non-keratinized, non-differentiated, stratified squamous epithelium. The morphology of JE cells varies along its width. For instance, cells in the layer facing the underlying gingival tissue are more cuboidal while cells facing the tooth surface are more flattened and run parallel to the tooth. The JE normally starts from the cemento-enamel junction (CEJ) up to the gingival margin (GM). The gingival connective tissue adjacent to the JE contains an extensive vasculature which allows high influx of inflammatory cells into the JE.

JE tissue is unique because it possesses two distinct basal lamina structures: an external basal lamina that connects the JE with the gingival connective tissue and an internal basal lamina (IBL) that attaches the JE to the tooth [119]. The external basal lamina resembles the general basal lamina structure found between epithelial cells and connective tissues. On the other hand, IBL structure is a specialized ECM enriched in glycoconjugates and contains laminin 332 but lacks other major components of the basal lamina such as collagen type IV and type VII and most of other laminin isoforms. The IBL adheres to the outermost cell layer of the JE by hemidesmosomes and simultaneously adheres to the tooth surface. Therefore, the IBL and hemidesmosomes represent

the attachment structure between the JE and the teeth and are crucial for successful sealing between the JE and the tooth surface.

While this and previous sections have discussed the structure of basement membranes, the next sections will focus on the tooth and its surface in order to understand which properties of the tooth surface favor the attachment of the IBL and the JE.

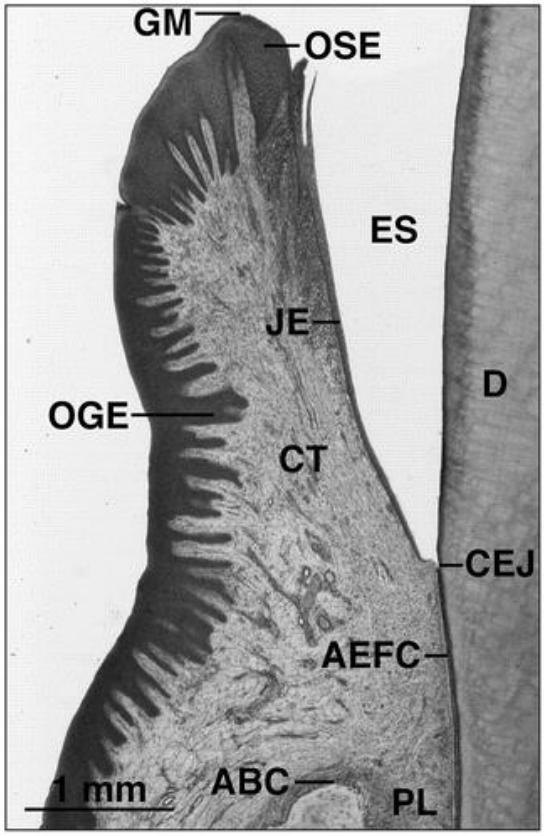

Figure 2.14. A light microscope image of a human tooth, focusing on the crown part and the surrounding junctional epithelium (JE). GM, gingival margin; OSE, oral sulcular epithelium; OGE, oral gingival epithelium; (ES), the enamel space; (CEJ), cemento-enamel junction; (CT), connective tissue; ABC, alveolar bone crest; AEFC, acellular extrinsic fiber cementum; PL periodontal ligament; D, dentin. Reprinted with permission from [119].

2.6. Tooth anatomy

Teeth consist of two major parts: the crown, which is the white visible part of the tooth; and the root, which is buried in the bones and part of the periodontal tissue [120, 121]. Teeth do not have a homogenous anatomy, though. Through examining a cross section of the crown, we can find tooth pulp in the inner-most layer at the center of the tooth. The pulp contains nerves and blood

vessels and it represents the soft tissue part of the tooth. The pulp is surrounded by a mineralized layer called dentin. The outer-most layer of the crown is the enamel tissue which is also a mineralized tissue [122]. The root of the tooth contains the same inner layers (the pulp and the dentin); however, the outer-most layer is the cementum instead of the enamel. A schematic of these layers is depicted in Figure 2.15. The composition and functions of each layer are discussed in the following sections.

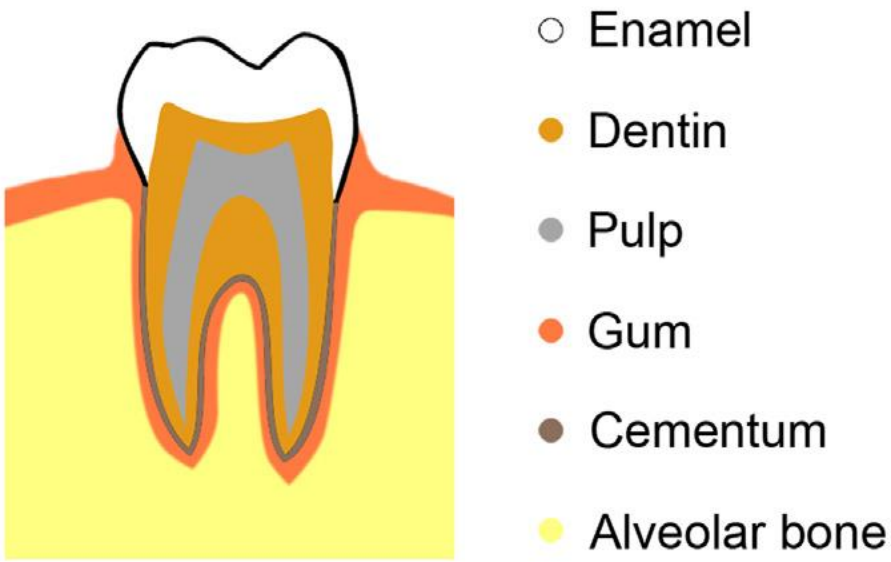

Figure 2.15. A schematic of tooth structure. Reprinted with permission from [123].

2.6.1. Enamel

The enamel is the outer-most layer of the tooth crown. It is the hardest tissue of the human body [122, 124]. The enamel is composed of 96% hydroxyapatite minerals [$Ca_{10}(PO4)_6(OH)_2$] and 4% organic components and water. Organic components are mainly proteins and lipids; 90 % of the organic part is a protein called amelogenin which has a critical role in enamel development [123, 125, 126]. During maturation, ameloblast cells, which secret amelogenin, are detected in the enamel but they disappear from mature enamel. Therefore, the enamel is considered an acellular tissue [127]. Hydroxyapatite minerals in the enamel form nanorod crystals with cross section of 25-100 nm and length of 0.1-100 µm [127]. The presence of amelogenin is crucial for crystal stabilization, growth and morphology. Other proteins are found in trace amount in the enamel such as enamelin and ameloblastin, which have roles in crystal nucleation and morphology[123]. Proteinases such as serine proteinase and matrix metallopeptidase are also found in the enamel.

They have a role in enamel degradation and rebuilding. Other inorganic anions and cations can substitute calcium and phosphate in mineral crystals of enamel, including carbonate (CO_3^{2-}), fluoride (F^-), SO_4^{2-}, magnesium (Mg^{2+}), and chloride (Cl^-) ions.

2.6.2. Dentin

The dentin can be considered the bulk of the tooth. It's the mineralized tissue under the enamel in the crown and under the cementum in the root [128]. The dentin has a lower inorganic to organic ratio than the enamel with 70 wt.% is inorganic minerals and 20 wt.% of proteins and lipids. Therefore, the dentin is less mineralized than enamel which is why the dentin is less brittle and more flexible than the enamel [129, 130]. Unlike the enamel, the dentin is a cellular tissue as it contains cells called odontoblasts [131]. Another main difference between the dentin and the enamel is the presence of collagenous proteins in the dentin. The main protein is collagen type I, accounting for 90% of the total organic matrix [129]. Microscopically, the dentin is divided into two structures: intertubular and peritubular dentin. The intertubular dentin is composed mainly of collagenous proteins such as collagen type I, III, and V, while the peritubular dentin is a hyper mineralized and collagen-free dentin lining the dentinal tubules as shown in Figure 2.16 [130]. The peritubular dentin contains non-collagenous proteins such as dentin sialoproteins, dentin matrix proteins, dentin phosphoproteins, osteopontin and osteocalcin.

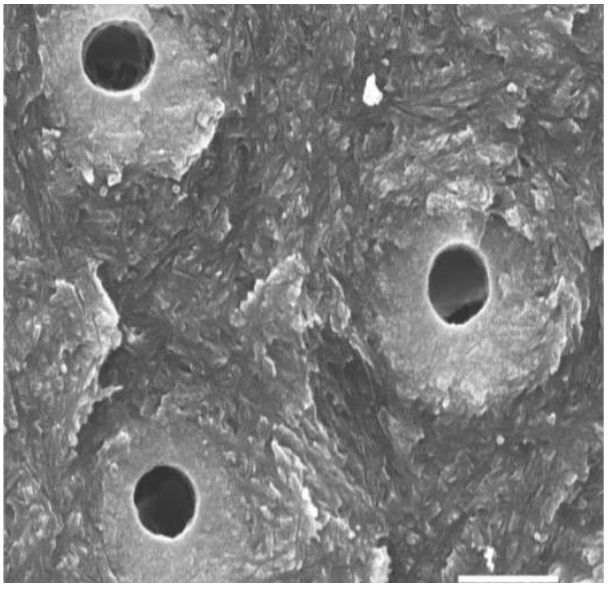

Figure 2.16 SEM image of dentin showing the intertubular dentin and peritubular dentin . Dentinal tubules are the hollow dark cylinders perpendicular to the surface.

2.6.3. Cementum

The cementum is an avascular mineralized connective tissue found on the outermost layer of tooth root [132]. The cementum has a cellular part near the apex of the root. It contains cementoblasts that help repair damaged root. The other part of the cementum is an acellular part that can be found along the cervical part facing the periodontal ligament. This part functions as anchorage for periodontal ligament fibres.

The cementum is similar to bones in its composition. It contains 50% minerals and 50% organic components [114, 133]. Collagenous proteins represent most of the organic components. In fact, collagen I represents 90% of the organic components, while other collagenous proteins include collagen III and XII. Similar to bones, non-collagenous proteins are present including sialoproteins, fibronectin, osteopontin, osteocalcin, proteoglycan and several growth factors.

2.7. Role of tooth proteins in junctional epithelium attachment

The previous section shows that the tooth surface comprises the enamel and the cementum. Therefore, the immediate conclusion would be that these two parts are involved in the connection with the JE and its IBL. However, previous studies showed that the JE can still be restored and adhere to the dentin after removal of tooth cementum and exposure of the underlying dentin [134]. Therefore, it can be inferred that despite compositional differences, enamel, dentin, and cementum can adsorb IBL protein and create a sealing with the JE. A previous study attempted to investigate the effect of the surface properties of the teeth (particularly, dentin) on the adsorption of the IBL and the JE [23]. The aim was to separate the mineral and the organic components of the dentin and compare their ability to adsorb IBL proteins and promote JE cell adhesion and proliferation. The study showed that the organic component (demineralized dentin) favors adsorption of more basal lamina proteins compared to the mineral component (deproteinized dentin). The authors noted that the proteins that are adsorbed on demineralized dentin are involved in cell adhesion, immune response and response to stimulus which are critical to produce a tight seal against external bacteria [23]. Demineralized dentin showed higher epithelial cell adhesion and proliferation compared to deproteinized dentin. These results support the correlation between basal lamina protein adsorption and epithelial cell sealing and pave the way into further exploration of the role of tooth proteins in

mediating the tight sealing between the teeth and the JE. This will be the starting point of my work, followed by an attempt to use the most promising proteins to modify the surface of implants and promote their sealing with the JE and the IBL proteins.

3. Thesis objectives

Previous studies highlighted the significance of tooth proteins (specifically dentin proteins) in promoting adsorption of basal lamina proteins [23]. Therefore, the first objective of this work is to investigate which tooth proteins bind tightly to BL proteins. To achieve this objective, we designed a model to study the interaction between tooth proteins and BL proteins. We used BL proteins and not just IBL proteins because BL proteins are the first biological components that interact with all implants that breach the skin. The model includes depositing a layer of BL proteins on a glass substrate. After ensuring that this layer is well-adhered, a liquid solution of tooth proteins is added on the BL protein layer and the two are allowed to interact with each other. After this, we gently wash away the tooth protein layer to remove weakly bound tooth proteins. The tooth proteins that have high affinity towards BL proteins are not washed away; these are collected and identified using proteomics analysis. These proteins are compared to the proteins present in the BL protein layer and in the tooth protein extract to identify the origin of the proteins collected after the washing step.

The second objective is to conjugate the tooth protein that were found to have the strongest affinity for the BL protein layer to percutaneous device surfaces (i.e. Ti-6Al-4V and PEEK). Conjugating tooth proteins has an advantage over conjugating BL proteins which is ensuring that sites of interactions between BL protein and cell receptors are not blocked by immobilization on implant surfaces [135, 136]. We covalently immobilized the protein to the implants to ensure long-term stability. To achieve a covalent bond between proteins and implant surface, both should possess functional groups that can interact with each other. Proteins contain many carboxylic and amino groups that can readily form amide bonds in the presence of appropriate crosslinkers; however, neither Ti-6Al-4V nor PEEK possess appropriate functional groups. Therefore, we first introduced carboxyl groups on the biomaterial surfaces through diazonium chemistry [137]. Then, we covalently coupled the proteins to the implants using the 1-ethyl-3- [3-dimethylaminopropyl] carbodiimide (EDC) crosslinker [138]. We characterized the above-mentioned surfaces using X-ray photoelectron spectroscopy (XPS) for chemical and elemental analyses, and atomic force

microscopy (AFM) for assessing surface morphology. We then compared the materials modified with the tooth protein with unmodified materials in terms of their capacity for BL protein adsorption, which in turn influences material-cell adhesion. We did so by incubating the modified and unmodified materials in solutions containing the most relevant BL proteins and then analyze the proteome of the proteins that adsorbed on material surfaces. The proteome of each surface was obtained using mass spectrometric analysis. We then assessed epithelial integration to the surfaces and correlated with the affinity of these surfaces to basal lamina proteins. We used human gingival fibroblasts as the cell model. We seeded the cells on the modified and unmodified surfaces and determined cell viability and proliferation by Alamar blue assay at 3 timepoints (1day, 3 days, and 7 days). These results aim to provide more insights on developing implants that can achieve soft tissue integration through adsorbing key BL proteins and promoting cell adhesion and proliferation.

4. Methods

4.1. Tooth protein extraction

Teeth were collected from patients attending the McGill University Undergraduate Dental Clinic. The teeth were collected after obtaining the approval from the Faculty of Medicine (McGill University) research ethics board with the protocol number A01-M02-18A. They were stored in a 10% thymol solution at 4° C for further use. Tooth proteins were extracted from teeth based on a previously established protocol [139]. Tooth proteins include collagenous and non-collagenous proteins that were extracted using guanidine hydrochloride (guanidine-HCl) and ethylenediaminetetraacetic acid (EDTA) as extraction buffers, respectively. Guanidine is used to desolubilize collagen by weakening the hydrophobicity of collagen, the main factor that stabilizes collagen conformation [140]. EDTA is used to chelate metal ions without destroying proteins, thus preserving their integrity [141]. The first extraction buffer was prepared by dissolving 4 M Guanidium-HCl in 50 mM Tris-HCl solution, pH 7.4. The second buffer consisted of 0.5 M EDTA in 50 mM Tris-HCl solution, pH 7.4. After preparation, both buffers were stored at 4° C. Three protease inhibitors were added on the extraction buffers just before the extraction to prevent protein breakdown; the protease inhibitors are 100 mg/ml of benzamidine, 1 mg/ml of leupeptin, and 0.05 M of phenylmethylsulfonyl fluoride (Sigma–Aldrich, StLouis, MO, USA).

To produce tooth powder, liquid nitrogen was added on a clean and dry biopulverizer (Biospec Products, Bartlesville, OK, USA) as shown in Figure 4.1. After that, a tooth was placed inside the biopulverizer to freeze it before crushing it into powder by striking a steel piston with a hammer several times [142]. The tooth powder was collected, weighed and transferred to a 50 ml tube. Guanidine-HCl buffer was added to the tube with the powder (50 ml of buffer per 1 g of tooth powder). The tube was then placed on a rotator at 4° C for 24 hours. After that, the tube was centrifuged for 15 minutes using 1000 g acceleration. The supernatant containing the extracted proteins was collected in a separate tube and stored at 4° C. The extraction step was repeated again for another 24 hours and the supernatant containing proteins was collected as well. The remaining pellet was used for another two extractions; these were performed using the same procedure just described but using the EDTA buffer instead of the Guanidine-HCl buffer. All extractions were pooled and filtered using Centricon 20 centrifugal filter units (Ultracel PL membrane) by centrifuging at 4000 g acceleration until the volume was reduced to 1 ml for each buffer. Each concentrated sample was diluted in either 8 M urea (guanidine-HCl extract) or 5 mM NH_4HCO_3 (EDTA extract) to wash any remaining guanidine or EDTA. After this, the samples were re-concentrated back to 1 ml by filtration. The total protein concentration was measured using the Micro Bicinchoninic acid (Micro BCA) assay (Pierce, Rockford, IL) following manufacturer instructions. Samples were stored at – 20 ° C till further use.

Figure 4.1 An image of a biopulverizer with a steel piston. Depicted from: https://www.labcompare.com/1258-Laboratory-Mill/12607956-BioPulverizer/

4.2. Interactions between tooth proteins and Matrigel

In order to model the interaction between tooth proteins and basal lamina proteins, we used the set up shown in Figure 4.2. In this experiment, Matrigel (BD Biosciences, Mississauga, Canada) is used to model basal lamina proteins. Matrigel contains proteins derived from Engelbreth-Hom-Swarm mouse tumor cells. Matrigel is a liquid at 4 ° C however, it turns into a gel at 37° C. Phosphate buffer saline (PBS) was used to dilute Matrigel with a Matrigel to PBS v/v ratio of 1:5. Then, a volume of 50 µL of the diluted Matrigel was added on a coverslip inside a well plate and transferred to an incubator at 37° C to form a gel. A volume of 30 µL of pooled tooth proteins (15 µL of both collagenous extract in urea solution and non-collagenous extract in NH_4HCO_3 solution) were then added on top of the Matrigel and allowed to interact for 30 minutes. Weakly bound tooth proteins were washed away using 100 µL deionized water. The Matrigel disk with the remaining tooth proteins was labelled as Mat-tooth. These proteins are compared to Matrigel proteins and to the tooth proteins to identify the origin of the proteins in the Mat-tooth samples.

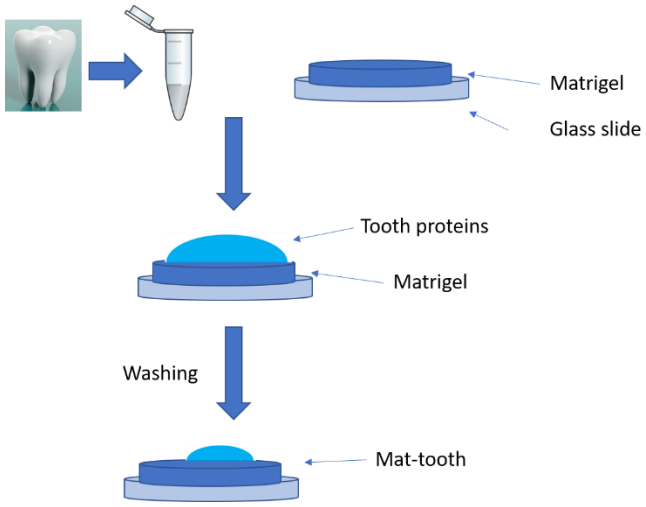

Figure 4.2. Experimental setup used to investigate the interaction between tooth proteins and Matrigel. Tooth proteins are extracted and added on a gel layer of Matrigel proteins. After that, the tooth proteins are washed away to remove weakly bound proteins leaving only proteins tightly bound to Matrigel.

4.3. Mass spectrometry-based proteomics to identify interactions between tooth proteins and Matrigel.

Mass spectrometric analysis was used to identify the proteins in Mat-tooth, Matrigel and tooth protein samples. This technique provides quantitative profiling of a large protein mixtures adsorbed on a specific surface and identifies the adsorbed proteins with their relative abundance. Proteins were detached from the glass slides surfaces using 2% (w/w) trypsin for 18 h at 37° C.

Peptide separation and mass spectrometric analyses were performed using a nano-HPLC Proxeon (Thermo Scientific, San Jose, CA) linked to a mass spectrometer (LTQ-Velos, Thermo Scientific, San Jose, CA, USA) using an electrospray ionization with a survey scan in the range of m/z values 390–2000 tandem MS/MS [143, 144]. The peptides were separated based on their weight in the nano-HPLC Proxeon which allows in-line liquid chromatography with a capillary column with dimensions of 75 µm × 10 cm (Pico Tip™ EMITTER, New Objective, Woburn, MA) packed in-house by Magic C18 resin of 5 µm diameter and 200 Å pores size (Michrom BioResources, Auburn, CA). Equal amount of protein sample was subjected to reverse phase liquid chromatography electrospray ionization tandem mass spectrometry (LC-ESI-MS/MS). The nano-flow reversed-phase HPLC was performed with linear 100 min gradient ranging from 5% to 55% of solvent B in 65 min (97.5% acetonitrile, 0.1% formic acid) at a flow rate of 300 nL/min with a maximum pressure of 280 bar. Electrospray voltage and the temperature of the ion transfer capillary were 1.8 kV and 250°C, respectively. The resulting MS/MS spectra were searched against mouse and human databases (Swiss Prot and TrEMBL, Swiss Institute of Bioinformatics, Geneva, Switzerland, http://ca.expasy.org/sprot/) [144]. Then, protein identification was done using the Proteome Discoverer 1.3 software. Each protein gets a score that represents how many times its constituent peptides were detected. This value positively correlated with the abundance of the protein in the sample. Therefore, the identified proteins are compared using their score (protein score).

4.4. Surface modification via diazonium chemistry

Ti-6Al-4V samples (McMaster-Carr, Cleveland, OH) were obtained as rods and cut into disks with a diameter of 9 mm and length of 2 mm. PEEK samples (Modern plastics, Shelton, CT) were obtained as rods and cut into disks with diameter of 12.7 mm and length of 2 mm. All samples were polished sequentially using 800 and 1200 grit silicon carbide papers. Then, all samples were washed sequentially in acetone, ethanol and deionized H_2O for 10 minutes each. Samples were then dried and stored in vacuum till further use.

Surfaces of polished PEEK and Ti-6Al-4V implants were modified by introducing carboxylic groups using diazonium chemistry based on a previously established protocol [145]. Diazonium chemistry is a technique used to modify the surface of a wide range of materials such as polymers, metals and metal oxides [146-148]. With this technique, arylamines compounds are the precursors that contain the functional group that needs to be introduced [146]. Figure 4.3 depicts the general

structure of arylamines. Sodium nitrite reacts with the arylamine of choice in the presence of an acid to transform the arylamine into metastable diazonium salts. Diazonium cations are then transformed into radicals by the addition of a reducing agent, such as iron powder or hypophosphorous acid. The radicals can react with almost any surface and create covalent bonds [149]. Figure 4.4 depicts a schematic of the general steps in the diazonium reaction. In this work, we use diazonium chemistry to add carboxylic groups to the surface of Ti-6Al-4V and PEEK.

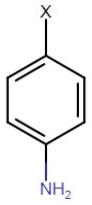

Figure 4.3. The general structure of arylamine precursor used in diazonium chemistry to introduce functional group labeled "X" on the surface of a material.

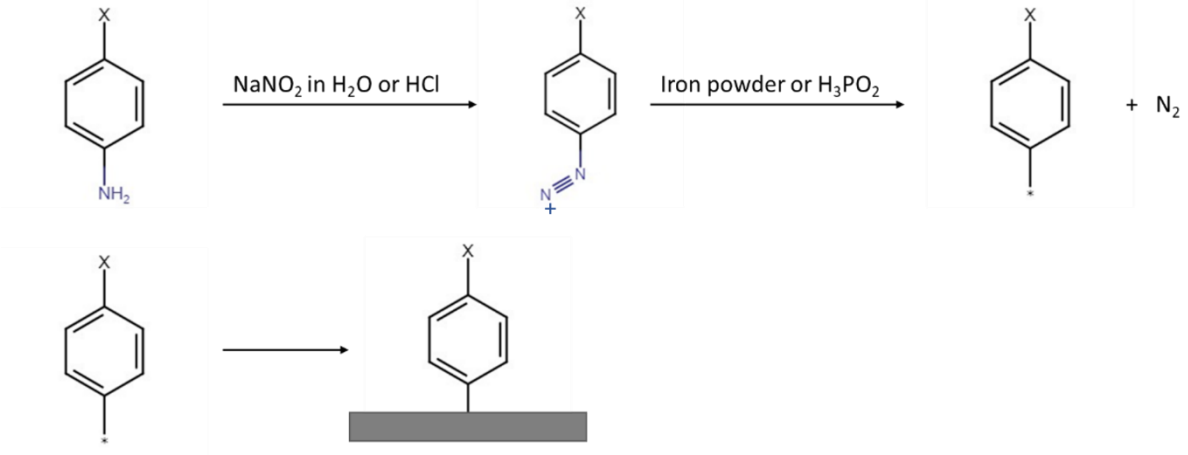

Figure 4.4. A schematic of the general steps in the diazonium chemistry reaction.

P-Amino-benzoic acid (PABA; an arylamine compound with a carboxylic group replacing the “X” in Figure 4.3) (SIGMA-ALDRICH, Oakville, ON) was used as the arylamine precursor. In a clean 200-ml flask, ten PEEK or Ti-6Al-4V disks were added to 50 ml distilled water. To reach a concentration of 100 mM of PABA, 343 mg of PABA were added to the flask. Cations were generated in-situ by addition of one equivalent of $NaNO_2$ (173 mg) (SIGMA-ALDRICH, Oakville, ON) to convert the amine group to aryldiazonium cation. The reaction was stirred for 5 minutes before adding 2.7 ml of hypophosprous acid (H_3PO_2) (SIGMA-ALDRICH, Oakville, ON) as reducing agent (0.5 M). H_3PO_2 reduces the aryldiazonium groups and the resulting free radicals attack the surface of PEEK and Ti-6Al-4V disks placed in the reactant solution. The disks were

left in the reaction solution for 16 hours. Then, they were collected, washed with 70 % ethanol and distilled H_2O for 10 minutes each. Then they were dried and stored in vacuum storage till further use. Carboxylated PEEK and Ti-6Al-4V were named COOH-PEEK and COOH-Ti, respectively while Ti-6Al-4V was shorten to Ti.

To confirm the presence of carboxyl group, 2,2,2 tri-Fluoro-ethanol (TFE) was added on both COOH-PEEK and PEEK. TFE reacts with carboxyl groups in the presence of di-tert-butyl-carbodiimide (DBC) and pyridine as a catalyst. Briefly, disks of control and modified samples were placed in small beakers inside a hermetically sealed larger. TFE (0.9 ml), DBC (0.3 ml) and pyridine (0.4 ml) were added sequentially inside the larger container but outside the beakers with the samples, and the reaction was left to proceed for 18 h. Since the reactants are volatile, their vapor would be able to reach the surface of the samples inside the beakers and react with carboxylic groups, if present. After the reaction, PEEK samples were denoted as F-PEEK while COOH-PEEK samples were denoted as F-COOH-PEEK.

4.5. Covalent attachment of collagen protein to implant materials

Collagen type I solution from rat tail was obtained from SIGMA-ALDRICH (Oakville, ON). Collagen was covalently coupled to the carboxylated surfaces through activation of the carboxyl groups with EDC (SIGMA-ALDRICH, Oakville, ON). The reaction between carboxylic groups and EDC forms an active intermediate (O-acylisourea) that reacts with primary amine groups of collagens to form an amide bond. However, O-acylisourea is unstable and can easily gets hydrolyzed by water. This rapid hydrolysis is prevented by addition of N-hydroxy succinimide (NHS) (Alfa Aesar, Thermo Fisher Scientific Chemicals, Inc., Ottawa, ON) that forms a more stable NHS ester intermediate that reacts slowly with primary amines to form a stable amide bond.

We followed a previously established protocol with some modifications [138]. Briefly, 200 mM EDC and 200 mM NHS solutions were prepared in 100 mM 2-(N-Morpholino) ethane sulfonic acid (MES) buffer at pH 6.0 separately. COOH-PEEK and COOH-Ti disks were put in the wells of a 24-well plate. Then, 100 µL of each of EDC and NHS solutions were added on each COOH-PEEK and COOH-Ti disks and then diluted with 1.0 ml of MES buffer to obtain a final concentration of 10 mM of both EDC and NHS. The reaction proceeded for 30 minutes before the addition of 30 µL of 98% ethanolamine (SIGMA-ALDRICH, Oakville, ON) to quench the reaction. The solutions were removed from the wells and fresh 1.9 ml MES buffer were added on

the disks. After that, 100 µL of collagen type I solution with a concentration of 2 mg/ml was added on the disks to reach a final concentration of 100 µg/ml. The reaction was left overnight then the disks were collected, rinsed with deionized water and sonicated in 10% sodium dodecyl sulfate (SDS) for 30 minutes to remove weakly adsorbed proteins. These samples were named as Col-COOH-PEEK and Col-COOH-Ti. Some samples were not sonicated in 10% SDS to test the effect of SDS on removal of adsorbed proteins. These samples were named Col-COOH-PEEK-noS and Col-COOH-Ti-noS. All disks were rinsed 3 times with distilled water, dried and stored in vacuum storage for characterization or cell culture. Collagen was added on pristine PEEK and Ti disks to show the difference between protein conjugation and adsorption. The same procedure mentioned above was used while replacing COOH-PEEK and COOH-Ti with PEEK and Ti, respectively. These samples were named Col-PEEK and Col-Ti. The disks were rinsed 3 times with distilled water, dried and stored in vacuum storage for characterization.

The stability of collagen on Col-COOH-PEEK and Col-COOH-Ti was tested by incubating the samples in a PBS solution at pH 7.4. Samples were removed from the solution after 1, 3, and 7 days for characterization. Samples were rinsed with distilled water, and dried before characterizing their surfaces.

4.6. Physical characterization

4.6.1. XPS

X-ray photoelectron spectroscopy (XPS) is a surface sensitive technique that is used to identify the chemical composition of the surface of a material. We used XPS (Thermo Fischer Scientific Inc, East Grinstead, UK) to confirm (1) the functionalization of the COOH-PEEK and COOH-Ti disks, (2) the functionalization of COOH-PEEK with TFE, and (3) Col-COOH-PEEK and Col-COOH-Ti. A monochromatic Al Kα X-ray source (1486.6 eV) was used as the source with an X-ray beam diameter of 400 µm. Survey scans were obtained over the range of 0-1350 eV with a pass energy of 200 eV at a step of 1.0 eV and a X-ray beam diameter of 400 µm. Data analysis was performed using the Avantage software (5.41v, Thermo Fisher Scientific Inc, East Grinstead, UK). High-resolution C1s spectra were obtained with a pass energy of 50 eV and an energy step of 0.1 eV with the same beam diameter as the survey and then deconvoluted using the same software. Gaussian–Voigt curves functions were used for peak fitting and an iterated Shirley

procedure was used for background subtraction. Atomic percentages of carbon bonds were calculated as percentages of the total atomic composition of the surfaces.

4.6.2. Quantitative assessment of carboxylic groups

The amount of surface carboxyl groups was measured using a toluidine blue O (TBO) assay [150, 151]. Briefly, PEEK, Ti, COOH-PEEK and COOH-Ti disks were incubated in 2 ml of 0.5 mM TBO in 100 mM NaOH at pH 10 at 37° C. At basic pH, TBO can form a complex with the carboxyl groups. After 4 hours, the TBO solution was removed and the disks were washed 3 times with 2 ml of 100 mM NaOH at pH 10 to remove any unreacted TBO. Then, the samples were transferred to 0.5 ml of 50% acetic acid solution for 10 min to dissolve the bound dye. The solution was then collected to analyze the concentration of the dye by measuring the absorbance at 562nm using a microplate reader (Cole-Parmer, IL, USA). The amount of carboxyl groups was determined using a calibration curve by assuming that TBO complexes an equimolar amount of carboxylic groups.

4.6.3. Atomic Force Microscopy (AFM)

AFM was used to assess the surface topography of PEEK, Ti, COOH-PEEK, COOH-Ti, Col-COOH-PEEK, and Col-COOH-Ti samples. AFM images were recorded in air using the AC mode of a Cypher VRS with ARC 2 controller instrument from Bruker with FS1500AuD probe (Oxford Inst). The probe had a resonance frequency of 2 MHz and spring constant of 6 N/m. The software Igor Pro was used to process the AFM images. Three different scan sizes were taken per sample, with lateral dimensions of 10 µm, 5 µm, and 2 µm. The image resolution is 512*512 pixels for all samples.

4.6.4. Contact angle

Wettability was determined by measuring water contact angle on sample surfaces, using the sessile drop method at room temperature on a goniometer (OAC 15, Data Physics, Filderstadt, Germany). Three drops of deionized were measured per specimen (n=3 per group) with a drop volume of 5 µL. Angle measurements were calculated with a video-based software (SCA 20, Dataphysics, Filderstadt, Germany).

4.7. Assessment of BL protein adsorption using Mass spectrometry-based proteomics

PEEK, Ti, Col-COOH-PEEK, and CoL-COOH-Ti samples were incubated in a solution containing the most relevant BL proteins (i.e. Matrigel). Matrigel was diluted in PBS to a ratio of (1:20). Aliquots (400 ul) of the diluted Matrigel solution were added on the surface of the samples and allowed to remain in contact for 45 min. All samples were then washed with distilled water three times to remove weakly adsorbed proteins. The proteome of each surface was determined using mass spectrometric analysis with a liquid chromatography electrospray ionization mass spectrometry (LCESI-MS/MS) instrumentation as described in section 4.3.

4.8. Cell culture

4.8.1. Alamar blue for proliferation assay

Human periodontal ligament fibroblasts (PDL) (Cedarlane Laboratories, ON, Canada) were used to evaluate the effect of the modification of PEEK and Ti surfaces on cell proliferation and viability. The cells were cultured in Dulbecco's Modified Eagle's Medium containing 2 mM L-glutamine (DMEM, Gibco®, ThermoFisher, Burlington, ON) supplemented with 10% fetal bovine serum (Gibco®, ThermoFisher, Burlington, ON) and 100 U/ml penicillin-streptomycin [23]. Cells were moved from the shipping vial into sterile tissue culture dish and 8 ml of media were added to the dish. Then, cells were incubated at 37 °C in a 5% CO_2 atmosphere to multiplicate. Cells were passaged when they reached ~ 70% confluence. Cells from passages 4-6 were seeded on samples.

PEEK, Ti, COOH-PEEK, COOH-Ti, Col-COOH-PEEK, and CoL-COOH-Ti disks were placed in a 24-well plate and disinfected with UV for 10 to 15 minutes then a drop of 50 µL of media containing approximately 10,000 cells was placed on each specimen. Cells were allowed to attach for 4 h before adding 1 ml of media.

Cell proliferation was evaluated at 1,3 and 7 days after cell seeding. Briefly, 100 µl of culture medium containing 10% of Alamar Blue® (ThermoFischer, Burlington, ON) was added to each well. After 4 h of incubation at 37^o C, 150 µl of the supernatant was transferred into a 96-well plate with a clear bottom. Fluorescence intensity was measured using a microplate reader (Cole-Parmer, IL, USA) with excitation and emission set at 560 and 590 nm, respectively. Cells seeded on tissue culture plates (TCPS) were used as positive controls, while PEEK and Ti samples incubated in

medium in the absence of cells were also tested in order to measure the background fluorescence of each biomaterial. This experiment was done in triplicates and each time, 3 samples of each type were used (n=9).

4.8.2. Live/dead fluorescence imaging

Live/dead staining assay was carried out according to an established protocol [152]. The assay uses fluorescein diacetate (FDA) to stain viable cells in green and propidium iodide (PI) to stain cells with compromised membranes in red. A stock solution of FDA was prepared by dissolving 5 mg FDA in 1 ml acetone while the stock of PI was prepared by dissolving 2 mg of PI in 1 ml PBS. 2 µL of each dye stock solution were added to 1 ml of culture media and then applied on the samples to stain the cells for 5-10 min. Then, the staining solution was removed; the samples were transferred to clean well plates and 1 ml PBS was added on the samples. Cells were analyzed with the Zeiss AX10 fluorescence microscope (Carl Zeiss, Göttingen, Germany). Images were obtained using 2.5X and 10X objective lenses.

4.9. Statistical analysis

All experiments were done with 3 to 9 samples per group ($n \geq 3$). Results are displayed as mean ± standard deviation (SD). For parametric data, statistical differences were assessed based on unpaired and paired Student's t-test (for comparison between 2 groups) and one-way ANOVA followed by Tukey HSD test (for comparison between 3 groups or more) (F-test was used to assess equal variance and Shapiro-Wilk test was used to test for normality). Statistical analysis was performed using GraphPad Prism 8.3 (CA, USA). Differences were considered significant when the *p*-value was lower than 0.05.

5. Results

5.1. Proteomics analysis of the interaction between tooth proteins and Matrigel

We investigated the interaction between tooth proteins and Matrigel as shown in Figure 4.2 in order to identify tooth proteins that favor the adsorption of BL proteins. Proteomic analysis of Mat-tooth samples, Matrigel, and tooth proteins showed that only few tooth proteins were identified in the Mat-tooth samples. Figure 5.1 shows protein scores of the key tooth proteins and Table 5.1 shows the relevant tooth protein abbreviations. The protein score reflects the total number of peptide spectral counts associated with each protein. Therefore, the protein score is

correlated with the amount of the protein in the sample and can be used to quantify the proteins relative to other proteins in the analyzed sample [153]. Collagen type XI shows statistically higher score than other tooth proteins adsorbed on Matrigel. hence, it represents the a promising candidate to functionalize dental implants materials (PEEK and Ti) to increase BL proteins affinity towards implant. However, in this work, we used collagen type I instead because it was more practical to use in terms of availability and price. This point is further discussed in the discussion section.

Table 5.1. A legend of the names and the abbreviations of the tooth proteins identified in Mat-tooth samples.

Identified Protein	**Abbreviation**
Collagen alpha-2(XI)	COL11A2
Serum albumin	ALB
Laminin subunit gamma-1	LAMC1
Histone H4	HistoneH4
Histone H2B	HistoneH2B
Alpha-2-HS-glycoprotein	AHSG
Histone H2AX	H2AFX
Collagen alpha-2(I) chain	COL1A2
Ubiquitin-60S ribosomal protein L40	UBA52
Prothrombin	F2
Matrix Gla protein	MGP
Pigment epithelium-derived factor	SERPINF1
Matrix metalloproteinase-20	MMP20
Vitronectin	VTN
Laminin subunit beta-1	LAMB1

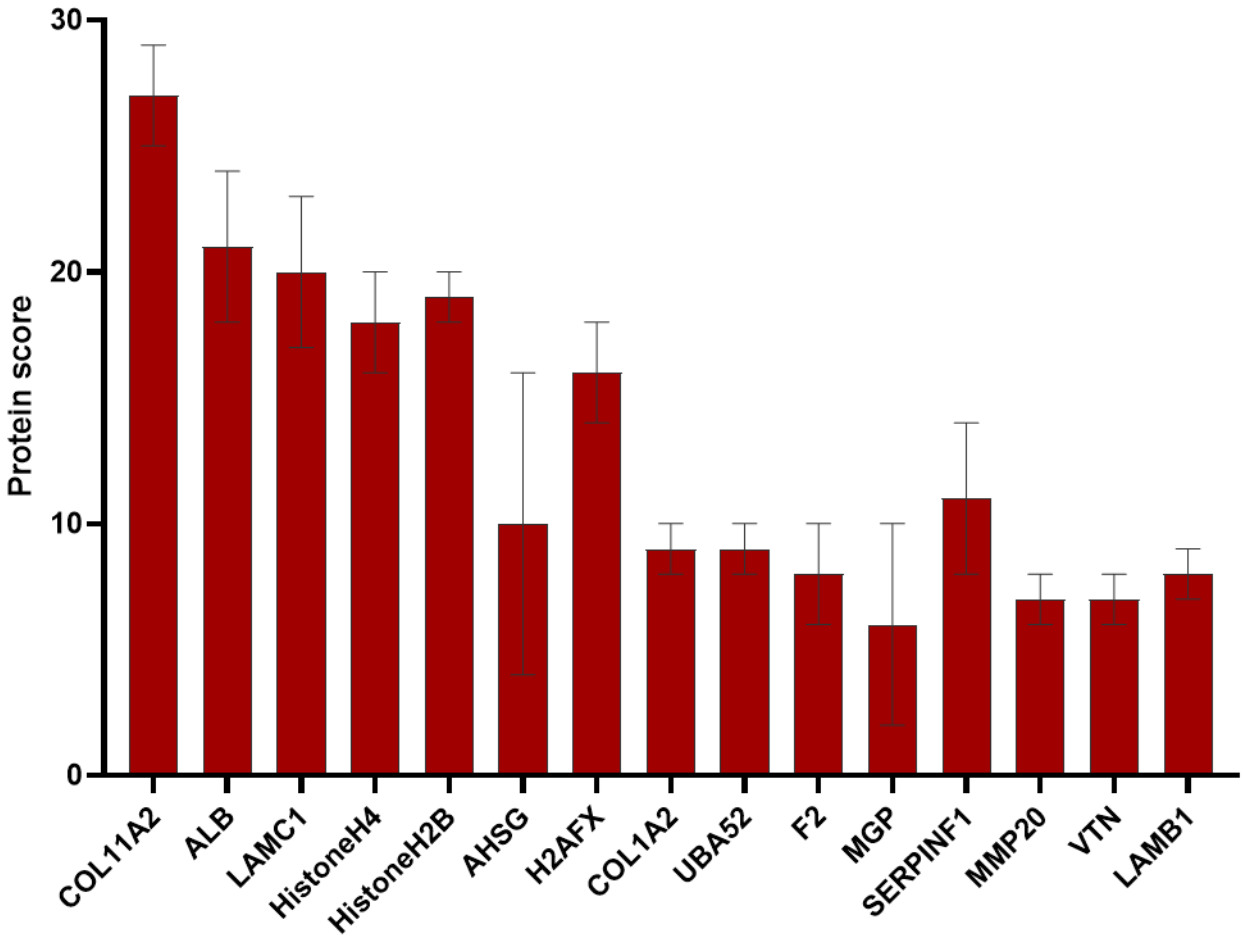

Figure 5.1. Protein scores of the key tooth proteins identified in Mat-tooth sample measured by mass spectrometry.

5.2. Characterization of PEEK and Ti after modification via diazonium chemistry

In order to conjugate collagen on the surface of PEEK and Ti, we first functionalized these materials with carboxylic groups to use them as anchors for covalent linking of collagen proteins. We characterized the surface of the materials before and after carboxylation using XPS. For PEEK samples, the atomic percentage of elements extracted from survey spectra showed the presence of only C and O on the surface of both PEEK and COOH-PEEK, and the amounts were not statistically different (Figure 5.2A). The high- resolution C1s spectra of PEEK and COOH-PEEK showed peaks corresponding to C-C, C-O, C=O and COO bonds (S1 A). Quantitative analysis of the relative amounts of these components showed a higher COOH content on COOH-PEEK compared to PEEK, in line with our expectations (Figure 5.2B). The successful introduction of

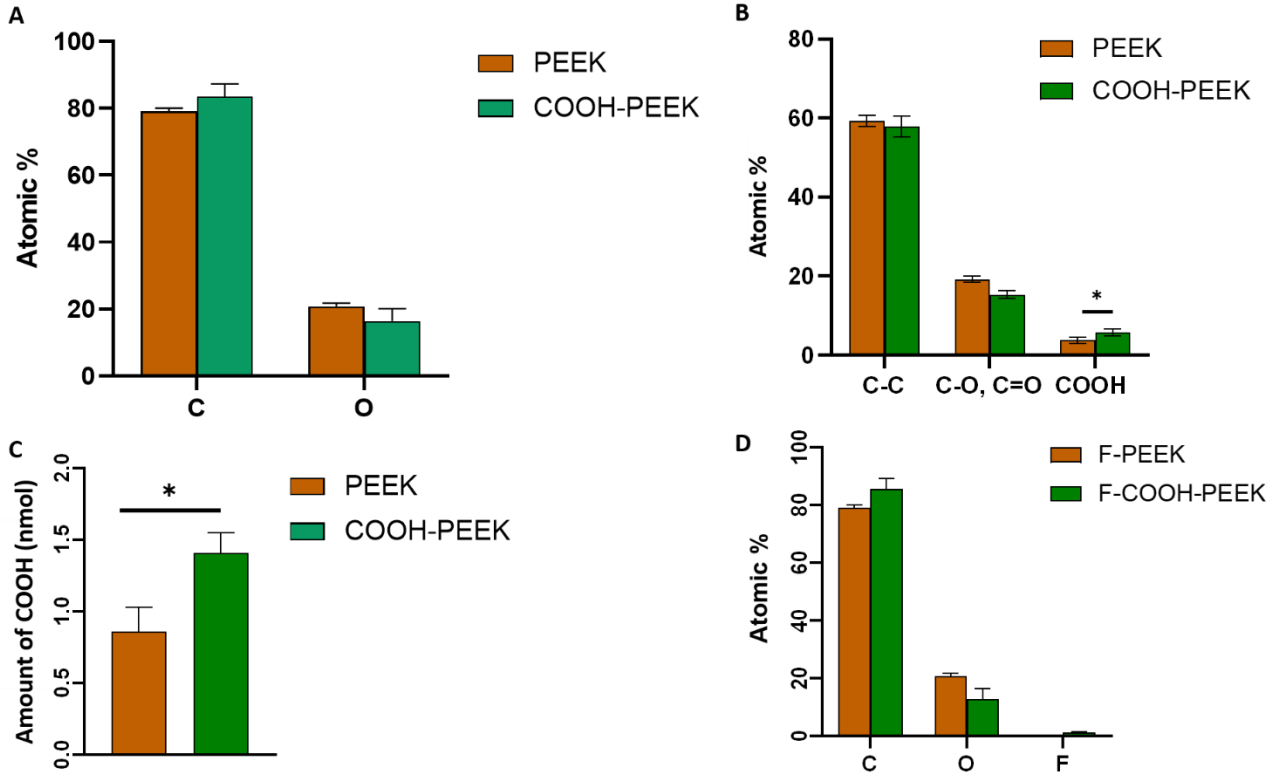

Figure 5.2. Surface characterization of PEEK. A) Atomic percentages of the elements detected on the surface of PEEK and COOH-PEEK obtained from XPS survey spectra B) Atomic percentages of different C bonds in comparison to the total elemental composition of the surfaces in both PEEK and COOH-PEEK obtained from XPS high resolution C1s spectra. C) Amount of carboxylic groups on PEEK and COOH-PEEK quantified using the TBO assay. D) Atomic percentages of the elements detected on the surface of F-PEEK and F-COOH-PEEK obtained from XPS survey spectra. All values are expressed as mean ± SD. The symbol (*) indicates significant differences between the different biomaterials with $p < 0.05$.

COOH groups on COOH-PEEK was further confirmed by the TBO assay, which showed higher

amount of carboxylic groups on COOH PEEK compared to PEEK (Figure 5.2C). As another confirming experiment, fluoride from the reaction with TFE was detected only on the surface of COOH-PEEK samples, which confirmed the presence of carboxylic groups on the surface of COOH-PEEK since TFE reacts with carboxylic groups (Figure 5.2D).

For Ti samples, the atomic percentage of elements obtained from XPS survey spectra showed the presence of C, O, Ti, Al, N and P on the surface of both Ti and COOH-Ti (Figure 5.3A). After carboxylation, the O, Ti, and N content decreases whereas C and P increase. The high-resolution C1s spectra show peaks corresponding to C-C, C-O, C=O and COOH bonds (Figure S1B). The quantification of these bonds showed higher COOH content on COOH-Ti compared to Ti confirming the successful attachment of COOH groups on the surface of Ti (Figure 5.3B). Similar to PEEK samples, the TBO assay showed higher amount of carboxylic groups on COOH-Ti compared to Ti (Figure 5.3C).

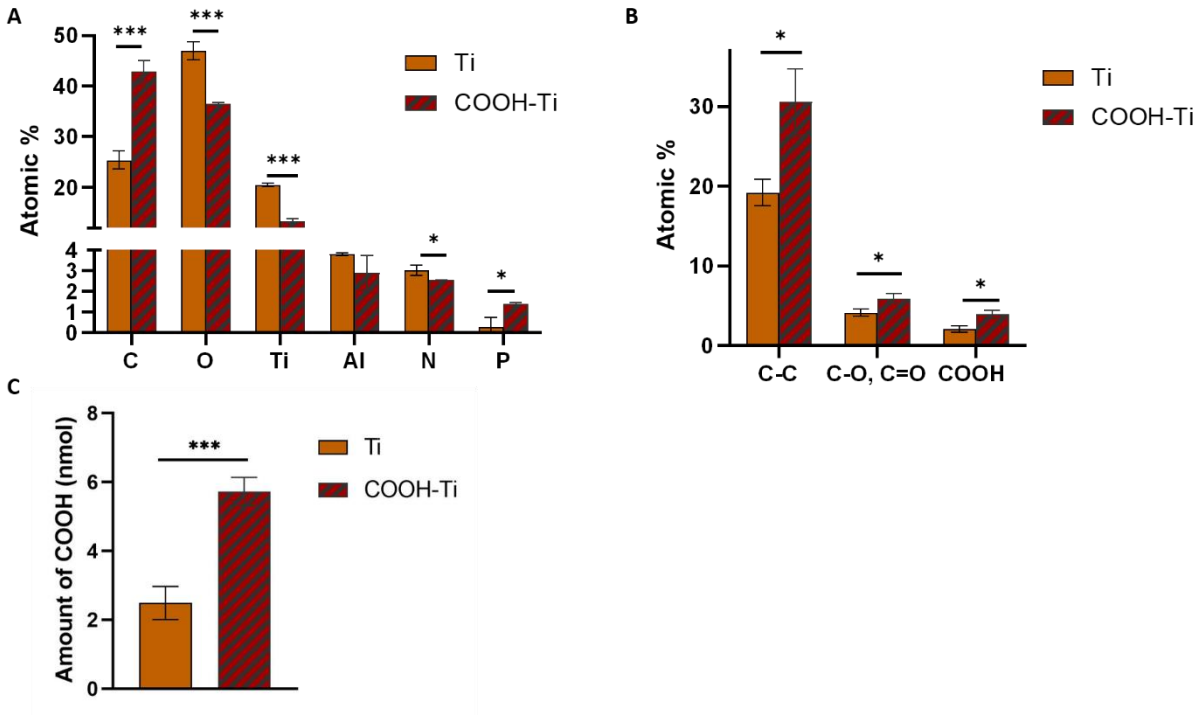

Figure 5.3 Surface characterization of Ti. A) Atomic percentages of the elements detected on the surface of Ti and COOH-Ti obtained from XPS survey spectra. B) Atomic percentages of different C bonds in comparison to the total elemental composition of the surfaces in both Ti and COOH-Ti obtained from XPS high resolution C1s spectra. C) Amount of carboxylic groups on Ti and COOH-Ti quantified using the TBO assay. All values are expressed as mean ± SD. The symbol (* and ***) indicate significant differences between the different biomaterials with $p < 0.05$ and < 0.001, respectively.

5.3. Characterization of PEEK and Ti after attachment of collagen

Collagen was added on the surface of PEEK, Ti, COOH-PEEK, and COOH-Ti using the NHS-EDC crosslinking strategy as described in section 4.5. In order to check the importance of washing and sonication in SDS solution after collagen modification to remove weakly adsorbed proteins, we analyzed XPS spectra of Col-PEEK and Col-COOH-PEEK before and after sonication (Figure S2). The decrease in N peak in both Col-PEEK and Col-COOH-PEEK compared to Col-PEEK-noS and Col-COOH-PEEK-noS confirms that sonication with SDS was able to remove most of the physiosorbed proteins. We then compared the surface elemental composition of Col-COOH-PEEK and Col-PEEK to confirm the importance of carboxylation on protein conjugation. Figure 5.4 A shows that C, O and N were detected on both surfaces, however higher N content was detected on Col-COOH-PEEK compared to Col-PEEK, which indicates the significance of conjugation on surface of the materials. Percentages of carbon bonds obtained from high-

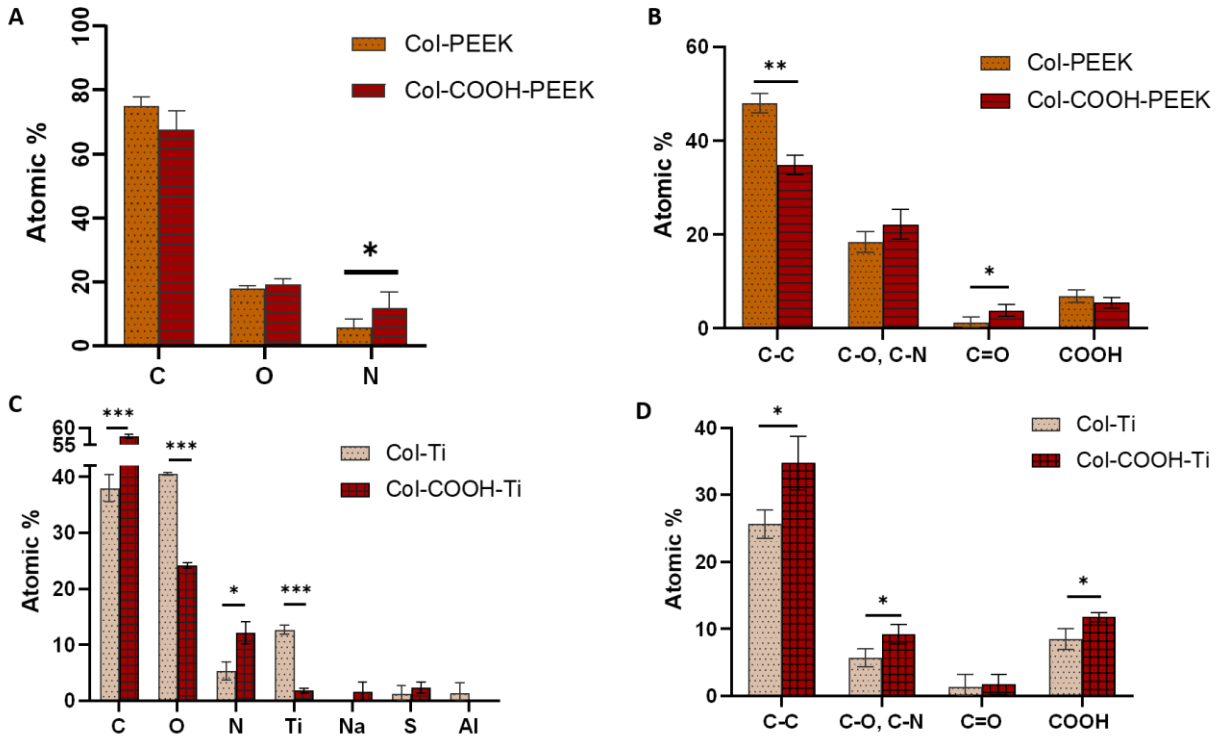

Figure 5.4. (A) Atomic percentages of the elements detected on Col-PEEK and Col-COOH-PEEK obtained from XPS survey spectra. (B) Atomic percentages of different C bonds in comparison to the total elemental composition in both Col-PEEK and Col-COOH-PEEK obtained from XPS high resolution C1s spectra. (C) Atomic percentages of the elements detected on Col-Ti and Col-COOH-Ti obtained from XPS survey spectra. (D) Atomic percentages of different C bonds in comparison to the total elemental composition in both Col-Ti and Col-COOH-Ti obtained from XPS high resolution C1s spectra. The symbols (*, ** and***) indicate significant differences between the different groups at $p < 0.05$, <0.01 and < 0.001, respectively.

resolution C1s spectra showed peaks corresponding to C-C, C-O/C-N, C=O and COOH bonds (**Error! Reference source not found.**B). For Ti samples, the elemental composition of Col-Ti and Col-COOH-Ti obtained from XPS survey spectra confirmed the role of COOH group on successful conjugation of collagen (Figure 5.4C). Quantification of carbon bonds from C1s high resolution spectra showed higher percentages of C-C, C-O, C-N and COOH bonds in Col-COOH-Ti compared to Col-Ti (Figure 5.4D).

The stability of collagen I on the surface of PEEK and Ti was investigated by collecting XPS spectra on samples of Col-COOH-PEEK and Col-COOH-Ti immersed in PBS for up to 7 days. No significant differences of the atomic percentage of C, O or N were observed during the whole experiment, in either Col-COOH-PEEK (Figure S3A) or Col-COOH-Ti (Figure S3B).

5.4. AFM imaging

AFM images of all samples are shown in Figure 5.5A-F. The root mean square (RMS) roughness values showed that both PEEK and Ti had similar roughness and that carboxylation did not significantly change the topography as seen in the RMS values of COOH-PEEK and COOH-Ti (Figure 5.5 G). After collagen modification, the RMS value increased in both Col-COOH-PEEK and Col-COOH-Ti with the latter showing larger increase. Collagen fibers can be clearly seen in Col-COOH-PEEK and Col-COOH-Ti and not in other images.

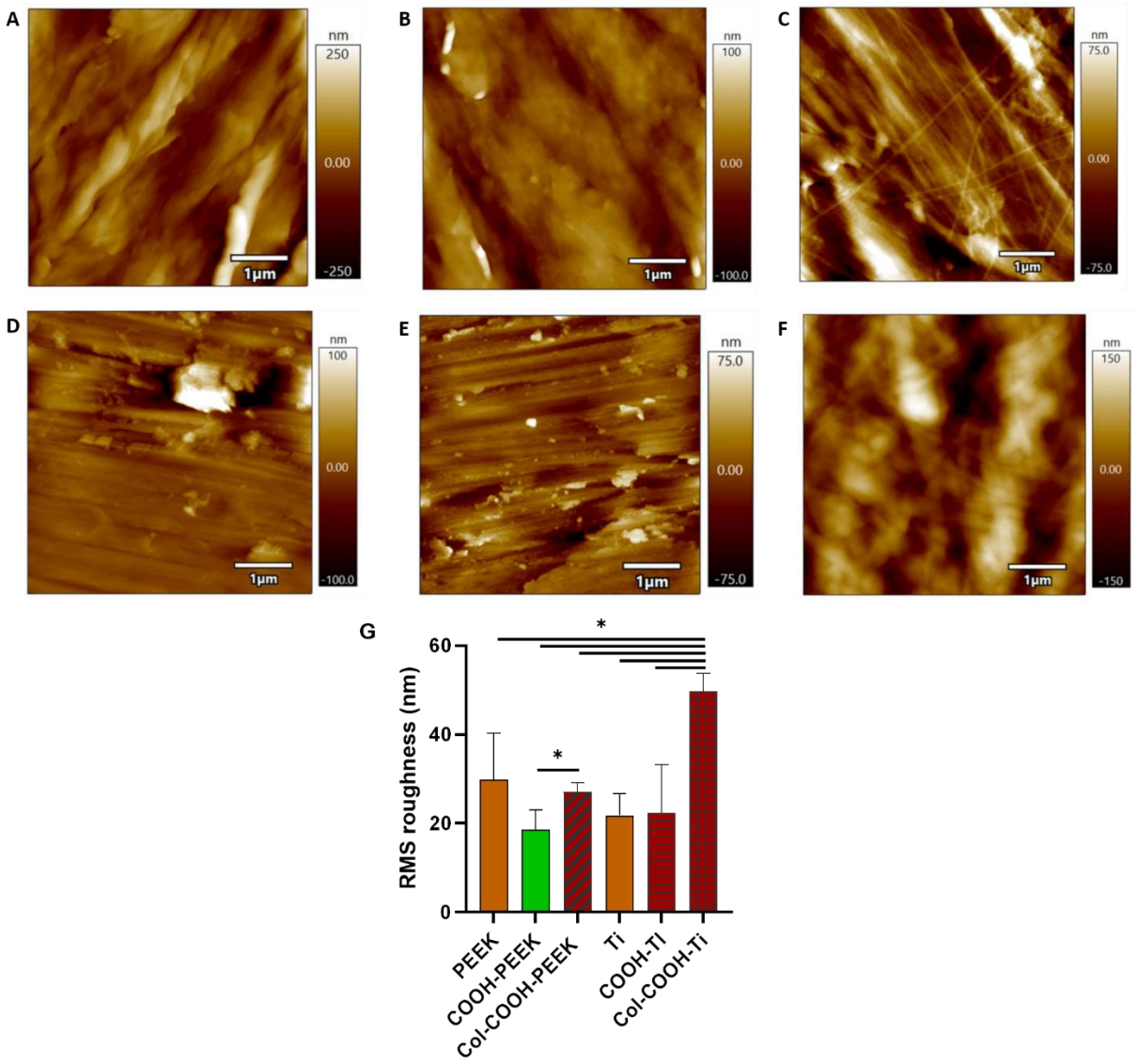

Figure 5.5. AFM images of (A) PEEK, (B) COOH-PEEK, (C) Col-COOH-PEEK, (D) Ti, (E) COOH-Ti, and (F) Col-COOH-Ti. (G) RMS roughness measurements of the six samples obtained from AFM imaging. The symbol (*) indicates significant differences with $p < 0.05$.

5.5. Water contact angle measurement

Water contact angle measurements show that Col-COOH-PEEK is more hydrophilic compared to PEEK and COOH-PEEK whereas there was no significant difference in wettability between PEEK and COOH-PEEK (**Error! Reference source not found.** A). For Ti samples, there was no significant difference in wettability among the three groups (Figure 5.6 B).

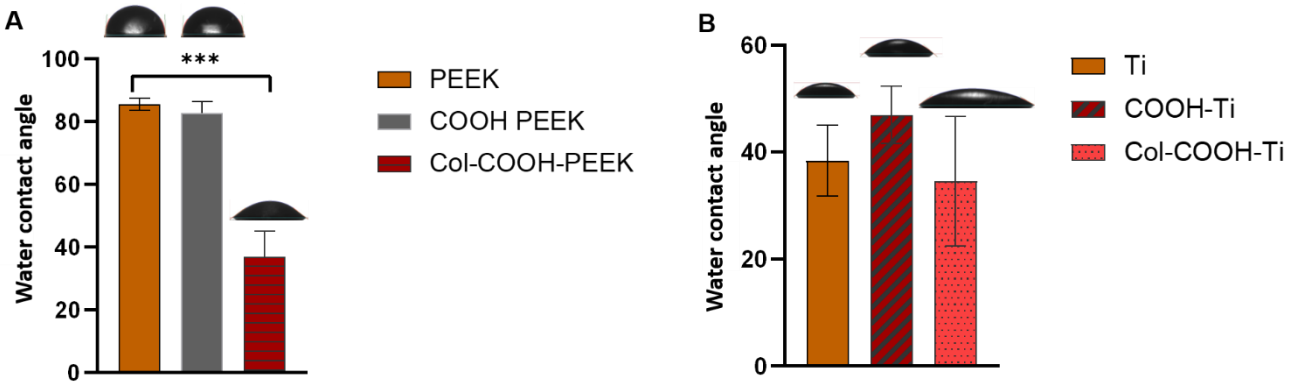

Figure 5.6. (A) Water contact angle measured on PEEK, COOH-PEEK and Col-COOH-PEEK. (B) Water contact angle measured on Ti, COOH-Ti and Col-COOH-Ti. The symbol (***) indicates significant differences with $p < 0.001$.

5.6. Effect of collagen I attachment on BL protein adsorption

Protein adsorption on biomaterials determines further interactions between cells and biomaterials. Therefore, in this experiment, we investigated the effect of attaching collagen proteins on PEEK and Ti on the adsorption of BL proteins. Protein scores of the key BL proteins adsorbed on PEEK, Col-COOH-PEEK, Ti and Col-COOH-Ti evaluated from mass spectrometry are shown in Figure 5.7A and Figure 5.7B; see Table 5.2 for an explanation of protein abbreviations. Both Ti samples adsorbed a larger variety of proteins than the PEEK samples. Fibronectin and peroxidasin homolog were the only two proteins that showed statistically higher adsorption on Col-COOH-PEEK than on PEEK, whereas laminin subunit gamma-1, nidogen-1, vimentin, heparan sulfate proteoglycan, myosin-9, fibronectin, and peptidyl-prolyl cis-trans isomerase B had statistically higher adsorption on Col-COOH-Ti compared to Ti.

Table 5.2 A legend of names and abbreviations of BL proteins adsorbed on PEEK, Col-COOH-PEEK, Ti, and Col-COOH-Ti identified by mass spectrometry.

Identified Proteins	Abbreviation	Presence in PEEK samples	Presence in Ti samples
Laminin subunit alpha-1	Lama1	Yes	Yes
Laminin subunit beta-1	Lamb1	Yes	Yes
Cluster of Laminin subunit gamma 1	Lamc1	Yes	Yes
Cluster of Nidogen-1	Nid1	Yes	Yes
Cluster of Vimentin	Vim	Yes	Yes
Basement membrane-specific heparan sulfate proteoglycan core protein	Hspg2	Yes	Yes

Cluster of Fibronectin	Fn1	Yes	Yes
Peroxidasin homolog	Pxdn	Yes	No
Cluster of Myosin-9	Myh9	Yes	Yes
Cluster of Fibrinogen beta chain	Fgb	Yes	No
Histone H2B type 1-B	Hist1h2bb	No	Yes
Histone H4	Hist1h4a	No	Yes
Actin, cytoplasmic 1	Actb	No	Yes
Serpin H1	Serpinh1	No	Yes
Peptidyl-prolyl cis-trans isomerase B	Ppib	No	Yes
60 kDa heat shock protein, mitochondrial	Hspd1	No	Yes

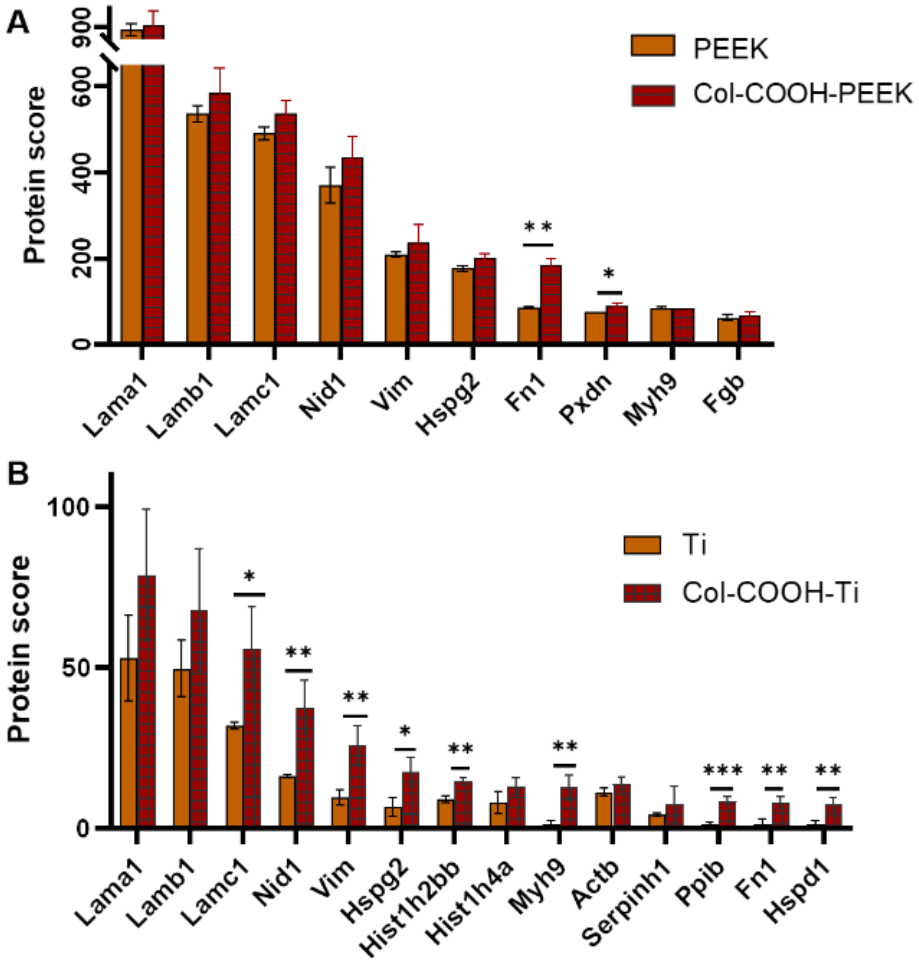

Figure 5.7. Proteomic scores measured by mass spectrometry for the adsorption of BL proteins on (A) PEEK and. Col-COOH-PEEK and (B) Ti and Col-COOH-Ti. All values are expressed as mean ± SD. The symbols (*, **, and ***) indicate significant differences between the groups with $p < 0.05$, <0.01, and <0.001, respectively.

5.7. Cell culture

5.7.1. Live/dead fluorescence imaging

The live/dead assay of PDL fibroblast cells showed that all samples were biocompatible, as no dead cells were visible at any timepoint (Figures 5.8 and 5.9). The high background in PEEK, COOH-PEEK, and Col-COOH-PEEK images is due to PEEK autofluorescence, which occurs in the same wavelength range as the green dye use for these assays. Because of this, a magnification higher than 2.5X was harder to obtain for the PEEK samples (Figure 5.8) while a 10X magnification was used for the Ti samples (Figure 5.9).

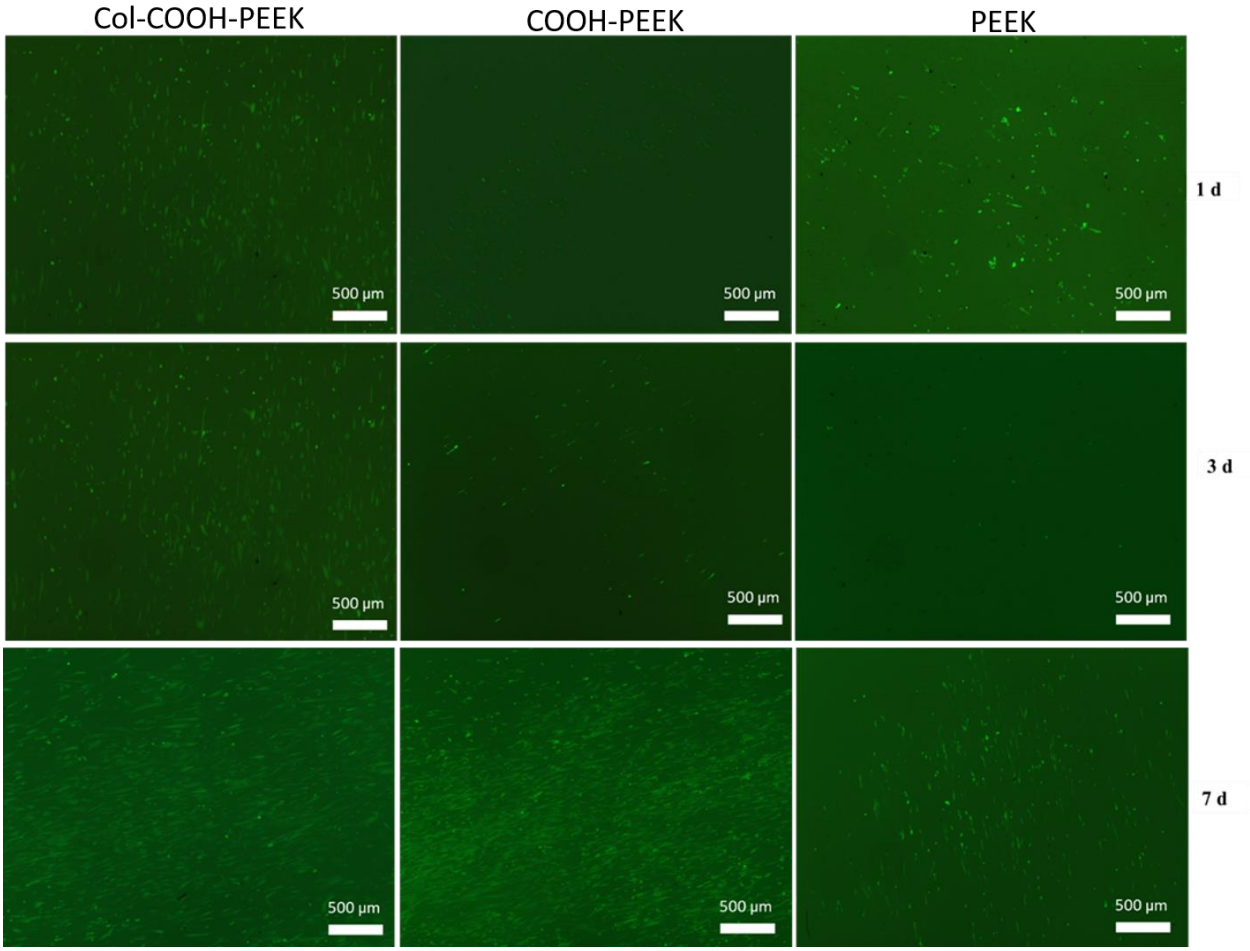

Figure 5.8 Live/dead assays of PDL fibroblast cells (magnification 2.5 X after 1d, 3d, and 7d of seeding on PEEK, COOH-PEEK and Col-COOH-PEEK.

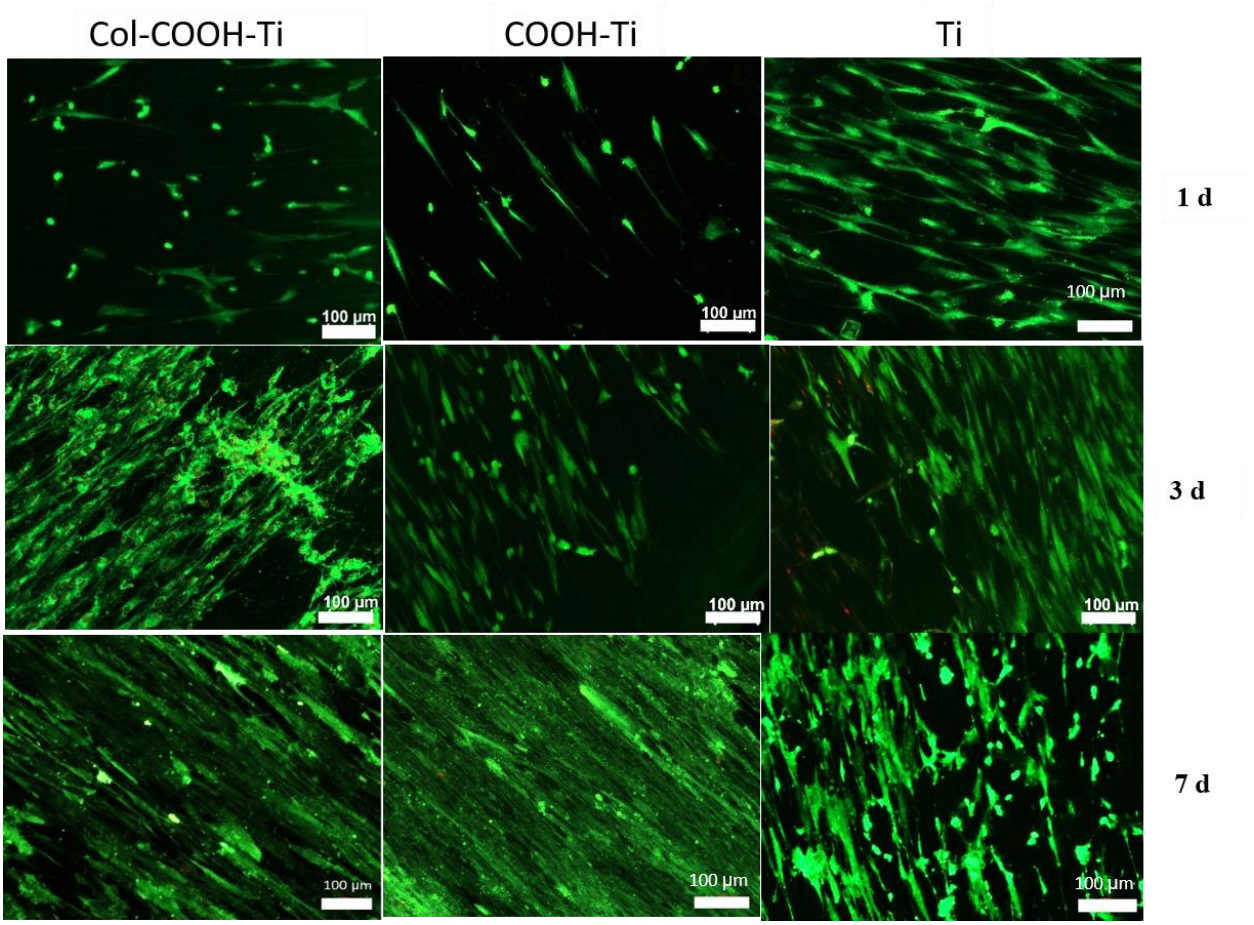

Figure 5.9 Live/dead assays of PDL fibroblast cells (magnification 2.5 X after 1d, 3d, and 7d of seeding on Ti, COOH-Ti, and Col-COOH-Ti.

5.7.2. Quantification of PDL fibroblast cell proliferation

PDL fibroblast cell proliferation was measured using the Alamar blue assay. Figure 5.10 A shows that Col-COOH-PEEK promoted statistically higher proliferation of PDL fibroblast cells compared to PEEK and COOH-PEEK on the seventh day after culturing. Although, there were no significant differences in cell proliferation at previous timepoints, Col-COOH-PEEK still showed higher proliferation than the other two groups (Figure 5.10 A). TCPS (the positive control) showed consistent proliferation over time. On day 1 it had statistically significant higher cell proliferation

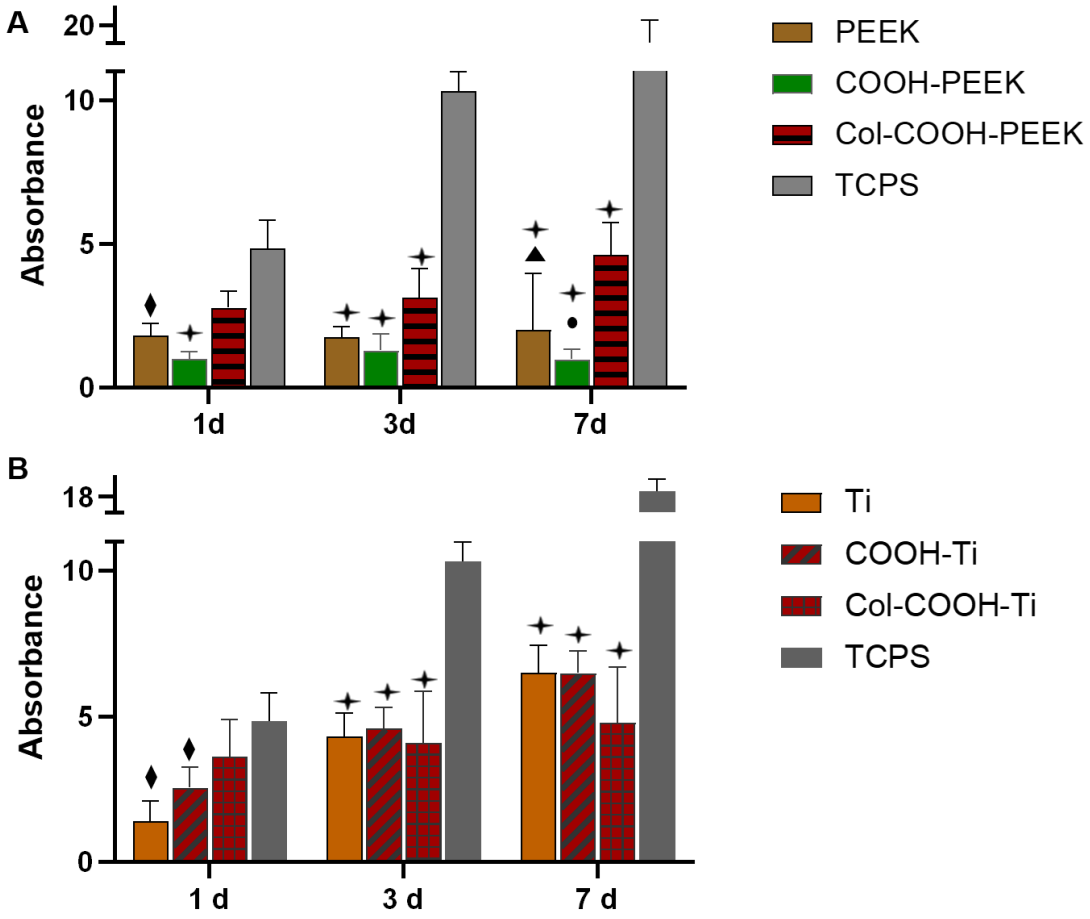

Figure 5.10. Proliferation rates of PDL fibroblast cells on (A) PEEK, COOH-PEEK, and Col-COOH-PEEK measured by Alamar blue assay (B) Ti, COOH-Ti, and Col-COOH-Ti measured by Alamar blue assay. TCPS is used as positive control in both A and B. Cell proliferation is demonstrated by the absorbance intensity values of cellular Almar blue on days 1, 3 & 7 after cell seeding (n= 9 per group). The symbols (♦ and ✦) indicate significant differences with TCPS with $p<0.01$ and $p<0.001$, respectively, while the symbols (▲ and ●) indicates significant differences with Col-COOH-PEEK ($p < 0.05$ and $p<0.001$, respectively).

than PEEK and COOH-PEEK but not Col-COOH-PEEK, however, it was higher than all of the groups in the other timepoints.

For Ti samples, Ti, COOH-Ti, and Col-COOH-Ti promoted proliferation of PDL fibroblast cells but no significant differences in cell proliferation between different Ti modifications were observed at any timepoint (Figure 5.10 B).

6. Discussion

6.1. Interaction of tooth proteins with BL proteins

At the interface between the teeth and the gingival tissue, the JE cells secret BL proteins that strongly adsorb on the teeth from one side and to the JE cell receptors from the other side, thus creating a strong seal between the teeth and JE cells. It was also shown before that BL proteins interact more strongly with the tooth proteins than the tooth minerals [23]. Therefore, the first objective of this work was to investigate the interaction between tooth proteins and BL proteins and determine which tooth protein bind tightly to BL proteins. We used Matrigel, which is composed of BL proteins derived from Engelbreth-Hom-Swarm mouse tumor cells, to model BL proteins. Matrigel contains all major components of human BL proteins such as laminins, collagen IV, nidogen, perlecan, and growth factors. Despite this similarity in composition, Matrigel does not necessarily have the exact amount of different protein that is found in BL layer in specific organs including tooth gingiva [154, 155]. Also, the crosslinking between the components is not necessarily replicating the in-vivo BL [156, 157]. The wide use of Matrigel as a model of BL is justified by two reasons: the first reason is the difficulty of producing large quantities of authentic tissue-specific BL matrices due to their minute amount (with a thickness of 50-100 nm) and complex structure; the second reason is that since the same components are found in both Matrigel and BL matrices, Matrigel provide both chemical and mechanical cues similar to in-vivo behaviors [155, 158]. For there reasons, we used Matrigel in this work to model BL matrix of gingival epithelial cells. We then used label-free mass spectrometry to analyze the adsorption of tooth proteins on Matrigel [112]. This technique allows identifying and quantifying large sets of proteins much faster than other protein identification methods such as western blot and immunoassays [78, 143]. It was successfully used in many studies, for instance, to identify protein content of murine

intervertebral discs [144], the proteins adsorbed from a mouse embryonic fibroblast on plasma-etched polystyrene surfaces [159], and Matrigel proteins adsorbed on several biomaterials [78].

Our first experiment shows that of the tooth proteins that have the highest affinity for Matrigel, two are isoforms of collagen (Col XI and Col I); Col XI has the highest score of all proteins, which is correlated with the amount of the protein of the tooth proteins that adsorbed on BL proteins. Col XI is a fibrillar protein composed of 3 α chains named α1, α2, and α3. It is composed of one triple helical collagenous domain, C-terminal non-collagenous domain, and N-terminal non-collagenous (N-terminal NC) domain. The three α chains have major differences in the N-terminal NC domain. Col XI co-assemble with other collagen types including Col I, II, and III and functions as a regulator of fibrillogenesis by nucleating collagen fibril formation [160]. The other proteins found in the experiment included laminins (laminin subunits β1 and γ1), histones (histone H4, H2B and H2AX), serum proteins (albumin, Alpha-2-HS-glycoprotein and prothrombin), and five other proteins shown in table 5.1. These proteins are not actually found in teeth (see section 2.6); their presence may be due to the use in our experiments of whole teeth, which may have had BM proteins adsorbed on their surface and remnants of neurons and blood vessels in the pulp. If we neglect these non-tooth proteins, we can conclude that Col XI and Col I are the two proteins present in teeth that interact more strongly with BL proteins, represented here by Matrigel. Hence, they are the best candidates to functionalize the surface of dental implants to increase their affinity with BL proteins. In our next set of experiments, we then modified the surface of PEEK and Ti with collagen I. We chose Col I because of its abundance in teeth and its presence in all of tooth parts in contact with gingival tissue, which are enamel, dentin, and cementum. Moreover, Col I was practical to use in terms of availability and price. However, further studies will aim to examine the effect of functionalizing Col XI on implants to study its effect on BL protein adsorption and cell interaction.

6.2. Characterization of PEEK and Ti and their modifications

We used 3 methods to verify the modification of PEEK and Ti surfaces with carboxylic groups: surface elemental analysis using XPS, TBO adsorption assay and TFE conjugation to carboxylic groups. We used XPS as the main characterization technique due to its high surface sensitivity. XPS provides information about surface composition within ~ 10 nm of the surface, which is ideal for detection of both diazonium modification and protein functionalization [161]. PEEK surface composition showed the presence of just C and O both before and after diazonium modification.

This result shows that reaction with PABA did not introduce N atoms on the PEEK surface, although they are present in PABA; this is because the amino group from PABA, transformed into a diazonium cation, is lost after forming a radical (Figure 4.4) [145]. The high-resolution spectra of C1s provided a way to analyze different carbon bonds in PEEK and COOH-PEEK, which confirmed higher percentage of carboxylic bond in COOH-PEEK compared to PEEK. The quantification of the peak corresponding to COOH bond was close to the value reported in the literature for PEEK functionalized with poly (acrylic acid) [162]. We also used TBO assay for quantitative assessment of the number of carboxylic groups [150, 151]. Although the assay confirmed that the amount of TBO dye on COOH-PEEK was higher than PEEK, there was TBO dye on PEEK, indicating some non-specific TBO adsorption on PEEK strong enough to withstand NaOH washing. The third method was using TFE due to its selective conjugation to carboxylic groups. The detection of a peak corresponding to F in F-COOH-PEEK but not in F-PEEK confirmed the presence of carboxylic groups only in COOH-PEEK samples, hence supporting the success of the diazonium reaction. The TFE method was a complementary method to the high-resolution spectra obtained from the COOH-PEEK and COOH-Ti.

As for Ti samples, all of the elements relative to the Ti alloy surface (namely Ti, Al and N present in the alloy composition and O due to the native surface oxide layer) decreased after addition of PABA in the COOH-Ti samples, while C increased; this result suggests a successful formation of a carboxylated layer on the sample surface. We found a very small amount of P on one of the Ti samples, which we attribute to contamination; P increased on COOH- Ti, most likely indicating the presence of remnants of hypophosphorous acid used during the diazonium reaction. Although the same method was used to modify both PEEK and Ti, we observed a higher amount of carboxylic groups on COOH-Ti compared to COOH-PEEK as shown in TBO assay in Figure 5.3 and Figure 5.2, respectively.

Proteins have been used extensively to coat several materials to change their surface properties [61, 64, 84]. The proteins can be either physically adsorbed on the surface of biomaterials or chemically conjugated to these surfaces. Physisorption is not ideal for long term applications since proteins can easily peel off and get degraded by body enzymes. Therefore, chemical conjugation of the proteins on surfaces of biomaterials can achieve long-term success. Among various conjugation methods, the EDC-NHS coupling method has several advantages. It is easy to perform

and independent on the surface of the material as long as it has the right functional groups. It also provides a zero-length spacer meaning that it directly links the protein to the biomaterial while it does not become a permanent part of the linkage [163]. We demonstrated this versatility of the EDC-NHS method by conjugating collagen proteins to two different types of biomaterials, PEEK and Ti. We used the atomic percentage of N of the surface obtained from XPS spectra as an indication of the amount of collagen since no N was detected prior to functionalization on PEEK or Ti (except for trace amount on Ti). Figure 5.4 shows that the atomic percentage of N on Col-COOH-PEEK and Col-COOH-Ti varied from 10 to17 %. These values were similar to the values reported by previous studies that conjugated collagen on Ti even though they used different linkages [91, 164]. The efficacy of the EDC/NHS coupling is shown by our control samples Col-PEEK and Col-Ti, prepared without carboxylic substrate modification. The amount of collagen physisorbed on these samples was easily rinsed away with SDS, and after rinsing, these substrates showed much lower N% and higher substrate signal (for the Ti samples) (Figure 5.4). The effect of washing the surfaces with SDS on removing most of adsorbed proteins is an agreement with previous research [165].

High resolution C1s spectra confirmed the survey results for the Col-Ti and Col-COOH-Ti samples. Since collagen possess C-N bonds (which has similar binding energy as C-O bond), we expected higher peak at binding energy of 286 eV corresponding to C-O and C-N bonds. This was confirmed in the case of Ti as shown in Figure 5.4. However, no statistical difference was observed in the atomic percentage of the C-O/C-N bond between Col-PEEK and Col-COOH-PEEK (Figure 5.4). This can be attributed to the presence of an ether bond (C-O-C) in the PEEK structure itself, which can mask differences in C-N amounts between the two samples.

Contact angle measurements showed no significant differences after carboxylation in both PEEK and Ti while Col-COOH-PEEK showed significantly lower contact angle compared to PEEK and COOH-PEEK. The reason that carboxylation did not affect the wettability can be attributed to the low density of carboxylic functional groups introduced on the surfaces as demonstrated in the TBO dye adsorption experiment (Figure 5.2c and 5.3c). Similar results were shown in pervious work where diazonium chemistry was used to introduce carboxylic groups on silk fibroin [166].

The AFM images confirmed the presence of collagen fibres in Col-COOH-PEEK and Col-COOH-Ti (Figure 5.5). the RMS roughness values were significantly higher in the collagen modified

samples with Col-COOH-Ti showing the highest roughness. Since there were no differences in the RMS values between PEEK and Ti, we attribute the increase in RMS values in collagen modified samples to the presence of collagen fibers. Based on this hypothesis, the differences between RMS values of Col-COOH-PEEK and Col-COOH-Ti can be explained by either difference in amount of collagen on the surface of the two materials or difference in collagen conformations. To test this hypothesis, future work should quantify the amount of collagen on each surface and augment the results with AFM imaging.

Finally, covalently bound collagen I on Col-COOH-PEEK and Col-COOH-Ti was stable for at least 7 days. We obtained this result by quantifying the atomic percentage of N on the surface of the samples for 7 days with no statistically significant difference over time (Figure S3). These results are in agreement with a previous study that investigated the stability of covalently bound collagen I on Ti for 2 days in similar pH [164].

6.3. Protein adsorption and cell proliferation

We used the label-free mass spectrometry technique again to evaluate the effect of collagen I immobilization on BL protein adsorption. Previous studies have used this technique to investigate the effect of physicochemical properties of biomaterials such as roughness and chemical properties on protein adsorption [78, 144, 167]. Several materials were investigated in these studies including Ti, polystyrene, PMMA, and poly (D,L-lactic acid) (PDLLA) using protein sets such as human serum proteins [167], mouse embryonic fibroblast conditioned medium [159], and BL proteins (Matrigel) [78]. However, this is the first study to our knowledge to investigate the proteomics signature of PEEK in contact with a large protein set such as BL proteins (Matrigel). Understanding BL protein adsorption on PEEK and comparing it with that of Ti provide more insight into the effect of material physicochemical properties on protein adsorption. In addition, investigating the effect of changing the surface chemistry of PEEK and Ti (through collagen conjugation) would shed more light on how we can tailor these physicochemical surface properties to favor adsorption of certain protein that would enhance cell adhesion. Results from PEEK samples showed that Col-COOH-PEEK adsorbed significantly higher amount of fibronectin and peroxidasin homolog than PEEK samples. For Ti samples, several BL proteins were adsorbed in higher amounts on Col-COOH-Ti compared to Ti including laminin, nidogen, and fibronectin. The comparison between PEEK and Ti is difficult because the range of BL protein scores in PEEK and Col-COOH-PEEK is on average 5 times higher than that of Ti and Col-COOH-Ti. This result is

surprising because a previous study by Gorth et al that used enzyme-linked immunosorbent assay (ELISA) method for protein quantification showed that the amount of laminin adsorbed on titanium was double the amount adsorbed on PEEK [168]. Possible reasons for this difference include different materials in Gorth's study, Ti grade 4 was used while in our study Ti-6Al-4V alloy was used; also, in Gorth et al, the Ti grade 4 substrate was rougher than the PEEK substrate, which is the opposite of our study. In fact, in a different study, the protein scores of adsorbed BL proteins on grade 2 titanium samples were in similar range to the current work shown in Figure 5.7 B [78].

We discussed in section 2.4 the importance of laminins and nidogens as structural components of the BL and their functional role in connecting epithelial cells with the underlying tissue. Therefore, the presence of laminins and nidogen with the highest amount among the adsorbed BL proteins on Col-COOH-Ti implies that this material has higher potential than Ti for subsequent steps of cell attachment and proliferation due to their physicochemical properties (Figure 5.7 B). Although laminin and nidogen had the highest scores among BL proteins of adsorption on Col-COOH-PEEK, these scores were not significantly different than their scores on PEEK (Figure 5.7 A). Fibronectin was the only BL protein that had significantly higher adsorption on both Col-COOH-PEEK and Col-COOH-Ti than on PEEK and Ti, respectively. Therefore, it is important to examine its function and whether it has a role in subsequent cell-biomaterial interactions. Fibronectin is a glycoprotein that has adhesive properties like laminins. It exists as a soluble form in the plasma or a non-soluble form in the ECM; the non-soluble form is more active and involved in many of the protein functions [169]. The non-soluble fibronectin contributes to ECM-cell adhesion through its multiple binding sites [59]. In fact, it can bind to other ECM components such as heparin sulphate and fibrin and to cell surface receptors such as integrins through multiple sequences; the most well-known one is Arg–Gly–Asp (RGD) [169]. There are around 20 different isoforms of fibronectin, which differ in their ability to bind different cell integrins. Fibronectin has also specific binding sites for collagens, which could explain its larger adsorption on Col-COOH-PEEK and Col-COOH-Ti than on PEEK and Ti. Fibronectin has a pivotal role during wound healing as it promotes cell migration, growth, and differentiation by adsorption of fibrin and upregulating focal adhesion expression [60, 170]. These functions of fibronectin suggest that the Col-COOH-PEEK and Col-COOH-Ti samples may promote fibroblast and epithelial cell adhesion and proliferation. Overall,

the results of the BL protein adsorption experiment suggest that functionalization of PEEK and Ti with collagen improves adsorption of key BL proteins that are able to promote cell attachment.

While protein adsorption represents the first reaction of the body towards a foreign material, a following and more important step is cell interaction. Therefore, ensuring cell adhesion and proliferation are crucial evaluation criteria for the success of the implant. Junctional epithelial cells and periodontal fibroblasts are relevant cell lines to test interactions of dental implants with soft tissue. However, we think periodontal ligament fibroblast cell line was enough as a proof-of-concept in this work. Col-COOH-PEEK consistently promoted proliferation of fibroblast cells compared to COOH-PEEK and PEEK, whereas there were no significant differences among Ti, COOH-Ti and Col-COOH-Ti. Previous research pointed out the superiority of Ti to PEEK in terms of fibroblast proliferation on their surfaces [171]. This is confirmed in the current result as the cell proliferation on Ti was greater than on PEEK. However, the presence of collagen on PEEK brought cell proliferation on the Col-COOH-PEEK samples up to the same values measured on the Ti samples. To the best of our knowledge, this is the first study to investigate the effect of modifying PEEK sample with collagen on improving fibroblast proliferation. On the other hand, several previous studies reported a trend of increasing fibroblast cell proliferation over time when seeded on Ti functionalized with collagen [61, 91]. In these studies, the presence of collagen on the surface of titanium samples led to much higher cell viability compared to bare titanium, which is different from the results we obtained in Figure 5.10 B. One explanation for these variations could be the difference of collagen protein conformation on the surface of Ti due to differences in the conjugation technique. In fact, a previous study showed that the wettability of the surface affected collagen conformation that consequently affected fibroblast cell adhesion and spreading [172]. Therefore, future work should focus on investigating the effect of conjugating collagen using EDC/NHS method on its conformation and subsequently cell adhesion and proliferation.

6.4. Future work and limitations

This work investigated the interaction between tooth proteins and BL proteins to determine which tooth protein has the highest adsorption into BL proteins, which led to the choice of collagen protein. Based on these results, collagen was conjugated on two dental implants materials, PEEK and Ti, to enhance their ability to adsorb BL proteins and improve soft tissue cell adhesion and integration. Col-COOH-PEEK and Col-COOH-Ti improved the adsorption of key BL proteins

such as laminin, nidogen, and fibronectin. They also improved PDL fibroblast cell viability although it was only statistically significant in Col-COOH-PEEK.

While these results show the promise of the proposed approach, many more experiments should be done to bring this technology closer to clinical translation including further in-vitro testing and performing ex-vivo and in-vivo testing. In-vitro assessment should include a gingival epithelial cell line due to the pivotal role of these cells in the formation of a tight seal with the teeth. In addition to testing viability and proliferation by MTS assay or Alamar blue assay, the formation of focal adhesion complexes that are evidence of cell adhesion on the materials should also be investigated. Ex-vivo testing can be performed using artificial full-thickness skin model with key structural and functional aspects of natural skin. An example is EpiDermFT, a model that serves as a reliable system to identify toxic or corrosive properties of percutaneous devices [173]. In-vivo tests could be done using a mice model such as those already established to assess skin integration of biomaterials in the dorsal skin in eight-week-old male C57BL/6 mice [119]. The tested materials should be in dorsal percutaneous defects. After a healing period of 1, 2 and 4 weeks, the implant sites will be retrieved, fixed, and sectioned for histological assessment of epithelial integration. The histological analyses will provide the relative number of epithelial cells attached to the different surfaces and compare the presence of attached organelles (i.e. hemidesmosomes, and tight junction proteins).

Another important aspect to investigate is the conformation of the proteins on the surface of the materials as pointed out in section 6.3. The physicochemical properties of the implant material directly affect the protein conformation on the surface [172]. Previous studies showed that in the interactions between fibroblast cells and ECM proteins, α1β1 and α2β1 integrin receptors interact with specific sequences found in collagen proteins such as aspartic acid–glycine–glutamate–alanine (DGEA) or glycine–phenylalanine–hydroxyproline–glycine–glutamate–arginine (GFOGER) [174, 175]. Therefore, collagen conformations that expose these sequences can lead to higher fibroblast cell adhesion than other conformations. in the current work, EDC/NHS coupling method was done so that covalent linkages were formed randomly with any free primary amine group on collagen proteins. With this in mind, in future work, collagen proteins can be selectively bound on material surfaces through one of their terminal groups to preserve their three-

dimensional configuration and ensure that sequences such as DGEA and GFOGER are accessible by cell receptors.

Another point that can be explored is the effect of other tooth proteins that were identified in the Mat-tooth protein sample mainly Col XI as it showed the highest score among the tooth proteins strongly adsorbed to Matrigel. Although Col XI is present in the teeth in lower amounts thanCol I, investigating the effect of functionalizing implants with Col XI and comparing them with Col I could provide even more biomimetic materials that could achieve better sealing with the gingival tissue. Col XI can be used to functionalize the surface of implants in the same way Col I was used in this study. After that, the biological activity (BL protein adsorption and epithelial cell proliferation) of functionalized surfaces can be compared with the results obtained from Col I-functionalized sufaces to determine if Col XI has more potential as surface coating to improve soft tissue integration compared with Col I.

In addition to the limitations highlighted above, another limitation of the current work is inherent to the use of mass spectrometry for protein identification. While this technique has the great advantage of being able to identify large number of proteins in one measurement, it does not accurately differentiate highly homologous proteins. The technique is based on breaking the protein into small peptide sequences and identify these peptides. Then, the identified peptides are compared to a database of protein sequences to be matched with the closest protein sequence. The more the identified peptides cover the whole protein sequence, the higher the accuracy of the identification process. But for highly homologous proteins, certain sets of peptides can identify more than one protein. Thus, this technique is ideally used as a filter to identify the most abundant proteins, and it should be coupled with other techniques such as ELISA to have a more precise identification and quantification.

7. Conclusion

This work used collagen proteins to modify the surface of materials used as dental implants, mimicking what nature successfully implements to protect the body from infections where skin is breached at the interface with teeth. We showed that collagen is likely a key factor in adsorbing BL proteins deposited by the JE. Collagen conjugated PEEK and Ti adsorbed higher amounts of key basal BL proteins (laminin, nidogen, and fibronectin) and resulted in higher fibroblast cell proliferation compared to bare PEEK and Ti (although not statistically different for Ti). Despite

the limitations highlighted in the previous section, this work represents a first step towards the fabrication of implants that will create a better seal with the skin compared to current percutaneous devices. This could be a solution for long-term prevention of infection around dental implants, transcutaneous implants, and catheters, thus tremendously reducing associated morbidity and healthcare costs.

8. Appendix

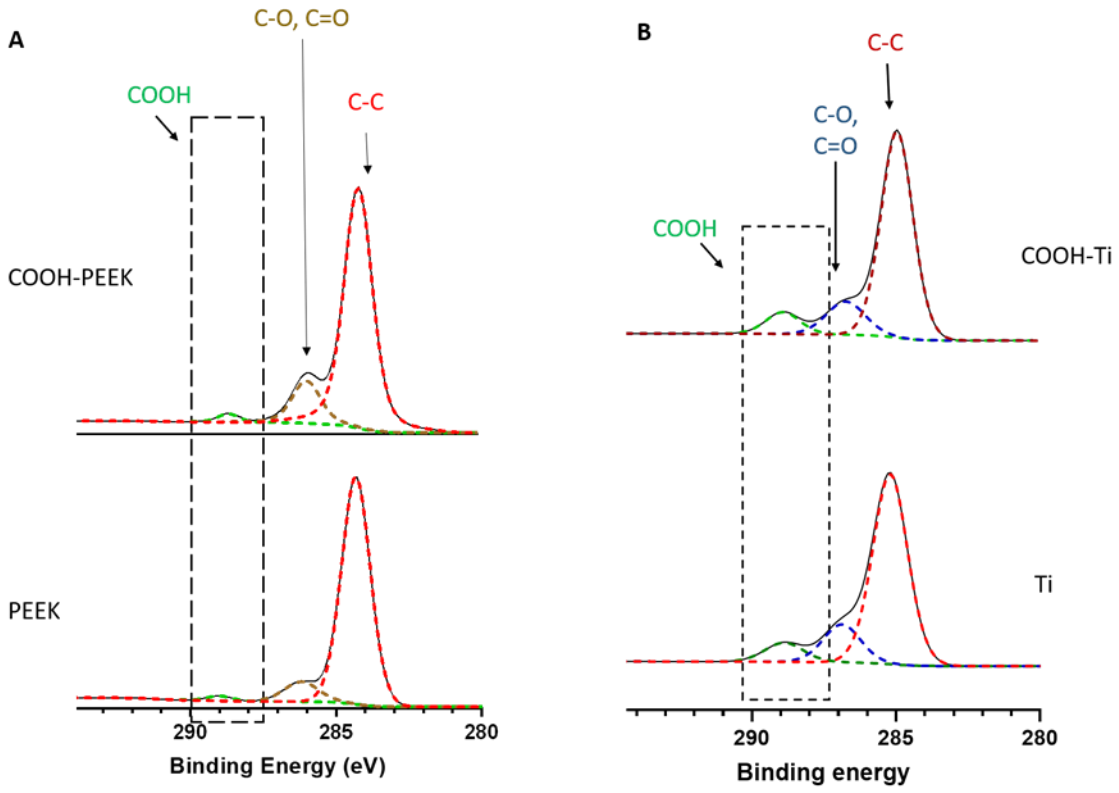

Figure S1. XPS high resolution spectra of C1s of (A) PEEK and COOH-PEEK and (B) Ti and COOH-Ti.

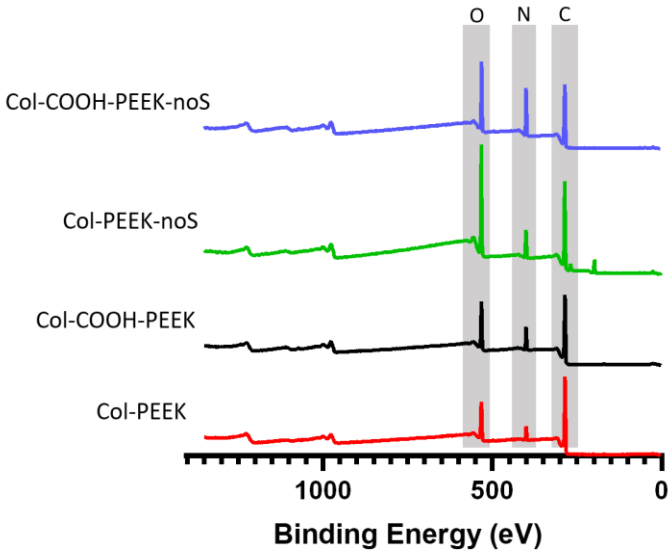

Figure S2. XPS survey spectra illustrating the surface elemental composition of col PEEK and col COOH PEEK before and after washing with (SDS) and sonication for 30 min (n=3 per group).

1. Characterization of collagen stability on biomaterials

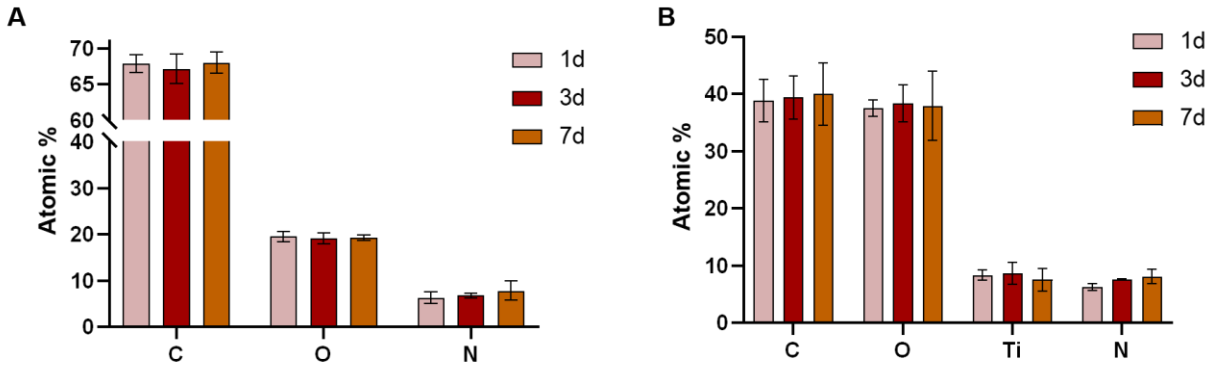

Figure S3. Atomic percentage of elements identified from XPS survey spectra of (A) Col-COOH-PEEK and (B) Col-COOH-Ti at 1d, 3d, and 7d.

9. References

1. von Recum, A.F., *Applications and failure modes of percutaneous devices: a review.* J Biomed Mater Res, 1984. **18**(4): p. 323-36.
2. Puckett, S.D., et al., *Nanotextured titanium surfaces for enhancing skin growth on transcutaneous osseointegrated devices.* Acta Biomaterialia, 2010. **6**(6): p. 2352-2362.
3. Pye, A.D., et al., *A review of dental implants and infection.* Journal of Hospital Infection, 2009. **72**(2): p. 104-110.
4. Pendegrass, C.J., A.E. Goodship, and G.W. Blunn, *Development of a soft tissue seal around bone-anchored transcutaneous amputation prostheses.* Biomaterials, 2006. **27**(23): p. 4183-4191.

5. Isackson, D., L.D. McGill, and K.N. Bachus, *Percutaneous implants with porous titanium dermal barriers: An in vivo evaluation of infection risk.* Medical Engineering & Physics, 2011. **33**(4): p. 418-426.
6. Aly, S.A., et al., *Success rates and factors associated with failure of temporary anchorage devices: A prospective clinical trial.* Journal of Investigative and Clinical Dentistry, 2018. **9**(3): p. e12331.
7. Campoccia, D., L. Montanaro, and C.R. Arciola, *The significance of infection related to orthopedic devices and issues of antibiotic resistance.* Biomaterials, 2006. **27**(11): p. 2331-2339.
8. Schierholz, J. and J. Beuth, *Implant infections: a haven for opportunistic bacteria.* Journal of Hospital Infection, 2001. **49**(2): p. 87-93.
9. Von Eiff, C., et al., *Infections associated with medical devices.* Drugs, 2005. **65**(2): p. 179-214.
10. Jacobsen, S.M., et al., *Complicated catheter-associated urinary tract infections due to Escherichia coli and Proteus mirabilis.* Clinical Microbiology Reviews, 2008. **21**(1): p. 26-+.
11. Atieh, M.A., et al., *The Frequency of Peri-Implant Diseases: A Systematic Review and Meta-Analysis.* Journal of Periodontology, 2013. **84**(11): p. 1586-1598.
12. Costa, S.F., M.H. Miceli, and E.J. Anaissie, *Mucosa or skin as source of coagulase-negative staphylococcal bacteraemia?* Lancet Infectious Diseases, 2004. **4**(8): p. 533-533.
13. Abdallah, M.N., et al., *Strategies for Optimizing the Soft Tissue Seal around Osseointegrated Implants.* Advanced Healthcare Materials, 2017. **6**(20).
14. Guy, S.C., et al., *In vitro attachment of human gingival fibroblasts to endosseous implant materials.* J Periodontol, 1993. **64**(6): p. 542-6.
15. Larsson, A., et al., *Histologic Evaluation of Soft Tissue Integration of Experimental Abutments for Bone Anchored Hearing Implants Using Surgery Without Soft Tissue Reduction.* Otology & Neurotology, 2012. **33**(8): p. 1445-1451.
16. Calliess, T., et al., *In vivo comparative study of tissue reaction to bare and antimicrobial polymer coated transcutaneous implants.* Materials Science & Engineering C-Materials for Biological Applications, 2016. **61**: p. 712-719.
17. Kim, H., et al., *Effects of surface topography on the connective tissue attachment to subcutaneous implants.* International Journal of Oral & Maxillofacial Implants, 2006. **21**(3): p. 354-365.
18. Alves, D. and M.O. Pereira, *Mini-review: Antimicrobial peptides and enzymes as promising candidates to functionalize biomaterial surfaces.* Biofouling, 2014. **30**(4): p. 483-499.
19. Allen, L.T., et al., *Surface-induced changes in protein adsorption and implications for cellular phenotypic responses to surface interaction.* Biomaterials, 2006. **27**(16): p. 3096-3108.
20. Wilson, C.J., et al., *Mediation of biomaterial-cell interactions by adsorbed proteins: A review.* Tissue Engineering, 2005. **11**(1-2): p. 1-18.
21. Roach, P., et al., *Modern biomaterials: a review-bulk properties and implications of surface modifications.* Journal of Materials Science-Materials in Medicine, 2007. **18**(7): p. 1263-1277.
22. Grossesiestrup, C. and K. Affeld, *Design Criteria for Percutaneous Devices.* Journal of Biomedical Materials Research, 1984. **18**(4): p. 357-382.
23. Abdallah, M.N., et al., *Comparative adsorption profiles of basal lamina proteome and gingival cells onto dental and titanium surfaces.* Acta Biomaterialia, 2018. **73**: p. 547-558.
24. Knabe, C., C. Grosse-Siestrup, and U. Gross, *Histologic evaluation of a natural permanent percutaneous structure and clinical percutaneous devices.* Biomaterials, 1999. **20**(6): p. 503-510.
25. Gristina, A.G., *Biomaterial-Centered Infection - Microbial Adhesion Versus Tissue Integration.* Science, 1987. **237**(4822): p. 1588-1595.
26. Duraccio, D., F. Mussano, and M.G. Faga, *Biomaterials for dental implants: current and future trends.* Journal of Materials Science, 2015. **50**(14): p. 4779-4812.

27. Liu, X., P.K. Chu, and C. Ding, *Surface modification of titanium, titanium alloys, and related materials for biomedical applications.* Materials Science and Engineering: R: Reports, 2004. **47**(3): p. 49-121.
28. Branemark, P.-I., *Osseointegrated implants in the treatment of the edentulous jaw. Experience from a 10-year period.* Scand. J. Plast. Reconstr. Surg. Suppl., 1977. **16**.
29. Jemat, A., et al., *Surface Modifications and Their Effects on Titanium Dental Implants.* BioMed Research International, 2015. **2015**: p. 791725.
30. Benic, G.I., et al., *Systematic review of parameters and methods for the professional assessment of aesthetics in dental implant research.* Journal of Clinical Periodontology, 2012. **39**(s12): p. 160-192.
31. Saini, M., et al., *Implant biomaterials: A comprehensive review.* World Journal of Clinical Cases, 2015. **3**(1): p. 52-57.
32. Bowers, K.T., et al., *Optimization of surface micromorphology for enhanced osteoblast responses in vitro.* International Journal of Oral & Maxillofacial Implants, 1992. **7**(3).
33. Gaviria, L., et al., *Current trends in dental implants.* Journal of the Korean Association of Oral and Maxillofacial Surgeons, 2014. **40**(2): p. 50-60.
34. Goharian, A., M.R. Abdullah, and M.R.A. Kadir, *9 - Bioinert Polymers (Polyetheretherketone)*, in *Trauma Plating Systems*, A. Goharian, Editor. 2017, Elsevier. p. 159-179.
35. Niinomi, M. and C.J. Boehlert, *Titanium Alloys for Biomedical Applications*, in *Advances in Metallic Biomaterials: Tissues, Materials and Biological Reactions*, M. Niinomi, T. Narushima, and M. Nakai, Editors. 2015, Springer Berlin Heidelberg: Berlin, Heidelberg. p. 179-213.
36. Faria, A.C., et al., *Experimental titanium alloys for dental applications.* J Prosthet Dent, 2014. **112**(6): p. 1448-60.
37. Torstrick, F.B., et al., *Getting PEEK to Stick to Bone: The Development of Porous PEEK for Interbody Fusion Devices.* Techniques in orthopaedics (Rockville, Md.), 2017. **32**(3): p. 158-166.
38. Johansson, P., et al., *Nanosized hydroxyapatite coating on PEEK implants enhances early bone formation: a histological and three-dimensional investigation in rabbit bone.* Materials, 2015. **8**(7): p. 3815-3830.
39. Deng, Y., et al., *Effect of surface roughness on osteogenesis in vitro and osseointegration in vivo of carbon fiber-reinforced polyetheretherketone-nanohydroxyapatite composite.* International journal of nanomedicine, 2015. **10**: p. 1425-1447.
40. Elias, C.N., *Factors affecting the success of dental implants.* Implant dentistry: a rapidly evolving practice. Rijeka: InTech, 2011: p. 319-64.
41. Dohan Ehrenfest, D.M., et al., *Classification of osseointegrated implant surfaces: materials, chemistry and topography.* Trends in Biotechnology, 2010. **28**(4): p. 198-206.
42. Jansen, J., et al., *Histologic evaluation of the osseous adaptation to titanium and hydroxyapatite-coated titanium implants.* Journal of biomedical materials research, 1991. **25**(8): p. 973-989.
43. Dhert, W., et al., *A histological and histomorphometrical investigation of fluorapatite, magnesiumwhitlockite, and hydroxylapatite plasma-sprayed coatings in goats.* Journal of biomedical materials research, 1993. **27**(1): p. 127-138.
44. de Groot, K., J.G.C. Wolke, and J.A. Jansen, *Calcium phosphate coatings for medical implants.* Proceedings of the Institution of Mechanical Engineers, Part H: Journal of Engineering in Medicine, 1998. **212**(2): p. 137-147.
45. Toth, J.M., et al., *Polyetheretherketone as a biomaterial for spinal applications.* Biomaterials, 2006. **27**(3): p. 324-334.
46. Mishra, S. and R. Chowdhary, *PEEK materials as an alternative to titanium in dental implants: A systematic review.* Clinical Implant Dentistry and Related Research, 2019. **21**(1): p. 208-222.

47. Rae, P.J., E.N. Brown, and E.B. Orler, *The mechanical properties of poly(ether-ether-ketone) (PEEK) with emphasis on the large compressive strain response.* Polymer, 2007. **48**(2): p. 598-615.
48. Buck, E., H. Li, and M. Cerruti, *Surface Modification Strategies to Improve the Osseointegration of Poly(etheretherketone) and Its Composites.* Macromolecular Bioscience, 2020. **20**(2): p. 1900271.
49. Kurtz, S.M. and J.N. Devine, *PEEK biomaterials in trauma, orthopedic, and spinal implants.* Biomaterials, 2007. **28**(32): p. 4845-4869.
50. Schwitalla, A. and W.-D. Müller, *PEEK dental implants: a review of the literature.* Journal of Oral Implantology, 2013. **39**(6): p. 743-749.
51. Tang, X., et al., *Influences of surface treatments with abrasive paper and sand-blasting on surface morphology, hydrophilicity, mineralization and osteoblasts behaviors of n-CS/PK composite.* Scientific Reports, 2017. **7**(1): p. 568.
52. Xu, A., et al., *Enhancement of osteogenesis on micro/nano-topographical carbon fiber-reinforced polyetheretherketone–nanohydroxyapatite biocomposite.* Materials Science and Engineering: C, 2015. **48**: p. 592-598.
53. Mahjoubi, H., et al., *Surface phosphonation enhances hydroxyapatite coating adhesion on polyetheretherketone and its osseointegration potential.* Acta Biomaterialia, 2017. **47**: p. 149-158.
54. Garrison, K.R., et al., *Clinical effectiveness and cost-effectiveness of bone morphogenetic proteins in the non-healing of fractures and spinal fusion: a systematic review*, in *NIHR Health Technology Assessment programme: Executive Summaries*. 2007, NIHR Journals Library.
55. Du, Y.-W., et al., *In vitro and in vivo evaluation of bone morphogenetic protein-2 (BMP-2) immobilized collagen-coated polyetheretherketone (PEEK).* Frontiers of Materials Science, 2015. **9**(1): p. 38-50.
56. Guillot, R., et al., *Assessment of a polyelectrolyte multilayer film coating loaded with BMP-2 on titanium and PEEK implants in the rabbit femoral condyle.* Acta biomaterialia, 2016. **36**: p. 310-322.
57. Han, C.M., et al., *Creation of nanoporous TiO2 surface onto polyetheretherketone for effective immobilization and delivery of bone morphogenetic protein.* Journal of Biomedical Materials Research Part A, 2014. **102**(3): p. 793-800.
58. Wu, J., et al., *Micro-porous polyetheretherketone implants decorated with BMP-2 via phosphorylated gelatin coating for enhancing cell adhesion and osteogenic differentiation.* Colloids and Surfaces B: Biointerfaces, 2018. **169**: p. 233-241.
59. Middleton, C.A., et al., *Fibronectin silanized titanium alloy: A bioinductive and durable coating to enhance fibroblast attachment in vitro.* Journal of Biomedical Materials Research Part A, 2007. **83a**(4): p. 1032-1038.
60. Pendegrass, C.J., M. El-Husseiny, and G.W. Blunn, *The development of fibronectin-functionalised hydroxyapatite coatings to improve dermal fibroblast attachment in vitro.* Journal of Bone and Joint Surgery-British Volume, 2012. **94b**(4): p. 564-569.
61. Ritz, U., et al., *The effect of different collagen modifications for titanium and titanium nitrite surfaces on functions of gingival fibroblasts.* Clinical Oral Investigations, 2017. **21**(1): p. 255-265.
62. Chimutengwende-Gordon, M., C. Pendegrass, and G. Blunn, *Enhancing the soft tissue seal around intraosseous transcutaneous amputation prostheses using silanized fibronectin titanium alloy.* Biomedical Materials, 2011. **6**(2): p. 025008.
63. Gordon, D.J., et al., *Modification of titanium alloy surfaces for percutaneous implants by covalently attaching laminin.* Journal of Biomedical Materials Research Part A, 2010. **94**(2): p. 586-593.
64. Zhu, Y., et al., *Polydopamine-mediated covalent functionalization of collagen on a titanium alloy to promote biocompatibility with soft tissues.* Journal of materials chemistry B, 2019. **7**(12).

65. Lee, S.W., et al., *Influence of microgroove dimension on cell behavior of human gingival fibroblasts cultured on titanium substrata.* Clinical oral implants research, 2009. **20**(1): p. 56-66.
66. Smith, B.S., et al., *Dermal fibroblast and epidermal keratinocyte functionality on titania nanotube arrays.* Acta biomaterialia, 2011. **7**(6): p. 2686-2696.
67. Jeyapalina, S., et al., *Efficacy of a porous-structured titanium subdermal barrier for preventing infection in percutaneous osseointegrated prostheses.* Journal of Orthopaedic Research, 2012. **30**(8): p. 1304-1311.
68. Chou, T.G.R., et al., *Evaluating antimicrobials and implant materials for infection prevention around transcutaneous osseointegrated implants in a rabbit model.* Journal of Biomedical Materials Research Part A: An Official Journal of The Society for Biomaterials, The Japanese Society for Biomaterials, and The Australian Society for Biomaterials and the Korean Society for Biomaterials, 2010. **92**(3): p. 942-952.
69. Farrell, B.J., et al., *Effects of pore size, implantation time, and nano-surface properties on rat skin ingrowth into percutaneous porous titanium implants.* Journal of Biomedical Materials Research Part A: An Official Journal of The Society for Biomaterials, The Japanese Society for Biomaterials, and The Australian Society for Biomaterials and the Korean Society for Biomaterials, 2014. **102**(5): p. 1305-1315.
70. Ge, X., et al., *Antibacterial coatings of fluoridated hydroxyapatite for percutaneous implants.* Journal of Biomedical Materials Research Part A, 2010. **95**(2): p. 588-599.
71. Tan, J., et al., *Anti-infection activity of nanostructured titanium percutaneous implants with a postoperative infection model.* Applied Surface Science, 2015. **344**: p. 119-127.
72. Larsson, A., et al., *Soft Tissue Integration of Hydroxyapatite-Coated Abutments for Bone Conduction Implants.* Clinical implant dentistry and related research, 2015. **17**: p. e730-e735.
73. Zhang, L., et al., *The dual function of Cu-doped TiO 2 coatings on titanium for application in percutaneous implants.* Journal of Materials Chemistry B, 2016. **4**(21): p. 3788-3800.
74. Jarrell, J.D., B. Dolly, and J.R. Morgan, *Rapid screening, in vitro study of metal oxide and polymer hybrids as delivery coatings for improved soft-tissue integration of implants.* Journal of Biomedical Materials Research Part A: An Official Journal of The Society for Biomaterials, The Japanese Society for Biomaterials, and The Australian Society for Biomaterials and the Korean Society for Biomaterials, 2010. **92**(3): p. 1094-1104.
75. Bruckmann, C., et al., *Periodontal ligament and gingival fibroblast adhesion to dentin-like textured surfaces.* Biomaterials, 2005. **26**(3): p. 339-346.
76. Nematollahi, M., et al., *Hexagonal micron scale pillars influence epithelial cell adhesion, morphology, proliferation, migration, and cytoskeletal arrangement.* Journal of Biomedical Materials Research Part A: An Official Journal of The Society for Biomaterials, The Japanese Society for Biomaterials, and The Australian Society for Biomaterials and the Korean Society for Biomaterials, 2009. **91**(1): p. 149-157.
77. Underwood, R.A., et al., *Quantifying the effect of pore size and surface treatment on epidermal incorporation into percutaneously implanted sphere-templated porous biomaterials in mice.* Journal of Biomedical Materials Research Part A, 2011. **98A**(4): p. 499-508.
78. Abdallah, M.-N., et al., *Biomaterial surface proteomic signature determines interaction with epithelial cells.* Acta biomaterialia, 2017. **54**: p. 150-163.
79. Ramenzoni, L.L., T. Attin, and P.R. Schmidlin, *In vitro effect of modified polyetheretherketone (PEEK) implant abutments on human gingival epithelial keratinocytes migration and proliferation.* Materials, 2019. **12**(9): p. 1401.
80. Rea, M., et al., *Marginal healing using Polyetheretherketone as healing abutments: an experimental study in dogs.* Clinical oral implants research, 2017. **28**(7): p. e46-e50.

81. Feng, X., et al., *Three-dimensionally-printed polyether-ether-ketone implant with a cross-linked structure and acid-etched microporous surface promotes integration with soft tissue.* International journal of molecular sciences, 2019. **20**(15): p. 3811.
82. Wang, X., et al., *Selective responses of human gingival fibroblasts and bacteria on carbon fiber reinforced polyetheretherketone with multilevel nanostructured TiO2.* Biomaterials, 2016. **83**: p. 207-218.
83. Pendegrass, C.J., et al., *The effect of adherens junction components on keratinocyte adhesion in vitro: Potential implications for sealing the skin-implant interface of intraosseous transcutaneous amputation prostheses.* Journal of Biomedical Materials Research Part A, 2012. **100**(12): p. 3463-3471.
84. Koidou, V.P., et al., *Peptide coatings enhance keratinocyte attachment towards improving the peri-implant mucosal seal.* Biomaterials science, 2018. **6**(7): p. 1936-1945.
85. Wang, J., et al., *Surface modification via plasmid-mediated pLAMA3-CM gene transfection promotes the attachment of gingival epithelial cells to titanium sheets in vitro and improves biological sealing at the transmucosal sites of titanium implants in vivo.* Journal of Materials Chemistry B, 2019. **7**(46): p. 7415-7427.
86. Yang, M., et al., *Dopamine self-polymerized along with hydroxyapatite onto the preactivated titanium percutaneous implants surface to promote human gingival fibroblast behavior and antimicrobial activity for biological sealing.* Journal of biomaterials applications, 2018. **32**(8): p. 1071-1082.
87. Pendegrass, C., M. El-Husseiny, and G. Blunn, *The development of fibronectin-functionalised hydroxyapatite coatings to improve dermal fibroblast attachment in vitro.* The Journal of bone and joint surgery. British volume, 2012. **94**(4): p. 564-569.
88. Chimutengwende-Gordon, M., C. Pendegrass, and G. Blunn, *The in vivo effect of a porous titanium alloy flange with hydroxyapatite, silver and fibronectin coatings on soft-tissue integration of intraosseous transcutaneous amputation prostheses.* The bone & joint journal, 2017. **99**(3): p. 393-400.
89. Fukano, Y., et al., *Epidermal and dermal integration into sphere-templated porous poly (2-hydroxyethyl methacrylate) implants in mice.* Journal of Biomedical Materials Research Part A, 2010. **94**(4): p. 1172-1186.
90. Oyane, A., et al., *Preliminary in vivo study of apatite and laminin-apatite composite layers on polymeric percutaneous implants.* Journal of Biomedical Materials Research Part B: Applied Biomaterials, 2011. **97B**(1): p. 96-104.
91. Marin-Pareja, N., et al., *Collagen-functionalised titanium surfaces for biological sealing of dental implants: effect of immobilisation process on fibroblasts response.* Colloids Surf B Biointerfaces, 2014. **122**: p. 601-610.
92. Ferraris, S., et al., *Nanogrooves and keratin nanofibers on titanium surfaces aimed at driving gingival fibroblasts alignment and proliferation without increasing bacterial adhesion.* Materials Science and Engineering: C, 2017. **76**: p. 1-12.
93. Tobin, D.J., *Biochemistry of human skin - our brain on the outside.* Chemical Society Reviews, 2006. **35**(1): p. 52-67.
94. Zaidi, Z. and S.W. Lanigan, *Skin: Structure and Function.* Dermatology in Clinical Practice, 2010: p. 1-+.
95. Gawkrodger, D., and Michael R. Ardern-Jones, *Dermatology E-Book: An Illustrated Colour Text*. 2016, Elsevier Health Sciences.
96. Montagna, W., *The structure and function of skin*. 2012: Elsevier.
97. *Extracellular Matrix and Egg Coats.* Extracellular Matrix and Egg Coats, 2018. **130**: p. 1-488.

98. Hashmi, S. and M.P. Marinkovich, *Molecular organization of the basement membrane zone.* Clinics in Dermatology, 2011. **29**(4): p. 398-411.
99. Katz, S.I., *The epidermal basement membrane zone—structure, ontogeny, and role in disease.* Journal of the American Academy of Dermatology, 1984. **11**(6): p. 1025-1037.
100. Uitto, J. and L. Pulkkinen, *Molecular complexity of the cutaneous basement membrane zone.* Molecular biology reports, 1996. **23**(1): p. 35-46.
101. McMillan, J.R., M. Akiyama, and H. Shimizu, *Epidermal basement membrane zone components: ultrastructural distribution and molecular interactions.* Journal of dermatological science, 2003. **31**(3): p. 169-177.
102. Timpl, R., et al., *Laminin--a glycoprotein from basement membranes.* Journal of Biological Chemistry, 1979. **254**(19): p. 9933-9937.
103. Durbeej, M., *Laminins.* Cell and Tissue Research, 2010. **339**(1): p. 259-268.
104. Yurchenco, P.D., *Basement membranes: cell scaffoldings and signaling platforms.* Cold Spring Harbor perspectives in biology, 2011. **3**(2): p. a004911.
105. Karsdal, M., *Biochemistry of collagens, laminins and elastin: structure, function and biomarkers*. 2019: Academic Press.
106. Boutaud, A., et al., *Type IV collagen of the glomerular basement membrane - Evidence that the chain specificity of network assembly is encoded by the noncollagenous NC1 domains.* Journal of Biological Chemistry, 2000. **275**(39): p. 30716-30724.
107. AUMAILLEY, M., et al., *Binding of nidogen and the laminin-nidogen complex to basement membrane collagen type IV.* European journal of biochemistry, 1989. **184**(1): p. 241-248.
108. Suleiman, H., et al., *Nanoscale protein architecture of the kidney glomerular basement membrane (vol 2, e01149, 2013).* Elife, 2013. **2**.
109. Aumailley, M., et al., *Nidogen mediates the formation of ternary complexes of basement membrane components.* Kidney international, 1993. **43**(1): p. 7-12.
110. Lössl, P., et al., *Analysis of nidogen-1/laminin γ1 interaction by cross-linking, mass spectrometry, and computational modeling reveals multiple binding modes.* PLoS One, 2014. **9**(11).
111. Fleischmajer, R., et al., *Skin fibroblasts are the only source of nidogen during early basal lamina formation in vitro.* Journal of Investigative Dermatology, 1995. **105**(4): p. 597-601.
112. LeBleu, V.S., B. MacDonald, and R. Kalluri, *Structure and function of basement membranes.* Experimental Biology and Medicine, 2007. **232**(9): p. 1121-1127.
113. Whitelock, J.M., J. Melrose, and R.V. Iozzo, *Diverse Cell Signaling Events Modulated by Perlecan.* Biochemistry, 2008. **47**(43): p. 11174-11183.
114. Nanci, A. and D.D. Bosshardt, *Structure of periodontal tissues in health and disease*.* Periodontology 2000, 2006. **40**(1): p. 11-28.
115. Buduneli, N., *Anatomy of Periodontal Tissues*, in *Biomarkers in Periodontal Health and Disease*. 2020, Springer. p. 1-7.
116. Seo, B.-M., et al., *Investigation of multipotent postnatal stem cells from human periodontal ligament.* The Lancet, 2004. **364**(9429): p. 149-155.
117. Schroeder, H.E. and M.A. Listgarten, *The gingival tissues: the architecture of periodontal protection.* Periodontology 2000, 1997. **13**(1): p. 91-120.
118. Frank, D.E. and W.G. Carter, *Laminin 5 deposition regulates keratinocyte polarization and persistent migration.* Journal of cell science, 2004. **117**(8): p. 1351-1363.
119. Bosshardt, D. and N. Lang, *The junctional epithelium: from health to disease.* Journal of dental research, 2005. **84**(1): p. 9-20.
120. Nanci, A., *Ten Cate's Oral Histology-E-Book: Development, Structure, and Function*. 2017: Elsevier Health Sciences.

121. Berkovitz, B.K., G.R. Holland, and B.J. Moxham, *Oral Anatomy, Histology and Embryology E-Book*. 2017: Elsevier Health Sciences.
122. Hu, J.C.-C., et al., *Enamel formation and amelogenesis imperfecta.* Cells Tissues Organs, 2007. **186**(1): p. 78-85.
123. Chen, H. and Y. Liu, *Advanced Ceramics for Dentistry: Chapter 2. Teeth*. 2013: Elsevier Inc. Chapters.
124. Woelfel, J.B. and R.C. Scheid, *Dental anatomy: its relevance to dentistry*. 1997: Williams & wilkins.
125. Yin, Y., et al., *Chemical regeneration of human tooth enamel under near-physiological conditions.* Chemical Communications, 2009(39): p. 5892-5894.
126. Wang, X., et al., *Direct growth of human enamel-like calcium phosphate microstructures on human tooth.* Journal of nanoscience and nanotechnology, 2009. **9**(2): p. 1361-1364.
127. Chen, H., et al., *Acellular Synthesis of a Human Enamel-like Microstructure.* Advanced Materials, 2006. **18**(14): p. 1846-1851.
128. Vallés Lluch, A., et al., *Bioactive scaffolds mimicking natural dentin structure.* Journal of Biomedical Materials Research Part B: Applied Biomaterials, 2009. **90**(1): p. 182-194.
129. Bertassoni, L.E., et al., *The dentin organic matrix–limitations of restorative dentistry hidden on the nanometer scale.* Acta biomaterialia, 2012. **8**(7): p. 2419-2433.
130. Goldberg, M., et al., *Dentin: Structure, Composition and Mineralization: The role of dentin ECM in dentin formation and mineralization.* Frontiers in bioscience (Elite edition), 2011. **3**: p. 711.
131. Balogh, M. and M. Fehrenbach, *Illustrated Dental Embryology, Histology, and Anatomy*. 1997, WB Saunders Publications.
132. CHO, M.-I. and P.R. GARANT, *Development and general structure of the periodontium.* Periodontology 2000, 2000. **24**(1): p. 9-27.
133. Gonçalves, P.F., et al., *Dental cementum reviewed: development, structure, composition, regeneration and potential functions.* Brazilian Journal of Oral Sciences, 2005. **4**(12): p. 651-658.
134. Polimeni, G., A.V. Xiropaidis, and U.M. Wikesjö, *Biology and principles of periodontal wound healing/regeneration.* Periodontology 2000, 2006. **41**(1): p. 30-47.
135. Ba, O.M., et al., *Protein covalent immobilization via its scarce thiol versus abundant amine groups: Effect on orientation, cell binding domain exposure and conformational lability.* Colloids and Surfaces B: Biointerfaces, 2015. **134**: p. 73-80.
136. Barros, D., et al., *An affinity-based approach to engineer laminin-presenting cell instructive microenvironments.* Biomaterials, 2019. **192**: p. 601-611.
137. Gehan, H., et al., *A General Approach Combining Diazonium Salts and Click Chemistries for Gold Surface Functionalization by Nanoparticle Assemblies.* Langmuir, 2010. **26**(6): p. 3975-3980.
138. Tavafoghi, M., et al., *Hydroxyapatite formation on graphene oxide modified with amino acids: arginine versus glutamic acid.* Journal of The Royal Society Interface, 2016. **13**(114): p. 20150986.
139. Goldberg, H.A. and J. Sodek, *Purification of mineralized tissue-associated osteopontin.* Journal of tissue culture methods, 1994. **16**(3-4): p. 211-215.
140. Wingfield, P.T., *Use of protein folding reagents.* Current Protocols in Protein Science, 2016. **84**(1): p. A. 3A. 1-A. 3A. 8.
141. Wang, Y. and J.M. Regenstein, *Effect of EDTA, HCl, and citric acid on Ca salt removal from Asian (silver) carp scales prior to gelatin extraction.* Journal of food science, 2009. **74**(6): p. C426-C431.
142. Kaartinen, M.T., et al., *Tissue transglutaminase and its substrates in bone.* Journal of Bone and Mineral Research, 2002. **17**(12): p. 2161-2173.
143. Siqueira, W.L., et al., *Quantitative proteomic analysis of the effect of fluoride on the acquired enamel pellicle.* PloS one, 2012. **7**(8): p. e42204.
144. McCann, M.R., et al., *Proteomic signature of the murine intervertebral disc.* PloS one, 2015. **10**(2): p. e0117807.

145. Mahjoubi, H., et al., *Surface Modification of Poly(d,l-Lactic Acid) Scaffolds for Orthopedic Applications: A Biocompatible, Nondestructive Route via Diazonium Chemistry.* ACS Applied Materials & Interfaces, 2014. **6**(13): p. 9975-9987.
146. Pinson, J. and F. Podvorica, *Attachment of organic layers to conductive or semiconductive surfaces by reduction of diazonium salts.* Chemical Society Reviews, 2005. **34**(5): p. 429-439.
147. Adenier, A., et al., *Attachment of polymers to organic moieties covalently bonded to iron surfaces.* Chemistry of materials, 2002. **14**(11): p. 4576-4585.
148. Palacin, S., et al., *Molecule-to-Metal Bonds: Electrografting Polymers on Conducting Surfaces.* ChemPhysChem, 2004. **5**(10): p. 1468-1481.
149. Bahr, J.L. and J.M. Tour, *Highly functionalized carbon nanotubes using in situ generated diazonium compounds.* Chemistry of Materials, 2001. **13**(11): p. 3823-3824.
150. Ying, L., et al., *Immobilization of galactose ligands on acrylic acid graft-copolymerized poly (ethylene terephthalate) film and its application to hepatocyte culture.* Biomacromolecules, 2003. **4**(1): p. 157-165.
151. Chen, J., et al., *Biocompatibility studies of poly (ethylene glycol)–modified titanium for cardiovascular devices.* Journal of bioactive and compatible polymers, 2012. **27**(6): p. 565-584.
152. Neuss, S., et al., *Assessment of stem cell/biomaterial combinations for stem cell-based tissue engineering.* Biomaterials, 2008. **29**(3): p. 302-313.
153. Silva-Boghossian, C.M., et al., *Quantitative proteomic analysis of gingival crevicular fluid in different periodontal conditions.* PloS one, 2013. **8**(10): p. e75898.
154. Aisenbrey, E.A. and W.L. Murphy, *Synthetic alternatives to Matrigel.* Nature Reviews Materials, 2020. **5**(7): p. 539-551.
155. Benton, G., et al., *Multiple uses of basement membrane-like matrix (BME/Matrigel) in vitro and in vivo with cancer cells.* International Journal of Cancer, 2011. **128**(8): p. 1751-1757.
156. Vukicevic, S., et al., *Identification of multiple active growth factors in basement membrane matrigel suggests caution in interpretation of cellular activity related to extracellular matrix components.* Experimental Cell Research, 1992. **202**(1): p. 1-8.
157. Hughes, C.S., L.M. Postovit, and G.A. Lajoie, *Matrigel: A complex protein mixture required for optimal growth of cell culture.* PROTEOMICS, 2010. **10**(9): p. 1886-1890.
158. Benton, G., et al., *Matrigel: From discovery and ECM mimicry to assays and models for cancer research.* Advanced Drug Delivery Reviews, 2014. **79-80**: p. 3-18.
159. Hammad, M., et al., *Identification of polymer surface adsorbed proteins implicated in pluripotent human embryonic stem cell expansion.* Biomaterials science, 2016. **4**(9): p. 1381-1391.
160. Smith, S.M. and D.E. Birk, *Focus on molecules: collagens V and XI.* Experimental eye research, 2012. **98**(1): p. 105-106.
161. Golczak, S., et al., *Comparative XPS surface study of polyaniline thin films.* Solid State Ionics, 2008. **179**(39): p. 2234-2239.
162. Zheng, Y., C. Xiong, and L. Zhang, *Formation of bone-like apatite on plasma-carboxylated poly(etheretherketone) surface.* Materials Letters, 2014. **126**: p. 147-150.
163. Damink, L.O., et al., *Cross-linking of dermal sheep collagen using a water-soluble carbodiimide.* Biomaterials, 1996. **17**(8): p. 765-773.
164. Sharan, J., et al., *Bio-functionalization of grade V titanium alloy with type I human collagen for enhancing and promoting human periodontal fibroblast cell adhesion–an in-vitro study.* Colloids and Surfaces B: Biointerfaces, 2018. **161**: p. 1-9.
165. Rezvanian, P., et al., *Enhanced biological response of AVS-functionalized Ti-6Al-4V alloy through covalent immobilization of collagen.* Scientific reports, 2018. **8**(1): p. 1-11.

166. Murphy, A.R., P.S. John, and D.L. Kaplan, *Modification of silk fibroin using diazonium coupling chemistry and the effects on hMSC proliferation and differentiation.* Biomaterials, 2008. **29**(19): p. 2829-2838.
167. Romero-Gavilán, F., et al., *Proteome analysis of human serum proteins adsorbed onto different titanium surfaces used in dental implants.* Biofouling, 2017. **33**(1): p. 98-111.
168. Gorth, D.J., et al., *Decreased bacteria activity on Si_3N_4 surfaces compared with PEEK or titanium.* International journal of nanomedicine, 2012. **7**: p. 4829-4840.
169. Pankov, R. and K.M. Yamada, *Fibronectin at a glance.* Journal of cell science, 2002. **115**(20): p. 3861-3863.
170. Sousa, S., P. Moradas-Ferreira, and M. Barbosa, *TiO 2 type influences fibronectin adsorption.* Journal of Materials Science: Materials in Medicine, 2005. **16**(12): p. 1173-1178.
171. Gheisarifar, M., et al., *In vitro study of surface alterations to polyetheretherketone and titanium and their effect upon human gingival fibroblasts.* The Journal of Prosthetic Dentistry, 2020.
172. Marín-Pareja, N., et al., *Different organization of type I collagen immobilized on silanized and nonsilanized titanium surfaces affects fibroblast adhesion and fibronectin secretion.* ACS applied materials & interfaces, 2015. **7**(37): p. 20667-20677.
173. Ataç, B., et al., *Skin and hair on-a-chip: in vitro skin models versus ex vivo tissue maintenance with dynamic perfusion.* Lab on a chip, 2013. **13**(18): p. 3555-3561.
174. Yamamoto, M., et al., *Identification of integrins involved in cell adhesion to native and denatured type I collagens and the phenotypic transition of rabbit arterial smooth muscle cells.* Experimental cell research, 1995. **219**(1): p. 249-256.
175. Knight, C.G., et al., *The Collagen-binding A-domains of Integrins α1β1 and α2β1recognize the same specific amino acid sequence, GFOGER, in native (Triple-helical) collagens.* Journal of Biological Chemistry, 2000. **275**(1): p. 35-40.